UNIVERSITY OF CAPE TOWN

DEPARTMENT OF MECHANCIAL ENGINEERING

RONDEBOSCH, CAPE TOWN, SOUTH AFRICA

The further Research, Development and Design of a Robotic Unmanned Ground Vehicle Platform for Urban Search and Rescue

Prepared by David Lwabona

Robotics and Agents Research Laboratory

University of Cape Town

Supervised by Stephen Marais

Robotics and Agents Research Laboratory

University of Cape Town

April 2013

The further Research, Development and Design of a Robotic Unmanned Ground Vehicle Platform for Urban Search and Rescue

Robotics and Agents Research Laboratory

David Lwabona

28th May 2013

Summary

This report details the further research, development and design of a Robotic **U**nmanned **G**round **V**ehicle (**UGV**) Platform for use in **U**rban **S**earch **A**nd **R**escue (**USAR**) . The platform depicted in Figure 0.1, is dubbed **Ratel** (the Afrikaans name for honey badger) and it is the the 5th generation **UGV** developed in the **R**obotics and **A**gents **R**esearch **L**aboratory (**RARL**) at the **U**niversity of **C**ape **T**own (**UCT**) .

Figure 0.1.: The Ratel UGV.

Disasters in urban areas, such as tornadoes and earthquakes can lead to damaged or structurally compromised buildings. Victims are often found under the debris of damaged buildings or trapped in voids. **USAR** is the first step in urban disaster management and recovery that rescue responders employ. This operation deals with the location, rescue and initial medical treatment of victims [1]. Mobile **USAR UGVs** have been successfully used to act as a sensory extension of emergency responders and to assist them to perform **USAR** related tasks [2].

The initial development on **Ratel's** robotic platform was performed by MSc student Eugene Dreyer. The unit proved to be a viable rescue robot, however, it still required several improvements and alterations before it could be successfully deployed in the field. The further design and development of the platform consisted of four main sections, namely the **Power Supply and Distribution System**, **Platform Actuation**, **Caterpillar Tracks** and **System Control and Communications**.

Power Supply and Distribution System

The previously developed power supply and distribution system was mainly used to verify the locomotion system of the platform and several desired features were not present. The voltages of the fully charged batteries were higher than the maximum allowable input supply voltage that the DC/DC converters were rated for. For this reason the platform could not be powered by the batteries and had to rely on regulated power from a power supply being supplied via a tether. The second version of the system developed in this project had improved current and voltage capabilities and thus allowed the platform to be driven without a tether. It additionally was used to control the lights and included current sensors that were used to verify the correct operation of the batteries and to estimate the remaining charge of the batteries. The two boards that were used to regulate and distribute power to the robot's devices are depicted in Figure 0.2.

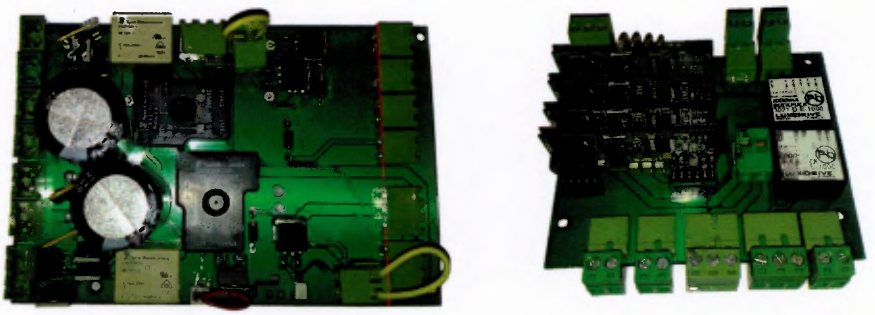

(a) The power distribution board. (b) The power regulation board.

Figure 0.2.: The boards of the power supply and distribution system.

Platform Actuation

In the previous development of the robotic platform, the actuation system consisted of a motor assembly for actuation of the drive tracks and flippers, yet no means of controlling the speed, current limit and other aspects of the motors were available. The final actuation system includes embedded microcontrollers that were used to control the operation of the motors.

Optical and magnetic end stops were utilised to calibrate the flippers to specific positions, seeing that the optical encoders of the motor assemblies were relative encoders and would reset every time the **UGV** was powered on. The introduction of the microcontrollers and the custom designed current sensor boards made the position control of flippers possible and allowed the monitoring of the amount of current drawn by each motor.

Caterpillar Tracks

At the beginning of the project the tracks were timing belts with teeth on a single side. The smooth side made contact with the terrain while the platform was being driven and the toothed side meshed with the pulleys. In order to increase traction, **TPU** sheets were cut into trapezoidal blocks that acted as the feet of the tracks. Superglue was used to attach these feet to the smooth sides of the belts in a pattern of two rows per drive belt and one row per flipper belt. The completed caterpillar tracks can be viewed in Figure 0.3.

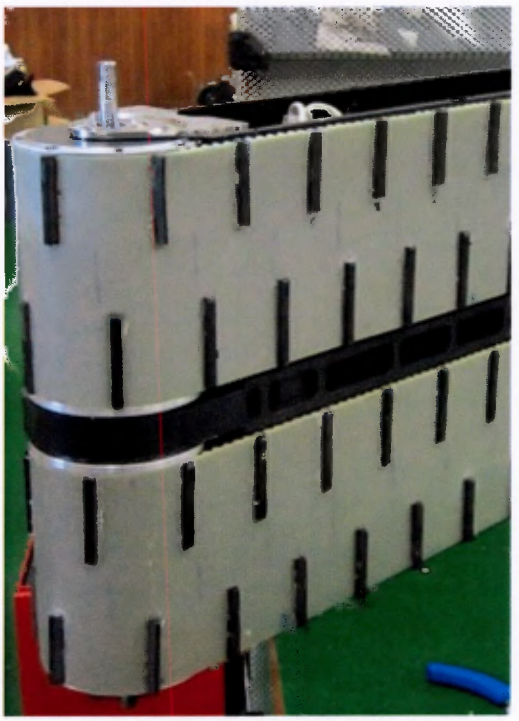

Figure 0.3.: The completed tracks.

System Control and Communications

In the previous development the wireless communications system consisted of a set of Ubiquiti RouterStation Pro radios. One was mounted in the platform and the other was mounted on the operator control station. Testing showed that these units were not reliable and a set of Ubiquiti Bullet M5 wireless radios were purchased. These units established a reliable wireless link that enabled teleoperation of the rescue robot.

The user interface of the **UGV** presents an operator with three video streams for driving it around. A Xsens **I**nertial **M**easurement **U**nit (**IMU**) was used in conjunction with the

Laboratory **V**irtual **I**nstrumentation **E**ngineering **W**orkbench (**LabVIEW**), a graphical programming environment, to produce a 3D image of the platform, that conveyed its roll, pitch and yaw in a visual manner, as can be seen in Figure 0.4. This image additionally presented the position of the flippers and was used by an operator to quickly and intuitively understand the platform's orientation in space. Additional information that the user interface presented included the numerical values of motor speeds, current draws and flipper positions.

The addition to the custom designed embedded microcontrollers presented a way of achieving position control over the flippers. Since the pre-selected motor controllers were speed controllers, position control was achieved by sending a specific speed values to the speed controllers and monitoring the feedback of the quadrature encoders. Once the motors had reached their desired position value, the controllers were told to stop toggle the stop boolean for the motors.

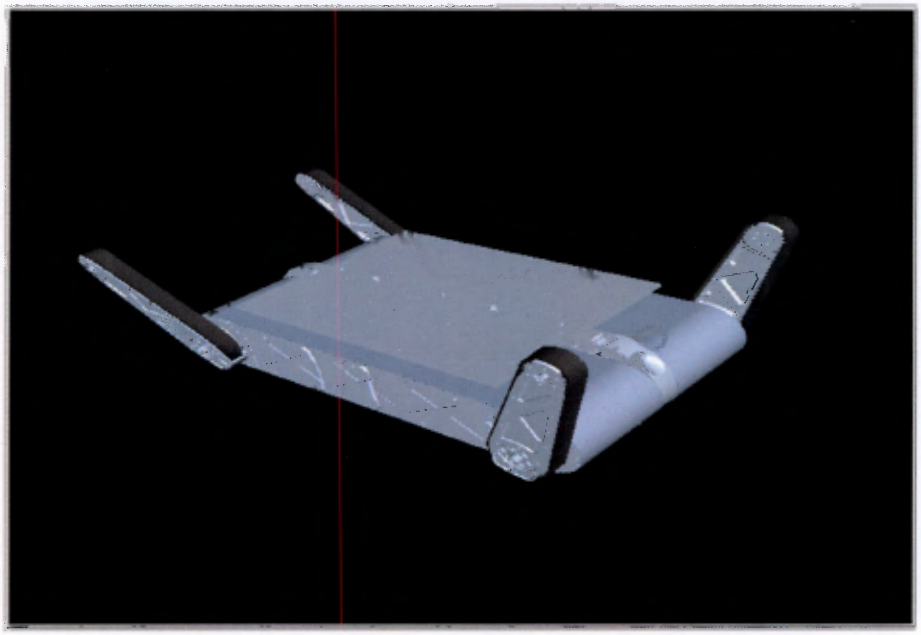

Figure 0.4.: The 3D model of the robotic platform in LabVIEW.

Testing, Conclusions and Recommendations

Tests were performed to evaluate the proficiency of the individual subsystems and of the assembled platform as a whole. These tests measured the position control accuracy of the flipper system, as well as the current draw after several changes were made to the initial drive system. Additional features that were inspected included the traction capabilities of the platform after alterations were performed to the tracks and aspects of the wireless link were also scrutinized. Further tests were run to investigate camera and lighting systems and the capabilities of the power supply and distribution system were gauged. Conclusions were drawn from the test's results, as well as from the lessons learnt during working on the platform.

Plagiarism Declaration

This thesis is submitted in complete fulfilment of a M.Sc. (Mechanical Engineering) at the University of Cape Town.

I know the meaning of plagiarism and declare that all of the work in the document, save for that which is properly acknowledged, is my own. Each contribution to, and quotation in, this document from the work(s) of other people has been attributed, and has been cited and referenced according to the style for IEEE Transactions.

I have not allowed, and will not allow anyone to copy my work with the intention of passing it off as their own.

Signed by candidate

Signature Removed

David Lwabona

02 April 2013

Acknowledgements

Special thanks goes to my supervisor,Stephen Marais, for his support and guidance throughout the development of the project and for giving us the opportunity to fly to Mexico City to take part at RoboCup 2012.

I would also like to say thanks to Glen Newins, the workshop manager at UCT, and to the rest of the workshop staff for always working quickly and for their excellent machining skills.

Many thanks go out to Tracy Booysen for her help with the electronics and for making an effort to make the lab a fun place to be.

Thanks are also owed to the postgraduate students of the Robotic and Agents Research Laboratory for their willingness to assist for long hours. Special thanks does to Eugene Dreyer for his insights and wisdom.

Lastly, I would like to thank my brother Bilo and my mother Eva for their constant support and encouraging words.

Contents

List of Figures

List of Tables

Glossary of Terms

ADC - Analog-to-Digital Converter

AHRS - Attitude and Heading Reference System

AP - Access Point

ASTM - American Society for Testing and Materials

CAD - Computer Aided Design

CAN - Controller Area Network

DAC - Digital-to-Analog Converter

DMF - Dimethylformamide

EC - Electronic Commutated

EOD - Explosive Ordnance Disposal

GUI - Graphical User Interface

HazMat - Hazardous Materials

I2C - Inter-Integrated Circuit

MOSFET - Metal-Oxide-Semiconductor Field-Effect Transistor

MRP - Mobile Robot Platform

NI - National Instruments

NIST - National Institute for Standards and Technology

PCB - Printed Circuit Board

PU - Polyurethane

PVC - Polyvinyl Chloride

PWM - Pulse Width Modulation

RARL - Robotics and Agents Research Laboratory

SOC - State Of Charge

SPDT - Single Pole Double Throw

SPST - Single Pole Single Throw

TCP - Transmission Control Protocol

THF - Tetrahydrofuran

TPU - Thermoplastic Polyurethane

TTL - Transistor-Transistor Logic

TVL - Tele-Vision Lines

UAV - Unmanned Aerial Vehicle

UCT - University of Cape Town

UGV - Unmanned Ground Vehicle

USAR - Urban Search And Rescue

USV - Unmanned Surface Vehicles

UUV - Unmanned Underwater Vehicle

WTC - World Trade Center

1. Introduction

Natural and man-made catastrophes such as earthquakes, floods and mining accidents often lead to the loss of life and cause a substantial amount of damage. Frequent outcomes of such disasters in urban areas are unstable, damaged or fully collapsed structures [1]. Survivors can find themselves trapped underneath debris or in confined spaces. **U**rban **S**earch **A**nd **R**escue (**USAR**) is the first step of the urban disaster recovery procedures that follow such catastrophes. It is an operation that deals with the location, rescue and initial medical treatment of victims in urban disaster zones [1]. The conditions seen in the following two figures are a typical sight in such situations.

Figure 1.1.: The collapsed Kashmir building in Srinagar, India on the 21st August 2009 [4].

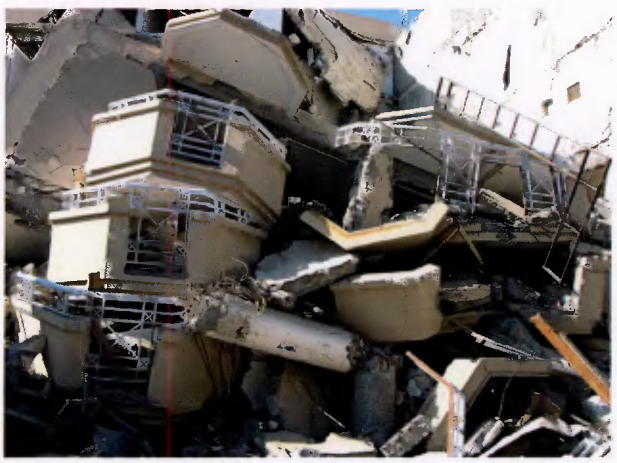

Figure 1.2.: Destruction in the Canterbury region owing to the 2011 Christchurch earthquake [5].

Searching for and retrieving victims in environments where a building's structural integrity is questionable and dangers such as fires and explosions are always present, makes this task exceptionally perilous and demanding. An aspect of **USAR** that is often stressed, is that it has to occur as fast as possible, for the reason that the mortality rate for trapped victims reaches its maximum after approximately 48 hours. Consequently emergency responders have to work as quickly as possible to reach victims, yet move carefully enough to avoid becoming victims themselves or worsening the situation [2].

Figure 1.3.: The devastation caused by the Great Hanshin-Awaji Earthquake [6].

Figure 1.3 depicts the aftermath of the the Great Hanshin-Awaji Earthquake that hit Kobe City, Japan on the 17th of January 1995. This earthquake led to the deaths of approximately 6500 people and caused over $100 billion in damages. The events that occurred during the disaster relief procedures led to an increase in research interest of the deployment of robots in **USAR** situations[7]. This marks the birth of the **'Rescue Robotics'** field.

The destruction of the **W**orld **T**rade **C**entre (**WTC**) on the 11th September 2001 marks the first time that robots were implemented in **USAR** . The robots served as an extension to the rescue workers and provided video footage in addition to supplementary information about the state of the disaster zones, while rummaging around for victims [2]. The Inuktun micro-VGTV, Inuktun micro-Tracks and the Foster-Miller Solem are the three small **UGVs** that were initially used to look for victims. Later on larger **UGVs** were used to explore the spaces of the fallen towers [2]. The robots used in the **WTC** rescue efforts are displayed in Figure 1.4 and Figure 1.5 below.

Figure 1.4.: A Rescue Robot searching for survivors amidst the debris of the collapsed towers [8].

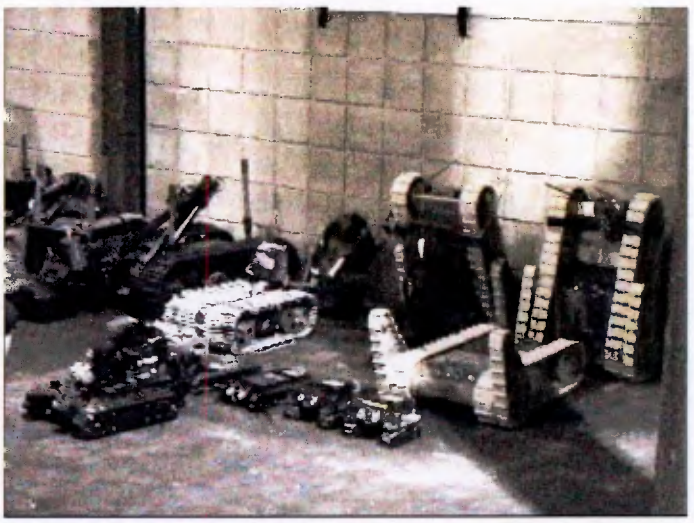

Figure 1.5.: The various robots that assisted rescue workers during the WTC collapse [8].

Since 911 the field has grown larger over the years and these days rescue robots come in various shapes, sizes and configurations, depending on the environment that they are meant to work in. On the ground **U**nmanned **G**round **V**ehicles (**UGVs**) assist rescue personnel during **USAR**, in the air **U**nmanned **A**erial **V**ehicles (**UAVs**) extend the responders' abilities and provide a bird's eye view of the disaster zone, while **U**nmanned **U**nderwater **V**ehicles (**UUVs**) and **U**nmanned **S**urface **V**ehicles (**USVs**) are used in water based rescue scenarios. The tasks of rescue robots range from search, reconnaissance and mapping, to the inspection of structural integrity and rubble removal; but at their core essentials they are teleoperated **M**obile **R**obotic **P**latforms (**MRPs**) that are meant to lend their senses to rescuers and allow them to act in hazardous environments, without putting themselves in danger [2].

Within this rather novel and diverse robotics field, the **R**obotics and **A**gents **R**esearch **L**aboratory

(**RARL**) at the **U**niversity of **C**ape **T**own (**UCT**) has been steadily developing its own **UGV**, dubbed **Ratel** (the Afrikaans name for honey badger), depicted in Figure 1.6.

Figure 1.6.: The fully assembled Ratel Rescue Robot.

Ratel is made up of a robotic **UGV** platform with four variable geometry tracks, also known as flippers. The platform consists of a robust aluminium body and provides real-time video feeds through two cameras, one at the front and the other the rear of the platform. A power supply and distribution system provides power to all electronic and electromechanical devices either through a tether or through an array of on-board batteries. Sensors built into this system make current readings of several components, including the five motors responsible for the platform's actuation available. A Xsens MTi, which is a miniature, gyro enhanced **A**ttitude and **H**eading **R**eference **S**ystem (**AHRS**), is used to visually provide the operator with a 3D model of the platform's orientation. This robotic platform is a complete system on its own and requires no additional features in order to traverse complex environments. As a means of improving its versatility, a number of additional systems were introduced to it. A robotic arm, controlled through inverse kinematics, is mounted on top of the platform. A sophisticated end

effector, that contains several sensors, is attached to the end of the manipulator arm and allows for delicate gripping manoeuvres. A sensor payload, mainly used for victim identification and navigation, provides a range of sensory data including CO_2 readings and real time video feed. Even though the system was primarily designed with **USAR** in mind, it is aptly suited for other areas, which include but are not limited to **E**xplosive **O**rdnance **D**isposal (**EOD**) and assistance in law enforcement. The **RoboCup Rescue League**, an international robotics competition, was used as a means of testing the viability of the platform as well as the proficiency of the other systems. The completed robotic platform, sans the other systems, is illustrated in Figure 1.7.

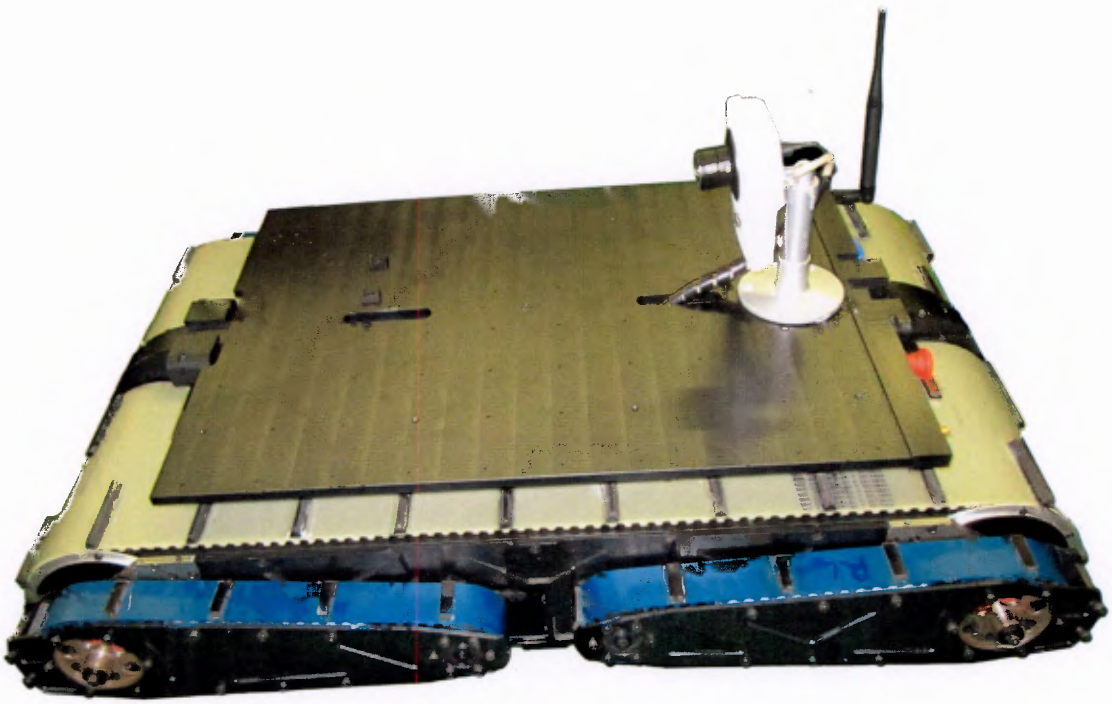

Figure 1.7.: The Final UGV Platform.

The subsequent chapter will examine the **RoboCup Rescue** environment and will present the previous development of **Ratel's** platform so as to be able to determine the improvements that are still required in order to make it deployable. Thereafter the features and functions associated with **UGVs** used in **USAR** and in other fields, where equally versatile mobility is required, will be examined in the following chapter, in order to identify desired features in line with the objectives of this project. Both custom built and commercially available units, such as the one depicted in Figure 1.8, will be examined. Thereafter the development that has taken place on the individual systems is presented, which is then followed by the testing of these systems. Finally conclusions are drawn and recommendations are made for the next iteration of the system.

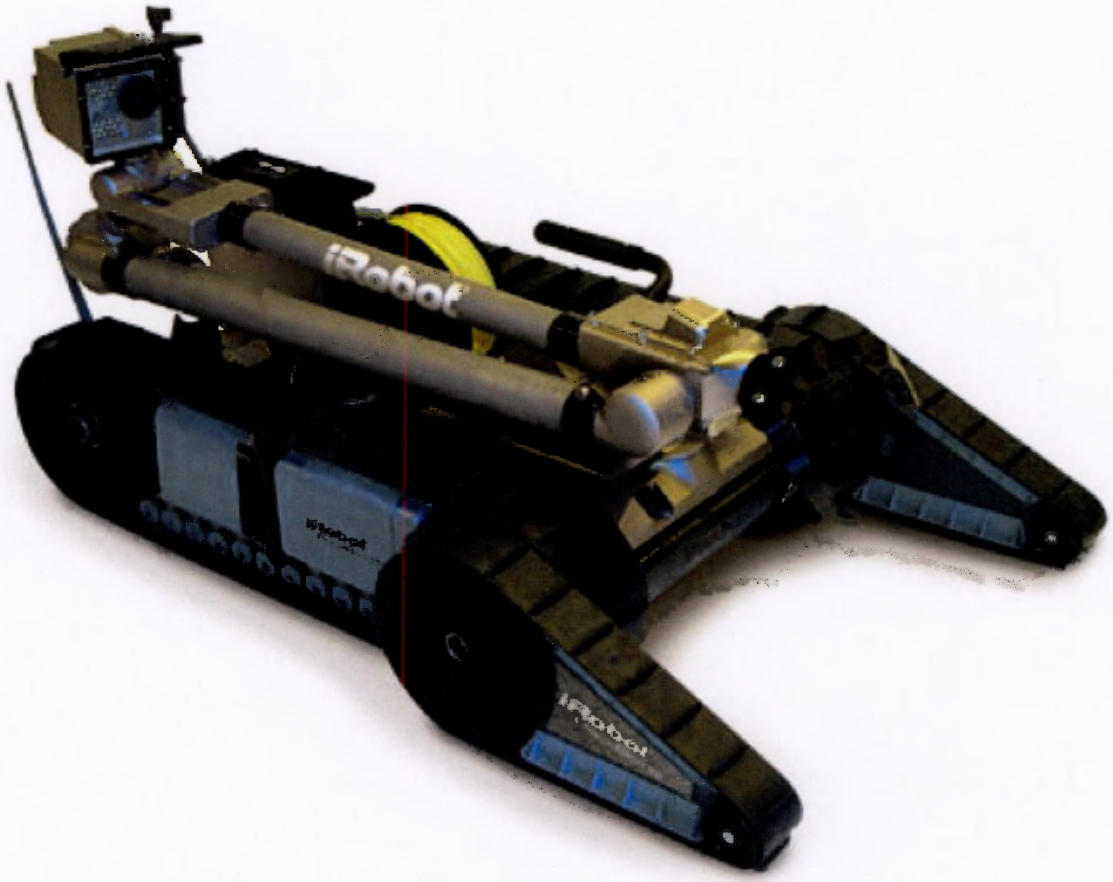

Figure 1.8.: The IRobot® PackBot [9].

2. Background Research

Robotics technology has made significant advances over the years and as a result robots have considerable effects on several facets of life in the present age. The majority of robots can be found in the industrial realm, where they effortlessly and quickly perform tasks ranging from assembly of vehicles, pick and place operations to quality inspection of products with precision and efficiency far superior to that of human workers [2]. Their usefulness and effectiveness in addition to continual technological progresses in robotics has gained the attention of professionals in areas outside the industrial environment. Today robots are involved in fields such as space and deep sea exploration,healthcare and military combat, to name a few.

The implementation of **MRPs** is poles apart from that of robots in factory settings. Unlike factory robots, where the environment is highly structured and constantly monitored, explorer robots have to deal with dynamic, unstructured and highly complex environments. This difference can be seen in the way these units are constructed and it is the reason for the relentless research and development in these fields. The following sections will explore the **RoboCup Rescue** environment and will be followed by an overview of the previous development of **Ratel**. Thereafter the desired features of the rescue robot that will make it deployable will be presented.

2.1. RoboCup Rescue Competition

Rescue robotics is an emerging technology and hence this field still has the need for significant improvements in numerous areas. Consequently competitions, such as **RoboCup Rescue**, have been created to promote research and development in mobility and artificial intelligence, amongst other areas. This competition annually brings together teams of students and researchers from around the globe. During the event participants demonstrate their proficiency in areas ranging from mobility and sensory perception to practical operator interfaces and assistive autonomous behaviour. Competitors test their systems in standardised test arenas that present some of the challenges of disaster-stricken urban areas. [10]

Six distinct arenas are provided for **RoboCup Rescue** , namely the yellow, orange, red, blue, yellow-black and black arena [10]. All arenas are constructed in accordance with the regulations created by the **N**ational **I**nstitute of **S**tandards and **T**echnology (**NIST**) in accordance with the **A**merican **S**ociety for **T**esting and **M**aterials (**ASTM**). As each arena is designed to test specific capabilities, no two arenas are the same, however, they do share structural and terrain specific characteristics. Seeing that the primary objective of the platform was to achieve sufficient mobility, only the mobility related elements of the arenas were considered. The simulated victims that are placed in the arenas were also taken into account. The information contained within these sections is derived from **"Robocup Rescue Robot League Rules 2011.2"** [10].

2.1.1. The yellow Arena

Only robots with a high level of autonomy participate in the yellow arena, where their navigation and victim identification capabilities are tested. The arena consists of an arbitrarily arranged maze that is made up of 1.2m wide hallways and larger rooms, with 15° pitching and rolling ramps. Sections of the yellow arena are displayed in Figure 2.1.

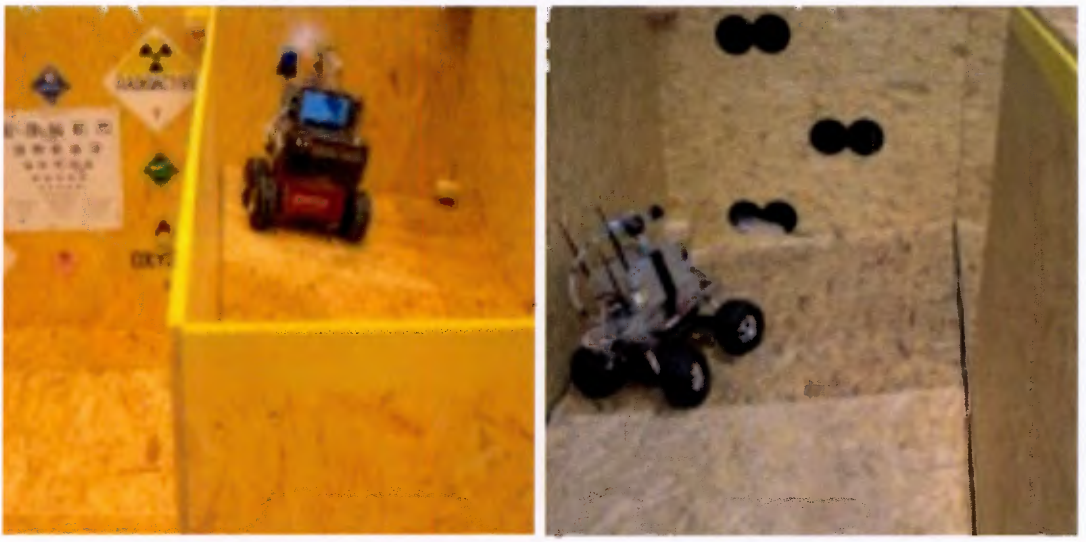

Figure 2.1.: Rescue Robots in the yellow arena [10].

2.1.2. The Orange Arena

Manoeuvrability in a more complex environment is being examined in this section of the competition. It has a similar configuration to the yellow arena in addition to stairs, planes with 45° inclinations, and vertically stacked pipes that make 20cm and 30cm high obstacles. The difficulty of the arena is intensified through the introduction of confined spaces below elevated platforms which tighten the vertical clearances of the ramps to a minimum of 500mm. Figure 2.2 depicts a section of the orange arena.

Figure 2.2.: The environment of the orange arena [10].

2.1.3. The Red Arena

Robots that compete in the red arena should be capable of reliably negotiating a stepfield which consists of 10cm square blocks of wood that have been cut to lengths of 10,20,30,40 and 50 cm. The blocks are arranged in such a way that the stepfield gains a topographically symmetric pattern. Robots traversing this arena are shown in Figure 2.3.

Figure 2.3.: Rescue robots traversing the red arena [10].

2.1.4. The Yellow-Black Arena

The yellow-black arena is the radio drop-out zone of the competition. Here teams must rely on their robot's autonomous behaviour to negotiate hallways with continuous 15° ramps. Figure 2.4 portrays a rescue robot driving around in the yellow-black arena.

Figure 2.4.: A rescue robot autonomously navigating the radio dropout zone of the competition [10].

2.1.5. The Black Arena

The black arena is the most unstructured arena. The environment closely resembles a collapsed urban structure and thus introduces a significant amount of complexity. This section has two specific aspects to it. The first aspect has a challenging terrain and it is reachable from the red arena, whereas the second aspect simulates a disaster that resulted in the release of hazardous materials. One or more vehicles are placed in this arena and it will contain simulated victims. Robots are to search vehicles for injured passengers and inspect car trunks for hazardous materials. One of these scenarios is depicted in the following figure.

Figure 2.5.: A rescue robot inspecting a car in the black arena [10].

2.1.6. Simulated Victims

Mannequins and baby dolls are used to simulate trapped survivors. They mimic human life signs through motion and the emission of heat, CO_2 and sound. They are placed in four scenarios that mimic the victim locations of real disaster sites, namely, surface, trapped, void or entombed. Mobility is tested by making teams accurately identify hazmat signs and eye charts that are placed with every victim. All robots need to determine all life signs before sending the required information to the operator. There are a total of four victims in the yellow, orange and red arena and a total of two victims in the yellow-black and the black arena. Figure 2.6 illustrates a trapped victim, along with a **Haz**ardous **Mat**erials (**HazMat**) Class 3 Flammable Liquid sign and a "Tumbling E" chart.

Figure 2.6.: A doll utilised as a simulated victim inside a box [10].

2.2. Previous Development on Ratel's Platform

After having examined the **RoboCup Rescue** environments that **Ratel** will have to traverse, it was imperative to have an understanding of the properties and capabilities of the platform up until its previous development by MSc student Eugene Dreyer [11], in order to be able to cultivate it to a point where it is deployable. This section will therefore present an overview of its modules.

2.2.1. Mechanical Structure

The structure of **RARL's** platform was designed by Mr Eugene Dreyer. It essentially consisted of a centre spine and two sidepods. A single sidepod was affixed to each side of the spine through 3mm dowel pins and M4 cap screws. The three modules are depicted in Figure 2.8. The platform was required to fit through an equilateral entry triangle of 24" that is typically cut into the side of a building if the conventional methods of entering and exiting said building are no longer available. This requirement was the rudimentary factor that led to the overall dimensions as well as mechanical structures of the platform's modules. Figure 2.7 shows how the fully assembled platform was designed to fit through the entry triangle.

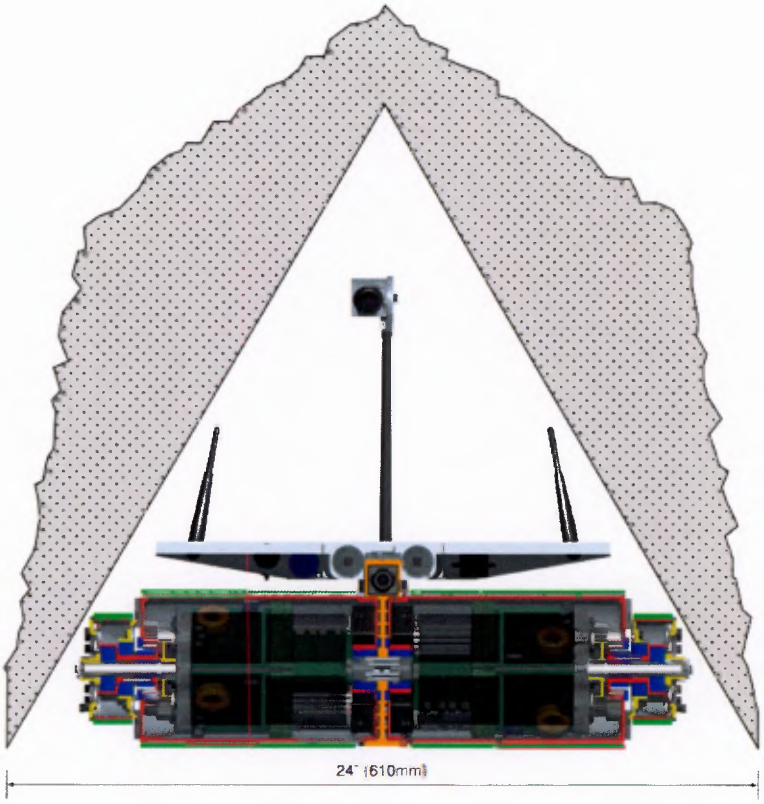

Figure 2.7.: ProEngineer CAD model showing how the platform was designed to fit through the 24" entry triangle [11].

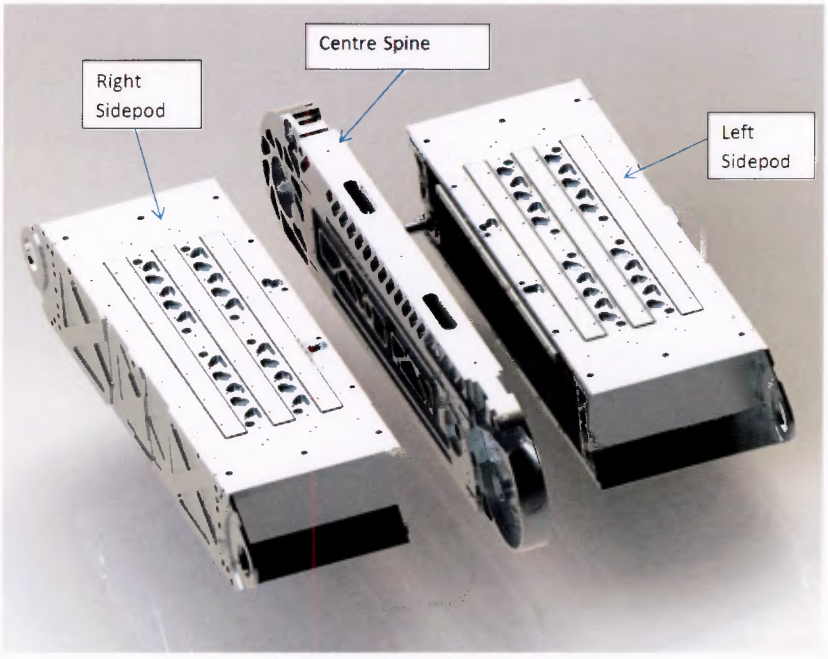

Figure 2.8.: The three basic modules that make up the platform.

Four identical variable geometry tracks, conventionally known as flippers, were attached one of the four corners of the platform through 3mm dowel pins, M4 cap screws and parallel keys. Figure 2.9 illustrates an isometric view of a flipper, while the Figure 2.11 that follows depicts a rendered view of the platform with the flippers attached.

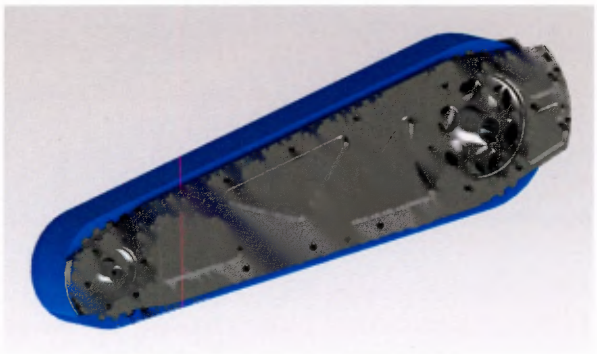

Figure 2.9.: A rendered CAD model of a flipper.

2.2.2. Locomotion

Five Maxon EC40, 120W motors actuated the platform. Four pulleys were mounted on each side of the spine, two at the front and two at the rear. The front pulleys contained Maxon speed controllers and two motors each. One of those motors on each side drove a track while the other actuates a front flipper. This configuration is illustrated in Figure 2.10. Unlike the front pulleys, the rear ones did not house any actuators or controllers. The rear flippers moved in unison as they were actuated by a single motor that was housed within the left sidepod.

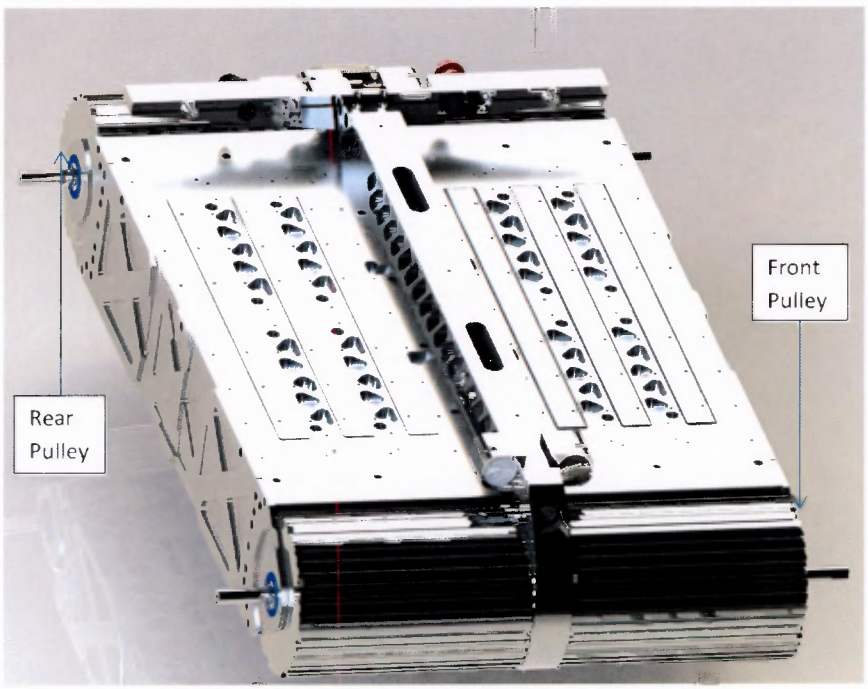

Figure 2.10.: Platform with drive pulleys.

All tracks were timing belts that had integral teeth on only one side and the non-toothed smooth side was in contact with the driving surface when the platform was in operation. No position control was implemented and thus the position of the flippers could not be set or maintained. In addition to this, the amount of current drawn by the driving mechanism was not monitored. The fully assembled platform is shown in the Figure 2.11 and an image of the previous platform is shown in Figure 2.12.

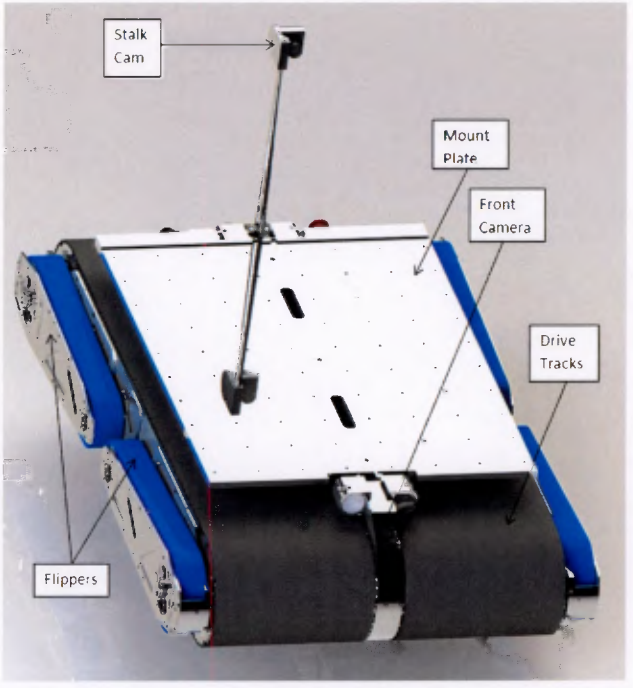

Figure 2.11.: Fully assembled rescue robot platform.

Figure 2.12.: The assembled platform in its previous development.

2.2.3. Electrical System

Power was provided to the robot platform either through a tether or by batteries. Six Li-Ion batteries were used to power the systems when the power tether was removed. The power distribution and regulation board took in 36V and 18V and provided 36V, 18V, 12V and 5V. There was also emergency stop functionality, in case something went wrong and power to the robot had to be cut off.

2.3. Tracks

There are numerous rubber track variations, but some those that have proven themselves at **RoboCup Rescue** and in the real world will be examined here.

2.3.1. Tracks of custom built rescue robots

The primary locomotion system of PARS's robot Adora from Iran consists of thin rubber feet bolted to a chain drive on either side of the platform [12]. The feet were placed in U-shaped brackets that forced them to retain a curved shape as seen in Figure 2.13 (a). Supplementary tracks are driven by two separate 110W brush-less DC motors that are situated between the main drive tracks. These tracks are located 10mm above the main tracks as can be seen in Figure 2.13 (b) and they serve the function of ensuring that objects underneath the platform do not hamper its movements. The tracks of the flipper arms have been constructed in a similar manner.

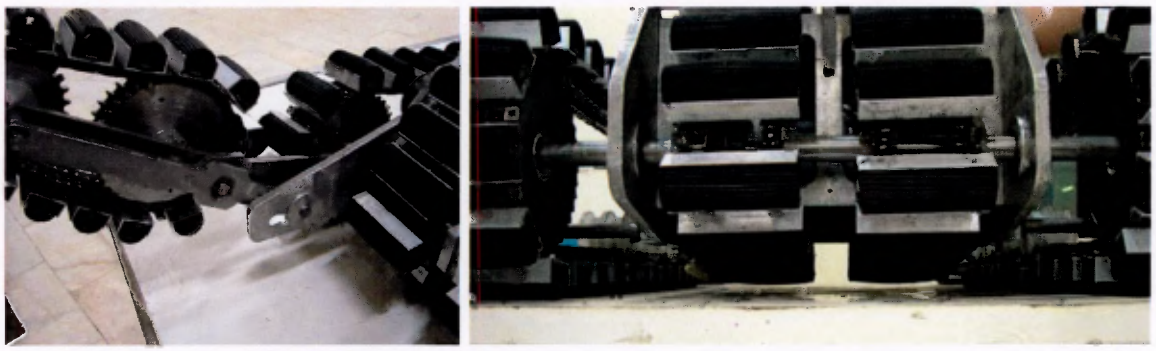

(a) A flipper track of Adora

(b) Adora's supplementary tracks sit 10mm above a horizontal terrain.

Figure 2.13.: The tracks of team PARS [12].

Very similar tracks were used by team SUCCESS from Thailand, albeit the track configuration was different [13]. The robot only had one pair of main tracks and they were significantly wider than those of Adora. The length of the teeth was uniform along the width of each track. SUCCESS' tracks are displayed in the Figure 2.14.

Figure 2.14.: SUCCESS demonstrating its ability of ascending and descending complex terrain [13].

Wide tracks with an Isotropic bumping and touching Grouser pattern that consisted of small rubber bumps attached onto tracks were employed by NuTech-R4 from Japan [14]. The main tracks had four distinct rows that contain bumps, of which the two outermost rows had large bumps and the two innermost rows had small bumps [14]. The flipper tracks employed two rows of small bumps for traction. NuTech-R4's track profile can be seen in Figure 2.15.

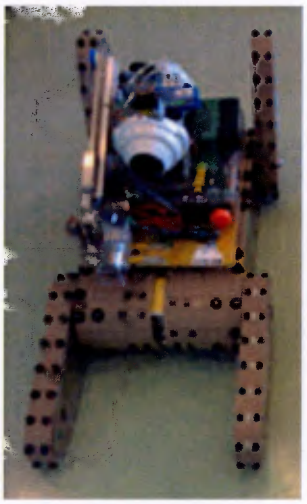

Figure 2.15.: Tracks of Japan's NuTech [14].

Quince and Kanaf are rescue robots developed by Pelican United and like NuTech-R4 they make implemented wide drive tracks. These tracks had three distinct rows of rectangular rubber feet. The outermost row consisted of the largest and widest teeth and the two innermost rows had the smallest teeth. The track profile and configuration of both rescue robot models can be seen in Figure 2.16.

(a) Quince travelling over a stepfield. (b) Kanaf manoeuvring over a stepfield.

Figure 2.16.: The Track profiles of Pelican's Quince and Kanaf [15],[16].

2.3.2. Tracks of commercial robots

In general it can be seen that only robots with wide tracks utilised varying feet sizes and multiple feet rows, whereas rescue robots and commercially available **UGVs** with thinner tracks that were situated close to the ends of the platforms, applied tracks with uniformly sized cleats that were arranged in a uniform pattern, as seen in Figure 2.17.

(a) The IRobot® 110 FirstLook [17]. (b) The 710 Warrior from IRobot® [18].

Figure 2.17.: Cleated tracks of IRobot UGVs.

IRobot's PackBot uses streamlined tracks with rounded cleats seen in Figure 2.18 to minimise detracking for both the main platform locomotion system and the flippers [9]. The tracks grant the PackBot high manoeuvrability through both rough and complex terrain.

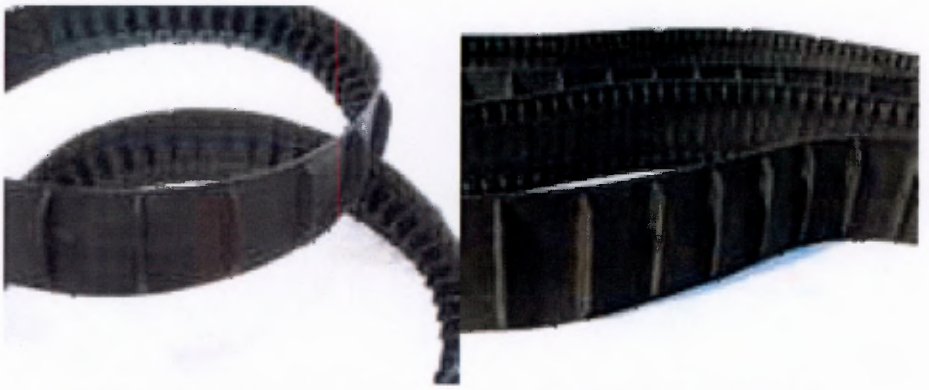

(a) PackBot's flipper tracks. (b) PackBot's main tracks.

Figure 2.18.: The PackBot's flipper tracks and main tracks [9].

2.4. Platform Sensors

While controlling the robot, camera views may not be enough when it comes to relating positional information of flippers and the attitude of the platform. An intuitive display of the robot's attitude and the positions of the flippers are vital and for this reason many teams use sensors that allow them to gain such information about their robots.

2.4.1. Shaft Encoders

Shaft encoders translate the rotary information of a revolving shaft into digital or analog signals. This data is then used to determine the angular speed, angular position and/or the direction of rotation of a shaft. This information can in turn be used to determine the speed and the displacement of a mobile robot.

Germany's Hector Darmstadt, like other **RoboCup Rescue** teams, used quadrature encoders to attain rotational information about their robot's motors. The team experienced the typical encoder errors described above. Readings from an **I**nertial **M**easurement **U**nit (**IMU**) as well as a digital compass were used in conjunction with encoders to attain odometry and compensate for encoder errors. [2]

AriAnA_AVA employed Maxon Gearhead DC motors that were coupled to Agilent's HEDL 5540 absolute optical shaft encoders, one of which is displayed in Figure 2.19. The encoders were connected to Maxon EPOS controllers that sent the encoder data to the motherboard via a **C**ontroller **A**rea **N**etwork (**CAN**) interface [19]. The data was then used to calculate the robot's position, velocity and acceleration.

Figure 2.19.: Agilent's HEDL 5540 quadrature encoder [20].

2.4.2. Inertial Measurement Unit

IMUs are routinely used to perform navigation and localisation through the acquisition of attitude and heading [2]. The sensors normally found inside such a device are accelerometers and gyroscopes. A digital compass/magnetometer is often present.

Pitch, roll and yaw data can be used to detect if a robots is tilting so much that it is on the verge of tipping over. A 3D model that shows the roll, pitch and yaw of the robot can be created. This is useful, as the operator can confirm the robot's attitude visually, which often takes much less time, and is more intuitive than reading the separate numerical values and trying to make sense of them, while simultaneously navigating the robot. A simple 3D model of Iran's team PARS is depicted below.

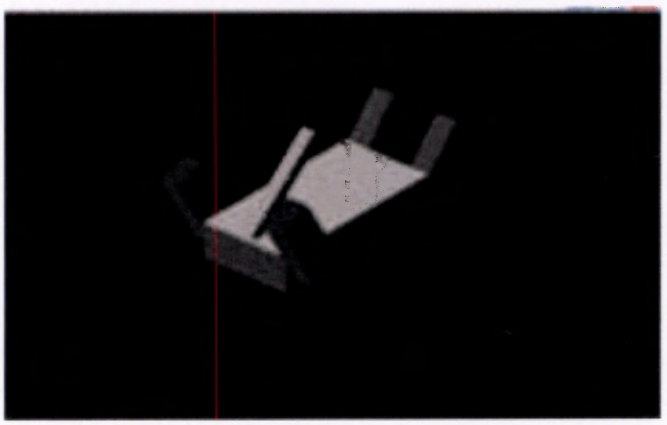

Figure 2.20.: Team PARS' 3D model of their robot [12].

In 2009 FH-Wels from Australia employed the Xsens MTi **IMU**, depicted in Figure 2.21, to attain their rescue robot's attitude, which was used for the calculation of distance of the laser scanner [21]. The collected data was then transmitted either via USB or RS232 to a wireless **l**ocal **a**rena **n**etwork (LAN) router and then to the operator station, where data processing took place. The displacement travelled was attained through the double integration of the acceleration readings.

Figure 2.21.: The MTi IMU from Xsens [22].

2.5. Motion Control

Another property that is important to a rescue mission is the ability to adequately traverse the debris filled areas of a collapse site, which strongly relies on an adequate control system [23] .

Discrepancies in velocity, position and motor torque are as a result of the disparities of load conditions caused by the terrain. Slopes, rubble and debris can lead to rapidly varying load conditions which intensify as the complexity of the terrain increases. An additional factor that results in deviations is that no two motors are exactly the same. Differences in internal friction could for example result in one motor requiring more power to rotate a required amount at any given scenario than the other. [24]

Motion control systems are designed to compensate for actuator errors and allow adequate motion capabilities. They come in one of two categories, either open-loop or closed loop. Open loop control implies that signals can be sent to the motor to set a desired output, but the input signal to the controller is not influenced by the motor's actual output. Thus the inaccuracy of the system can be substantial and errors accumulate over time. In contrast to open-loop systems, closed-loop systems use measurement data of the output variables to correct for deviations in the desired output.Although this control method can be more complex and expensive than its counterpart, it is also more accurate, ensures that a task is adequately achieved and eliminates the low level control that the operator has to continuously oversee. The most common control methods used, namely **P**, **PI** and **PID** control, are described in the subsequent sections.[24]

2.5.1. Proportional Controller

A proportional controller works by sending the proportion of the difference between the actual position and the set point, i.e. the error, to the plant, i.e. the motor [25]. It increases the overshoot and decreases the steady state error as well as the rise time. It can also decrease the settling time slightly. Its proportional gain (**Kp**) is multiplied by the error in order to adjust

the response. The increase in gain causes the stability of the system to decrease, seeing that a small error could cause a large response, until the system becomes unstable [24]. On the other hand, a small gain would cause the system to approach the set point slowly, seeing that a large error would result in a small response [25]. If the gain were increased by a substantial amount, the system would become unstable and end up oscillating around the set point. Essentially when using a proportional controller, one needs to determine compromise between overshoot and stability, since stability and overshoot are inversely proportional.

2.5.2. PI Controller

In order to remove the offset of a proportional controller, integral action can be applied in addition to the proportional action [25]. A controller that does this is known as a **P**roportional-**I**ntegral (**PI**) controller. It works by sending a proportion of the error in addition to the integral of the error to the motor. It has an integral gain (**Ki**) and a proportional gain (**Kp**) and increases both the overshoot and settling time, while it decreases the rise time and improves the steady-state error [24]. The rate at which the overshoot is reduced is proportional to the size of the error [25]. If this rate is too fast, then overshoot occurs; if this rate is too slow, then the system will respond too slowly. Such controllers can reduce the system's stability and can lead to oscillations about the set point.

2.5.3. PD Controller

A **P**roportional-**D**erivative (**PD**) controller works by sending a proportion of the error in addition to the derivative of the error to the plant. It has a derivative gain (**Kd**) and a proportional gain (**Kp**). It decreases the overshoot and improves the settling time of a system [24]. It only mildly affects the rise time and steady state error. The derivative action increases the rate at which the offset is reduced and thus improves the performance of systems that require long periods of time to reach the set point [25]. The stability of a system increases with increasing derivative action, however too much derivative action can lead to instability.

2.5.4. PID Controller

A **P**roportional-**I**ntegral-**D**erivative (**PID**) controller has a proportional gain (**Kp**), an integral gain (**Ki**) and a derivative gain (**Kd**). The implementation of a **PID** controller leads to a fast rise time with no overshoot and yields no steady state error [24]. It sends a proportion of the error in addition to the derivative of the error as well as the integral of the error to the motor. The proportional part of a **PID** controller deals with the present behaviour of the plant, the integral part deals with the past behaviour of a plant and the derivative part predicts the behaviour of the plant [25]. Its relative simplicity and good accuracy makes the **PID** controller a popular choice.

2.6. Power Management System

The accurate assessment of the remaining battery capacity of a mobile robot is vital during a mission as it allows for the estimation of the remaining time a robot can stay active. A power management system additionally allows the other systems on board the robot to be monitored.

AriAnA_AVA, a team made up of members from Thailand and Malaysia, designed a power management system in 2010. This device was the only component of their **UGV** that the operator could manually switch on and off [19]. Upon being turned on the system would switch on the devices that were to be wirelessly connected to the operator station and it would test the connection. A **l**ight **e**mitting **d**iode (**LED**) would blink if something went wrong during this testing procedure. After a successful wireless connection was established the operator could send instructions to the power management system to turn off specific devices on the platform.

2.7. Concluding Remarks

In the previous development, the mechanical structure of the platform was developed and accommodation for various electronic and electromechanical components was made available. However, the platform is not sufficiently developed to traverse any of the the **RoboCup Rescue** arenas in an adequate manner. The following aspects were considered absent or inadequate and required further development :

1. Insufficient traction.
2. No position control.
3. No current sensing.
4. The power system needs more control.
5. No control over lights.
6. Estimation of battery charge is needed.
7. No way of determining the charge left in the batteries.
8. Inadequate **G**raphical **U**ser **I**nterface (**GUI**) .

The systems listed above are considered the most essential for the platform to be able to sufficiently compete at **RoboCup Rescue** and to traverse real disaster zones, but other areas can also be improved.

Desired features can now be defined using the information attained in this chapter about the environment of the **RoboCup Rescue** competition, the capabilities of the **Ratel** platform and current technological trends. The following chapter focuses on the performance traits of the platform's systems and presents the validations behind each decision.

3. Performance Specifications

Table 3.1.: List of Primary Specifications of the Platform.

Location	Performance Specification	Value
Physical Specifications		
3.1.1.1	Height added by track feet.	< 10mm
3.1.1.2	Weight of the tracks .	< 3kg
Functional Specifications		
3.1.2.1	Straight line speed.	1.4m/s
3.1.2.2	Maximum rotational flipper speed	≥9 rpm
3.1.2.3	Shock absorption	Yes
3.1.2.4	High level of Traction	Yes
3.1.2.5	Multiple rows of feet on drive tracks	≥2 Rows
3.1.2.6	Ascending and descending of inclined planes	≥30°
3.1.2.7	Ascending and Descending of stairs	Yes
3.1.2.8	Supply Voltages	5V, 12V, 18V, 36V
3.1.2.9	Switching on and off of voltage lines	Yes
3.1.2.10	SOC estimation of the batteries.	Yes
3.1.2.11	Primary Communications Protocol.	I2C
3.1.2.12	Wireless Communications Protocol	802.11A
Control & User Interface		
3.1.3.1	Speed control of the main tracks and flippers.	Yes
3.1.3.2	Position Control of the flippers.	Yes, accuracy ≤1°
3.1.3.3	User Interface	Intuitive, joystick controller
3.1.3.4	Media Streaming	Real time video and sensor data streaming

Location	Performance Specification	Value
3.1.3.5	3D platform model	3D representation of the platform and the
3.1.3.6	Software used for running system	LabVIEW

Chapter 2 demonstrated the pertinent aspects of the **RoboCup Rescue** arenas as well as some of the required systems that were absent in the previous development of the platform. The chapter further displayed some of the existing solutions of these systems used by teams and by commercial **UGVs**. Drawing from the information that was delivered, it is possible to define the primary specifications, contained in Table 3.1, that will guide the further development of **Ratel's** platform. The system specific specifications will be displayed as each system is discussed in detail in upcoming chapters.

3.1. Justification and Description of Specifications

3.1.1. Physical Specifications

3.1.1.1. Height added by Track Feet

The platform was designed to be able to drive through a 24" equilateral triangle [11]. The feet of the tracks should therefore not be too high and jeopardise the platform's ability to drive through this triangle.

3.1.1.2. Weight of the tracks

The robot should be man portable [11], making it crucial to minimise the amount of extra weight that is added to the tracks through the addition of the feet.

3.1.2. Functional Specifications

3.1.2.1. Maximum Straight Line Speed

The straight line speed of the platform on a level, flat surface was specified by MSc student Eugene Dreyer to be 1.4m/s. The reasoning behind this decision was that since the robot is meant to replace a human disaster responder, it does not need to be able to move faster than a human's walking pace, which is approximately 1.4m/s [11].

3.1.2.2. Maximum Rotational Flipper Speed

During the initial development of the project, before the implementation of a control system, the flippers would be manually controlled by a user. For this reason, a maximum rotational flipper speed was chosen, since a value larger than this would be too fast for the user to manually control adequately. This could lead an operator to move the flipper past the intended value by mistake. The ability of the user to manually control the flippers can be considered to be an added feature and could be useful during debugging.

3.1.2.3. Shock Absorption

The platform is meant to be able to function in rough terrain, yet it has no suspension system to speak of and thus lacks shock absorption capabilities. While driving over complex terrain the camera feed will be very shaky and the lack of suspension may lead to high impact between the platform components and its environment. The ability to make the ride smoother should decrease the shakiness of the video feed as well as improve the operational life of the overall system.

3.1.2.4. High Level of Traction

After several tests it was concluded that the traction provided by the tracks of the previous development on the platform was insufficient. The traction of the tracks needs to increase, especially when one considers the slippery terrain that one could encounter in a real rescue situation, such as a wet floor.

3.1.2.5. Multiple Rows of Feet on Drive Tracks

It is a common to find debris scattered outside and inside a collapsed structure. Naturally it is an advantage when the debris hinders the mobility of a rescue robot as little as possible. While traversing debris-filled terrains items of such a site can get stuck underneath the robot's underbelly and hinder its movement. Feet with the specific function of preventing this from occurring should be present.

Just as important as preventing debris from getting jammed underneath the **UGV** is circumventing the robot from getting stuck on large obstacles, structural components or debris. Even though the platform's four flippers should prevent this, rare scenarios where the platform could be positioned in such a way that the flippers have no or insufficient contact with the terrain, or were the terrain is very loose or filled with loose debris that prevents the flippers from adequately removing the platform from a beached position were considered. The addition of an inner row of feet is a second layer of beaching prevention and this should add to the platform's ability to remove itself from a beached scenario.

The platform is susceptible to both of these problems, especially because it employs such wide tracks.The addition of more than one row on the drive tracks therefore has two purposes. The outermost rows will be the rows that the platform would drive on during regular driving operations and will be more suitable to turning than having a row of feet along the entire width

of the tracks. The innermost row should have shorter teeth that do not make contact with the terrain, especially during turning, and would reduce the platform's possibility of getting beached and would additionally prevent debris from getting stuck underneath it.

3.1.2.6. Ascending and Descending of Inclined Planes

The complex environments of urban collapse sites include a variety of challenges for rescue robot, one of which are inclined planes of varying degrees. **UGVs** working in such areas should have an adequate maneuverability that allows them to climb slopes, preferably of up to 45° and additionally to turn and change direction on them. Having this capability on slopes with larger incline angles would be an added bonus. Descending those slopes in a controlled manner without slipping is just as important.

Aside from the robot's motors, gearing and mechanical configuration, the tracks play a great role in its ability to meet the level of slope maneuverability that is desired. The right choice in material and shape for the teeth as well as their layout on the tracks will determine the robot's slope climbing abilities.

3.1.2.7. Ascending and Descending of Stairs

Seeing that urban environments, even those of collapsed buildings, contain stairs and step like obstacles, the ability to climb stairs of steps with different dimensions and turning on them increases the general maneuverability of the robot in urban disaster environments and greatly increases its overall ability to aid rescue workers. Descending stairs in a controlled manner with minimal slip is of equal importance.

As with the case of climbing inclined planes, this too is very dependent on both the material choice that is made for the feet as well as their shape and the configuration in which they are attached to the tracks.

3.1.2.8. Supply Voltages

Numerous electrical devices are housed within the robot and they require four distinct voltages to work. The batteries can produce only a part of the voltage requirements. Making all needed lines available and making sure that the current requirements are met is essential.

3.1.2.9. Switching on and off of Supply Voltages

The operator should be able to switch the four voltage lines on and off. This allows the resetting of devices remotely and is a useful tool when debugging.

3.1.2.10. State of Charge Estimation

The State of Charge (**SOC**) estimation will be a good indicator of the amount of time that the rescue robot still has available before the batteries go flat. This allows the operator to

return the robot to the operator station so that depleted batteries can be charged or replaced. This property is of great importance, seeing that retrieving a robot from the field is virtually impossible when its batteries have depleted, because the environment is too dangerous.

3.1.2.11. Primary Communications Protocol

The primary communications protocol was selected by MSc student Peter Henson, who developed the arm of Ratel, to be Inter-Integrated Circuit (**I2C**). It is the task of the MSc student Bradley Springer, who was responsible for the control aspect of the arm, to develop and test this communications protocol.

3.1.2.12. Wireless Communications Protocol

The **RoboCup Rescue** competition states that all teams have to use the 802.11a wireless standard. Unlike the commonly used 802.11g protocol, this wireless standard uses a 5GHz band, instead of a 2.4GHz one. This makes it less convenient with regard to signal penetration, but the 5GHz band is not used as readily as the 2.4GHz one, which minimises the chances of interference [26].

3.1.3. Control System and User Interface

3.1.3.1. Speed Control

Fluctuations in the load of the track and flipper motors can easily cause them to change their speeds. This is undesirable, especially when moving the driving tracks. Such disturbances can make the motors move at different speeds, which could for example result in the base making a turn even though the operator is directing it to go straight. Controlling a robot through complex areas is a difficult task even without such complications. Speed control is essential and needs to be implemented. The operator should additionally have the ability to change the track and flipper speed in real time.

3.1.3.2. Position Control

Position control is not particularly important when it comes to the driving tracks, but it is crucial for the flippers. The flippers are to be position controlled so they can be rotated to angles that are suitable to particular tasks, such as climbing stairs or descending slopes. Position control will also allow the flippers to retain a particular angular position even when the load in them is dynamically changing. 1° accuracy is acceptable, especially when dealing with the environment of RoboCup Rescue or that of an actual disaster site.

3.1.3.3. User Interface

The user interface should be intuitive and the learning and training before using it should take a minimal amount of time. **UGVs**, like the PackBot, are controlled with a gamepad [9] and thus an Xbox Controller should be used.

3.1.3.4. Media Streaming

During a rescue mission attaining data about the environment in real time is one of the most important properties of the robot. The real-time streaming of video footage and other sensors will allow the operator to react to events appropriately and in time [2].

3.1.3.5. 3D Robot Base Model

A 3D model of the robot base will allow the user to understand the base's orientation in space and will help in the assessment of whether the robot is on the verge of tipping over. This model will also make the illustration of the flippers positions visual and thus more intuitive. Being able to see the base will take less time for the operator to process the information and increase his/her ability to react faster.

3.1.3.6. Software

The **Lab**oratory **V**irtual **I**nstrumentation **E**ngineering **W**orkbench (**LabVIEW**) developed by **N**ational **I**nstruments (**NI**) was specified by **RARL** as the primary software package to be used for interfaces, embedded programming and communications throughout the **Ratel** rescue robot.

4. Overall System

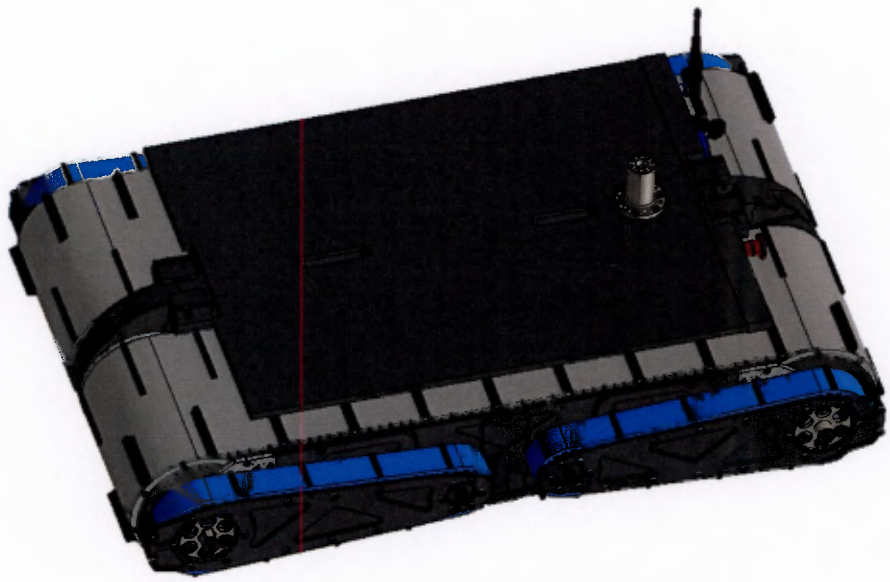

Figure 4.1.: The final platform assembly.

Figure 4.1 above illustrates the fully assembled robotic platform. The areas of the platform that required further development, as discussed in Chapter 2, were the actuation system and the caterpillar tracks. Other systems that required attention were the power supply and distribution module, as well as the system control and communications system. For a simplified analysis, the overall system was subdivided into these four modules.

The Power Supply and Distribution Subsystem

This system was made up of power regulation and distribution boards. Power was supplied to the boards either through a tether or via a set of six Makita 18V, 3.0Ah Li-ion batteries. A set of two batteries was connected in series batteries and then two of these sets were connected in parallel to produce a 36V line, with the energy capacity of 6.0Ah, as can be seen in Figure 5.3. The remaining two batteries were connected in parallel to provide an 18V line that was powered by two batteries with a total capacity of 6.0Ah.". DC/DC converters produced 12V and 5V lines from the 36V line. These lines were usually enabled, but an embedded microcontroller was used to enable and disable the lines, should the need to do so arise. Custom designed current sensor **p**rinted **c**ircuit **b**oards (**PCB**) were used to monitor the current flowing from the supply source to the components. This system also made the control over the platforms front and rear lights possible. The power supply and distribution system can be seen in Figure 4.2.

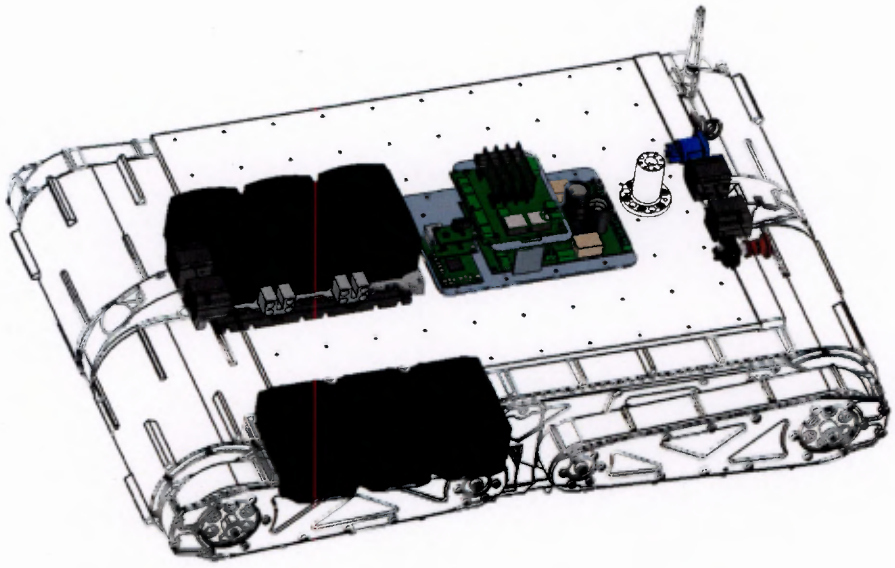

Figure 4.2.: The Power Supply and Distribution System.

The Platform Actuation System

The platform actuation system, depicted in Figure 4.3, consists of a combination of mechanical electromechanical and electronic components that have been carefully integrated to produce the desired requirements. This system was made up of the following components:

- Maxon EC40, 120W motors
- Maxon Planetary gearhead GP 42 C
- Maxon DECV 50/5 speed controllers
- Maxon Encoder HEDS 5540
- LM3S8962 embedded microcontrollers
- Optical switches
- Hall sensors

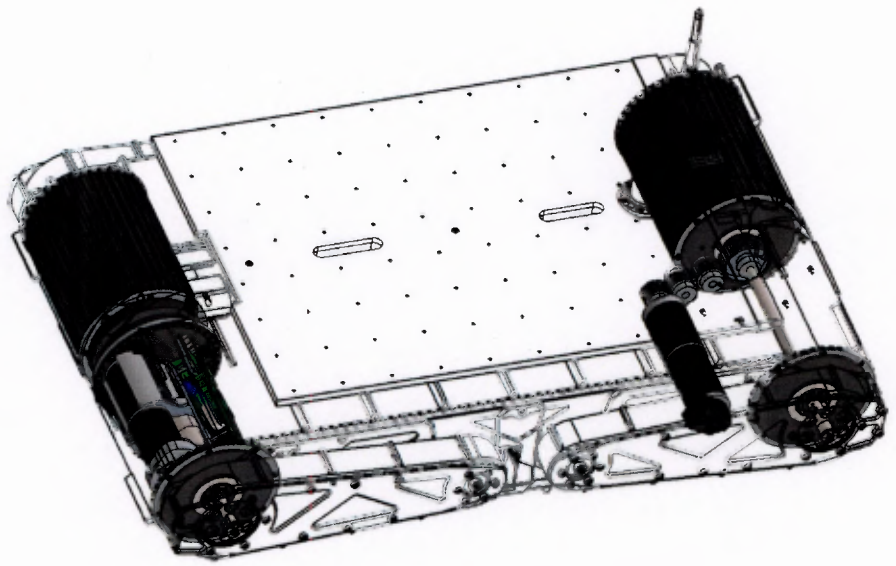

Figure 4.3.: The Platform Actuation System.

Caterpillar Tracks

The track subsystem portrayed in Figure 4.4 integrates with the sidepods and the actuation system of the platform. Its function is to provide traction as well as cushioning. Through it the front two driving pulleys move the platform and fully assembled **MRP** during its operations. The tracks consisted of **TPU** timing belts from **BELT TORQUE (PTY) LTD**. The two tracks were 170 mm wide and had 161 integral teeth on only one side. Two rows with two sets of polymer feet made from TPU sheets were glued onto the smooth side of the belts in order to increase traction.

The four flipper tracks were made up of the same timing belt material, but they were 32mm wide and had 73 integral teeth on one side. Like with the larger drive tracks, **TPU** feet were glued onto the smooth side of the flipper tracks that would make contact with the driving surface, so as to increase traction and thus mobility.

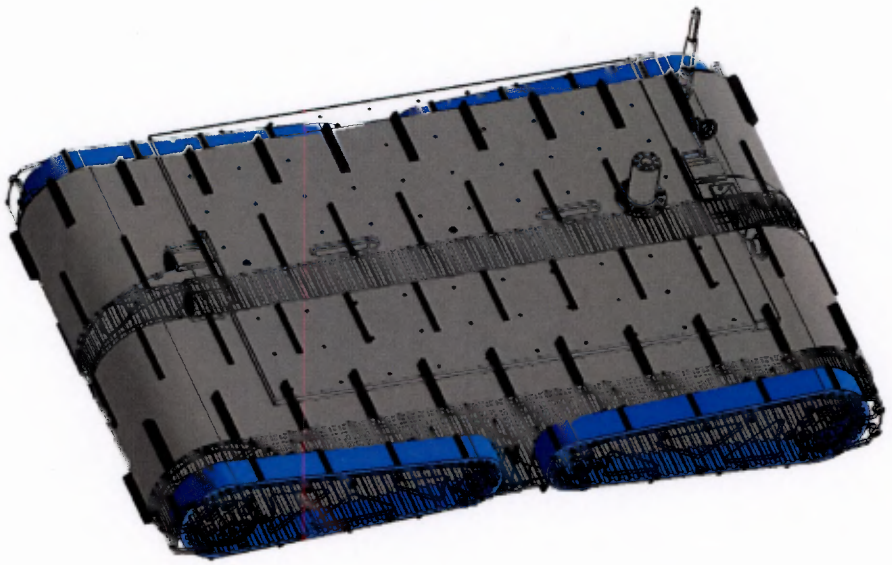

Figure 4.4.: The Caterpillar Tracks.

System Control and Communications

Wireless communications was achieved by implementing the Ubiquiti Bullet M5 wireless radios. The units provided a stable and consistent wireless link that made real time streaming of sensor data and commands available. The user interface has the following features and functionality:

1. A Xbox controller for game-like interaction with the platform
2. Real-time video feed from the front, rear and **H**igh **D**efinition (**HD**) camera
3. Current sensor information
4. Light bridge and hall effect sensor feedback to indicate the end stop of the flippers
5. Pitch, roll and yaw of the **UGV** is provided graphically in the form of a model of the platform
6. 3-Axis acceleration data and temperature indicator
7. Lighting and power board controls as well as the battery **SOC** values
8. Speed setting and indicator for drive tracks and flippers
9. Calibration and control buttons
10. Indication of established communications link

A more detailed look at the development and features of the systems discussed in this chapter can be found in the following chapters. Figure 4.5 depicts the overall dimensions of the fully assembled robotic platform.

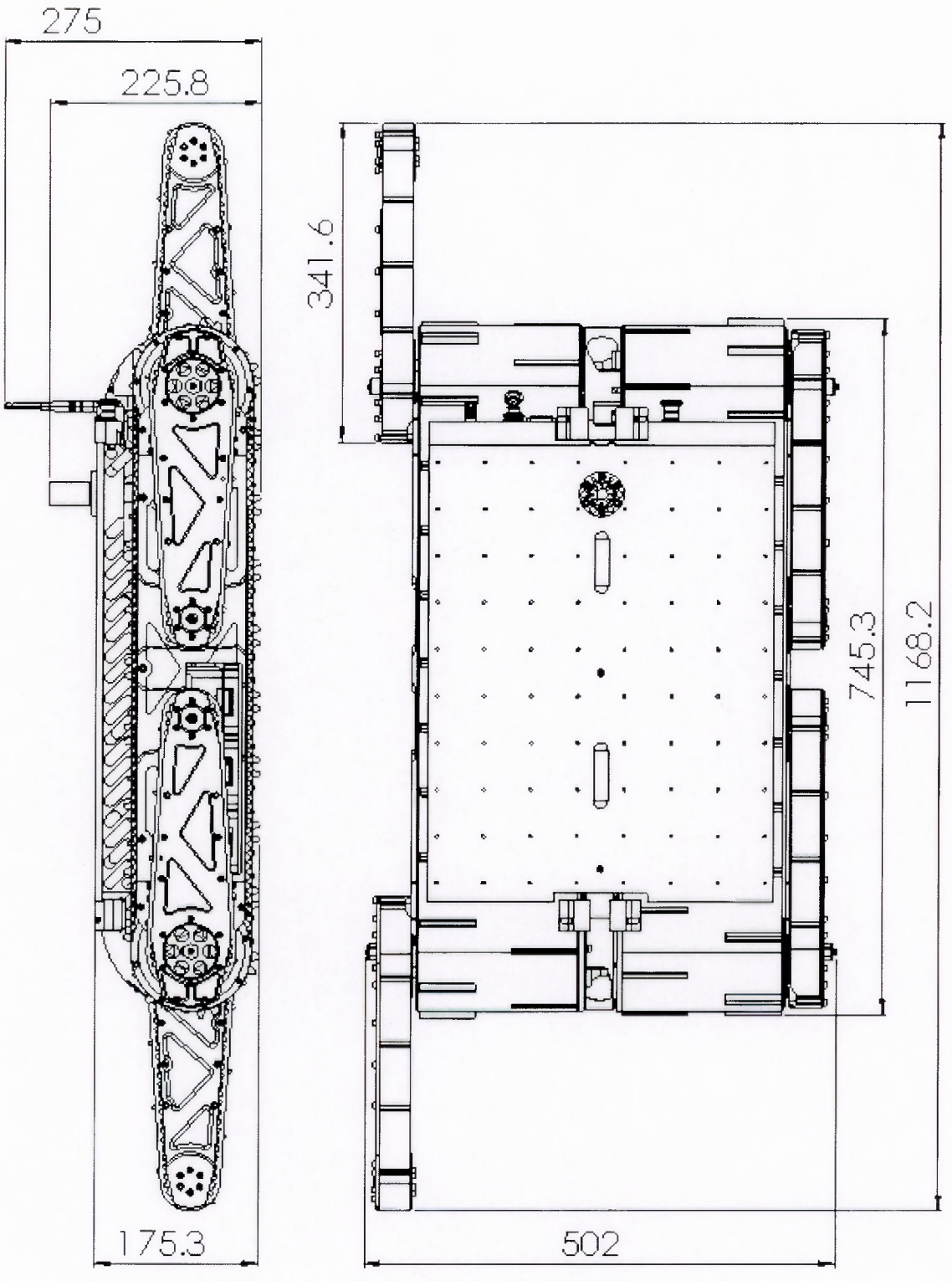

Figure 4.5.: The overall platform dimensions.

5. Power Supply and Distribution System

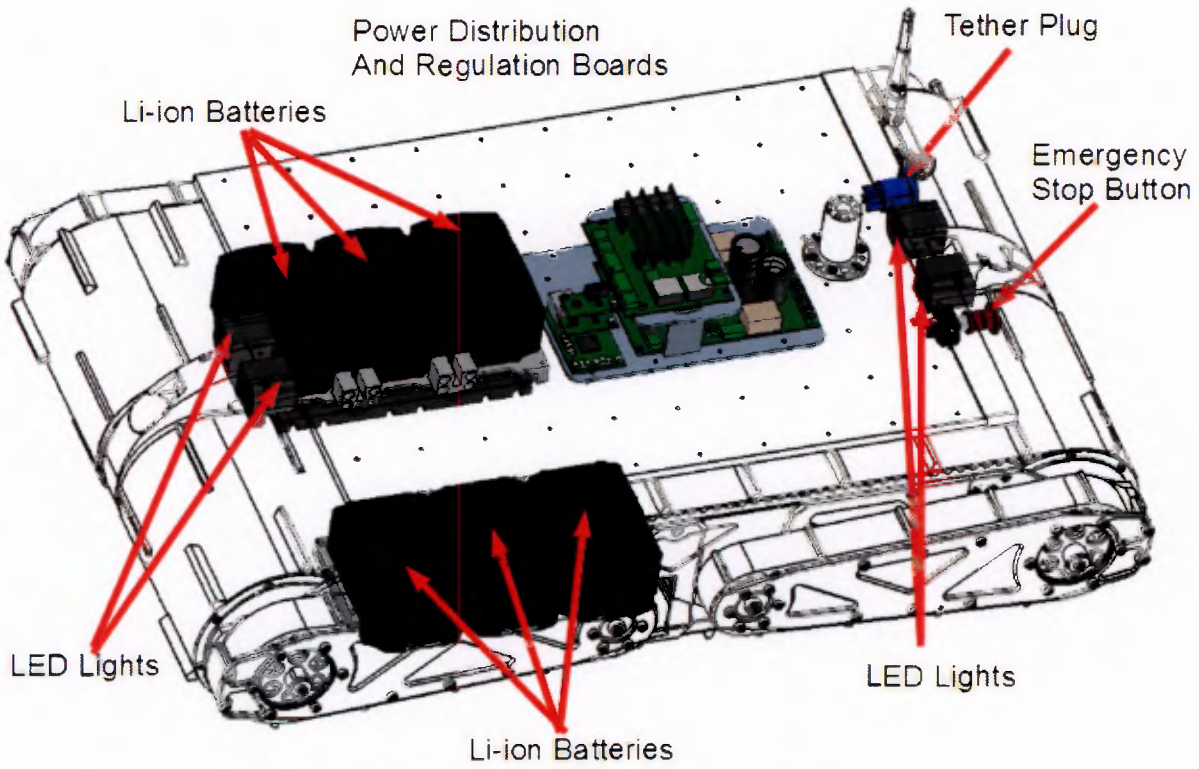

Figure 5.1.: The Power Distribution System.

In order to actuate the mechanical systems of **Ratel**, power had to be directed to various electronic and electromechanical devices. Apart from power distribution, an additional function of this system is to manage the lighting of the platform and monitor current drawn from batteries. The power supply and distribution system is highlighted in Figure 5.1. The system includes a **PCB** that takes care of the power regulation and distribution. It works in conjunction with a pair of custom designed current sensor boards and a custom designed ARM Cortex-M3 LM3S8962 embedded microcontroller. This chapter presents requirements of the systems and then shows the development that previously took place. Thereafter the changes and improvements will be briefly highlighted subsequent to which the final solution is presented.

5.1. Power Supply and Distribution Specific Specifications

The following specifications contained within Table 5.1 are derived from the primary specifications of Chapter 3. Here both essential and non-essential, but desired system requirements are presented. The table is followed by a set of validations behind each of the decisions made for this subsystem.

Table 5.1.: Power Supply and Distribution Specifications.

Location	Requirements	Desired Value
5.1.1	Dimensions	Should fit within a box of 226mmx176mmx100mm
5.1.2	Line voltages	48V, 36V, 18V, 12V, 5V
5.1.3	Current supply	up to 12A
5.1.4	Remote control voltage lines	Yes
5.1.5	Current monitoring	Current sensing of at least 10 A per line
5.1.6	Lighting	**LED** drivers for lights and **PWM** to control brightness levels
5.1.7	Interchangeable DC to DC converters	Yes

5.1.1. Dimensions

The power board requires several components to function adequately and some of them will take up a considerable amount of space, resulting in a large power board. It is thus essential to position the components in such a manner that reduces the overall space requirement, seeing that the sidepods already house a number of other systems and components. With all other devices installed, the amount of workable space that remains is a 100mmx226mmx176mm box. The side and top views of the left sidepod depicted in the next figure shows the amount of space that the power distribution board can occupy.

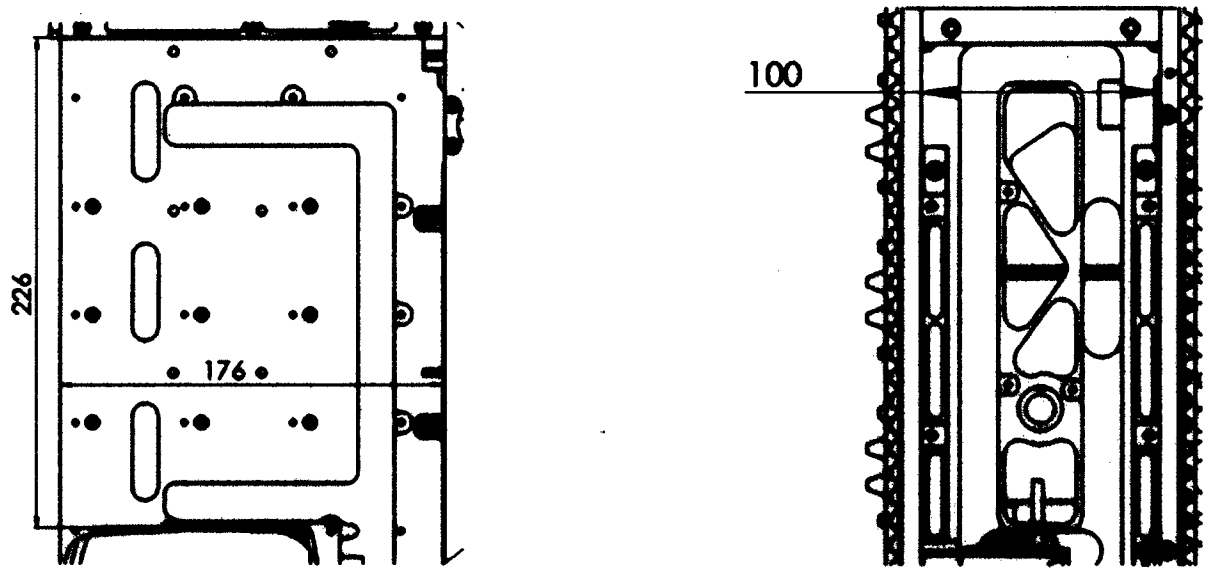

(a) Top view shows a 226mm x 176mm rectangle is unoccupied.

(b) Side view shows that 100mm is unoccupied.

Figure 5.2.: The side and top view of the left sidepod depicting the amount of free space left for the power distribution board.

5.1.2. Line Voltages

The systems of the platform and the rest of the rescue robot require 36V, 18V, 12V and 5V to function. The 48V is needed for the RouterStation Pro, the wireless radios chosen by Eugene Dreyer.

5.1.3. Current Supply

During operation the rescue robot consumes a generous amount of current. It was estimated that at absolute maximum power consumption the required amount of current would be in excess of 30A. However, this could not be supplied because not enough batteries could be stationed within the robotic platform, as a result of its space restrictions.

5.1.4. Remote Control of the Line Voltages

Having the ability of switching the line voltages on and off adds to the versatility of the robot and is advantageous during debugging. All lines except the 48V line should have this feature, seeing that the 48V line, which is intended for the RouterStation Pro, should always stay on for uninterrupted communications.

5.1.5. Current monitoring

Current monitoring of the batteries enables the operator to verify the correct operation of the power supply system and is useful during debugging. An added benefit of having this capability is using it to estimate the **SOC** of the batteries, which allows one to gauge the remaining operating time of the rescue robot.

5.1.6. Lighting

The lighting system is an essential part of Ratel's platform, especially when operating it under sub-optimal lighting conditions. Furthermore, a method of switching the **LEDs** on and off, as well as controlling their brightness was left unsettled in the previous development of the system.

5.1.7. Interchangeable DC to DC Converters

The converters, used to create the 12V and 5V, are essential and thus it would be advantageous to be able to replace them quickly, should one of them fail.

5.2. Previous Development of the Power Distribution System

In the previous development of the **UGV**, it was determined that the necessary voltage lines to power the fully assembled rescue robot were 36V, 18V, 12V and 5V. **Ratel** had two methods of delivering power to its devices, namely tethered and battery power. In tethered operation a power supply would be used to deliver the required power to the platform. During untethered teleoperation six Makita 18V BL1830 Li-Ion LXT 3.0Ah batteries were meant to produce the required power.

A prerequisite was to have a sufficient energy capacity and thus the two batteries were used to supply power to the 18V components were wired in parallel to increase the energy capacity from 3.0Ah to 6.0Ah. The remaining four batteries were used for the 36V line and for the same reason of doubling the energy capacity; they too were wired in series. The end result for the 36V line was two sets of batteries wired in series and in parallel, which produced a 36V line capable and had a maximum energy capacity of 6.0Ah. This battery configuration of the 18V line and that of the 36V line are portrayed in Figure 5.3.

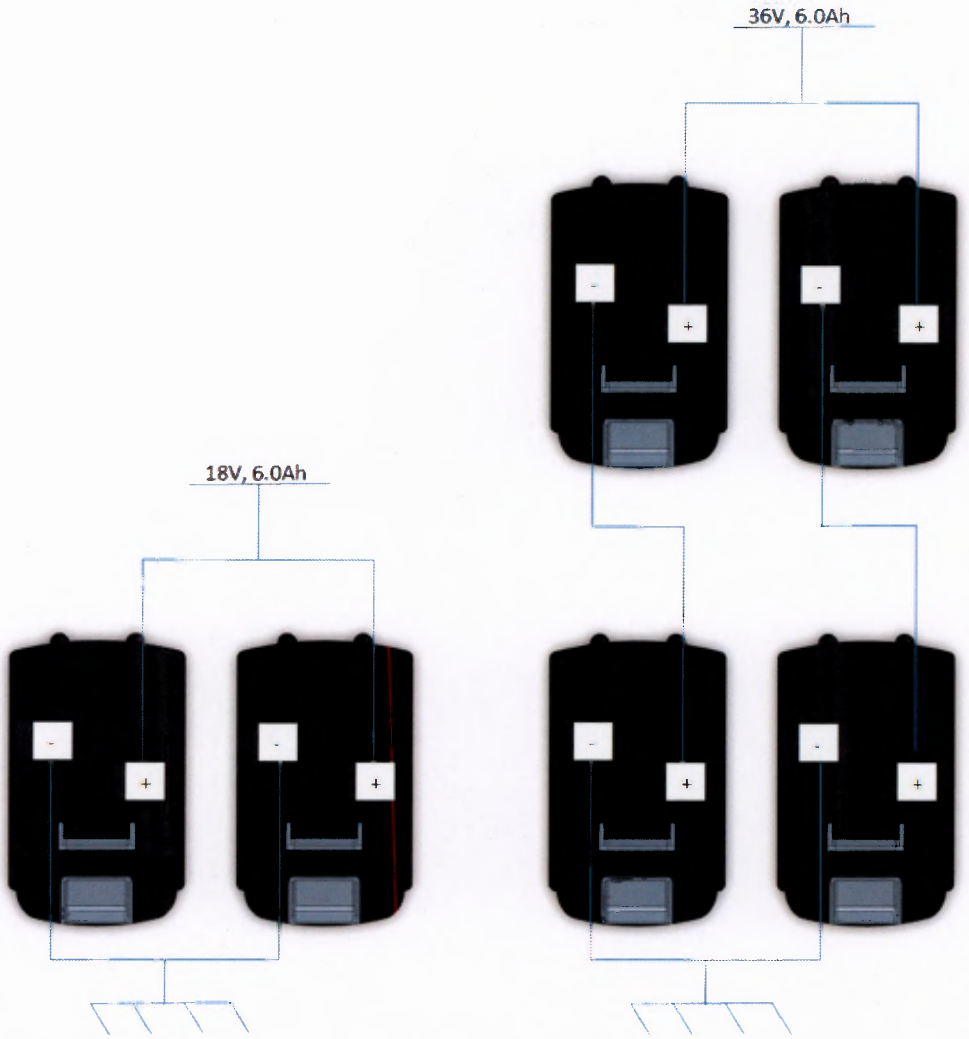

(a) The battery configuration of the 18V line. (b) The battery configuration of the 36V line.

Figure 5.3.: The battery configuration.

A **PCB** designed to handle the power regulation of the overall system was developed to fit in a sidepod. It facilitated connections to the electronic devices that required the four voltage lines. The 36V line was used to produce both the required 12 and 5V lines. Two 40W Mean Well and a single 15W Mean Well DC/DC switching power supplies produced the 12V and the 5V lines receptively. A single DC/DC converter was used to produce a single line, thus there were two 5V lines and two 12V lines. The converters input voltage range is between 18V and 36V and since a set of fully charged batteries connected in series could have a voltage of up to 41V, this board could not be used for wireless teleoperation. An emergency stop button worked by toggling the state of a set of **S**ingle **P**ole **S**ingle **T**hrow (**SPST**) relays that connected the supply power to the rest of the devices on the board. **S**ingle **P**ole **D**ouble **T**hrow (**SPDT**) relays were used to switch between battery power and tether power. The **PCB** is represented in Figure 5.4. The board offered the bare essentials for running Ratel under tethered power, but some essentials were outstanding and thus a new board had to be developed.

Figure 5.4.: The previous power distribution board developed by Eugene Dreyer.

5.3. The New Power Regulation and Distribution System

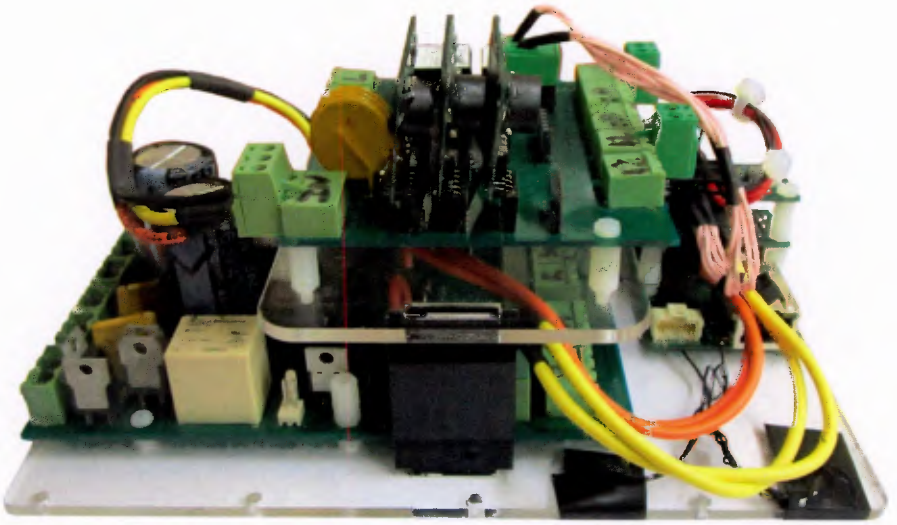

Figure 5.5.: The completed power distribution board.

A new power regulation and distribution **PCB** had the purpose of achieving the specifications contained in Table 5.1. This section will briefly explore the development and feature of the power regulation and distribution board depicted in Figure 5.5.

The relay and battery configurations were not changed from the previous version. Adding extra functionality to the board would also increase its footprint. An effort had to be made to reduce the size of the components as much as possible, because of the limited space available within the body of **Ratel's** platform. Another feature that required attention was that the 5V line in the previous generation board only had a power rating of 15W, which was not sufficient.

In the previous generation, the 36V and 18V lines were connected directly to the battery supply, however, several other things where changed. The new DC/DC converters, the Mean-Well NID60 boards, supplied more current, had a smaller footprint, included remote control functionality and had a higher supply voltage of 20V-53V. A single NID60 5V converter had a rated output power of 20W, while a single 12V converter had one of 48W. Having two for each power line doubled the rated power capabilities of the 5V and the 12V lines to 40W and 96W respectively. An added feature was that these boards were removable from the power board and could be easily replaced in case of failure. These converters had a remote control pin that permitted the remote toggling of the output line. Their size allowed four of them to be placed next to each other, while keeping the overall footprint small. A NID60 board is depicted in Figure 5.6 and its dimensions can be seen in Figure 5.7.

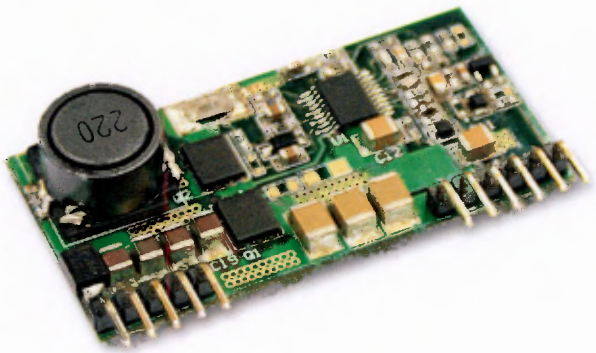

Figure 5.6.: A NID60 DC/DC converter [3].

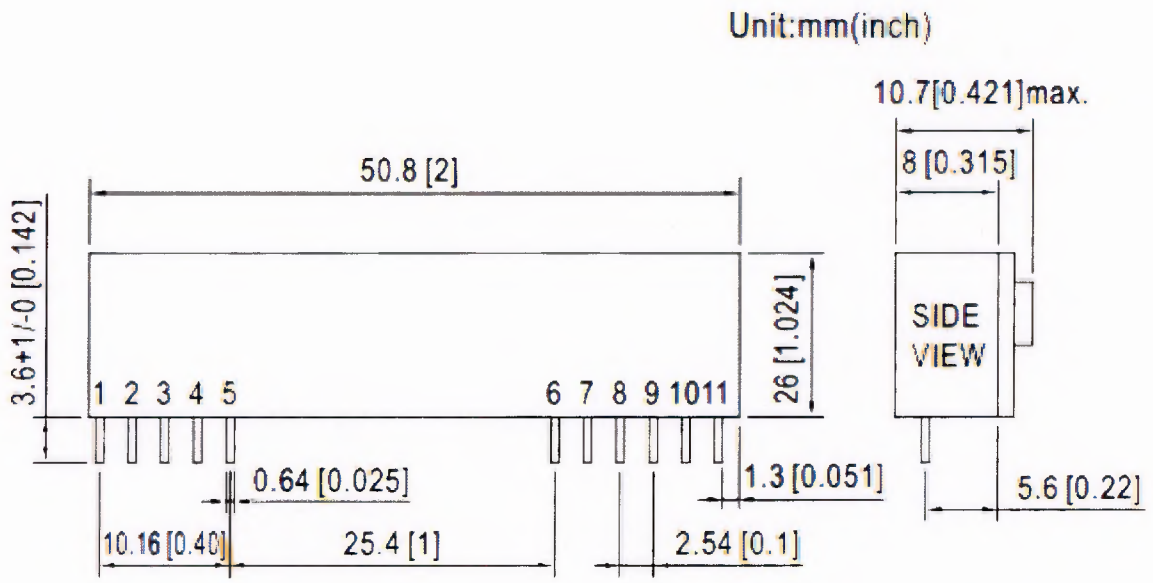

Figure 5.7.: Dimensions of the NID60 Converter [3].

The switching on and off of the 36V and 18V line was achieved through the implementation of a **Metal-Oxide-Semiconductor Field-Effect Transistor (MOSFET)** and **bipolar junction transistor (BJT)** circuit. A **transistor-transistor logic (TTL)** control signal was sent to the transistor, which in turn toggled the state of a set of three **MOSFETs** that controlled the flow of current through a voltage line.

The fuses that were used in the previous power board to protect the batteries from overcurrent were large and took over a minute to trigger, which was considered too long. In the board's second iteration, **polymeric positive temperature coefficient resettable fuses (PPTC)** were implemented, because of their small size and the added feature of them automatically resetting themselves once the fault condition was removed.The PTCs were rated for 6A and one PTC was connected in series to a pair of batteries that were also connected in series. Thus the overall current was limited to a maximum of 12A for both the 36V line and the 18V line. The batteries had internal fuses that were rated at 7.5A and therefore the PTC rating of 6A was chosen, so that the current would be limited before the internal fuses could blow and render a battery useless. An additional method of protection came in the form of diodes that were connected to terminals of each battery to prevent reverse current flow and to protect the batteries in case they were connected the wrong way around. Two LUXdrive 3021 BuckPuck **LED** power modules powered the two sets **LEDs** at the front and the rear of the platform. The 18V line powered the **LED** drivers and a microcontroller sent a **pulse width modulation (PWM)** signal to control the brightness of the **LEDs**.

As a result of space restrictions of the sidepods, the power board had to be made up of two separate boards. The larger board, depicted in Figure 5.13, takes in the supply voltages and produces multiple output pins for them. It also creates the 48V line that was initially needed for the Ubiquiti RouterStation Pro wireless radios. All battery protection and relays are soldered on to this board. Figure 5.11 depicts the board's EAGLE CAD model. The second and smaller of the two boards, depicted in Figure 5.10, contains the NID60 converters and the BuckPuck **LED** drivers. In order to control the voltage lines and the light, a LM3S8962 embedded microcontroller board was designed. Figure 5.12 illustrates features and shows what is plugged into its connector, while its EAGLE CAD model is depicted in Figure 5.14. The features and development of the board that was used is found in the following section. The configuration of the system, including the microcontroller and the current sensor can be viewed in Figure 5.8. Figure 5.9 illustrates how the power boards fit in the sidepod.

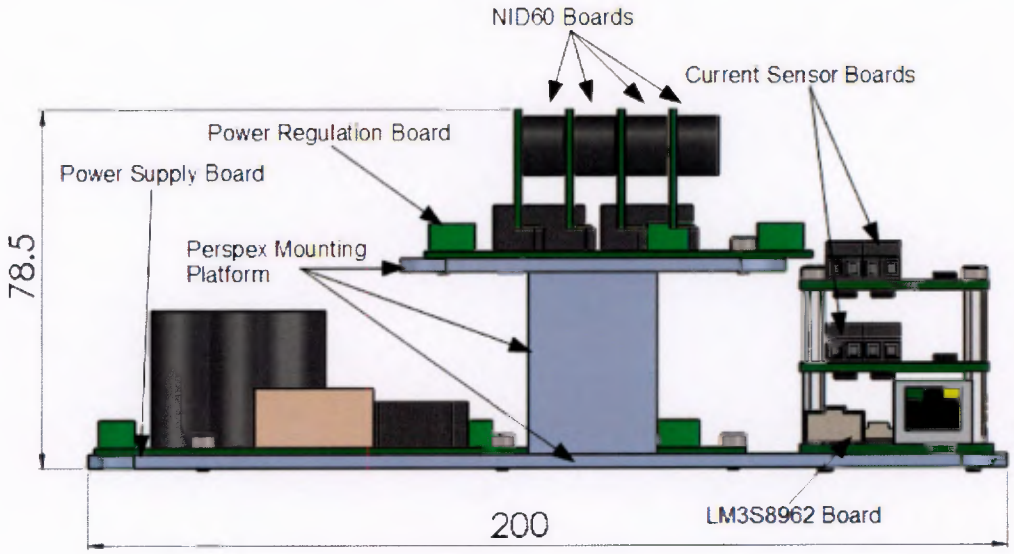

Figure 5.8.: The boards stacked on top of each other.

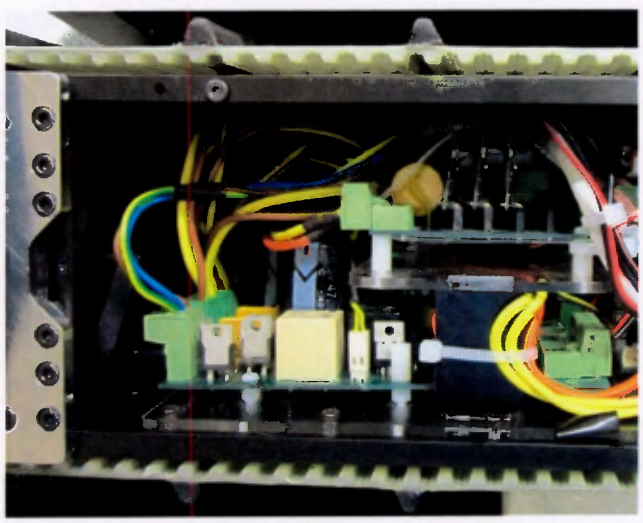

Figure 5.9.: The power board inside the left sidepod of the platform.

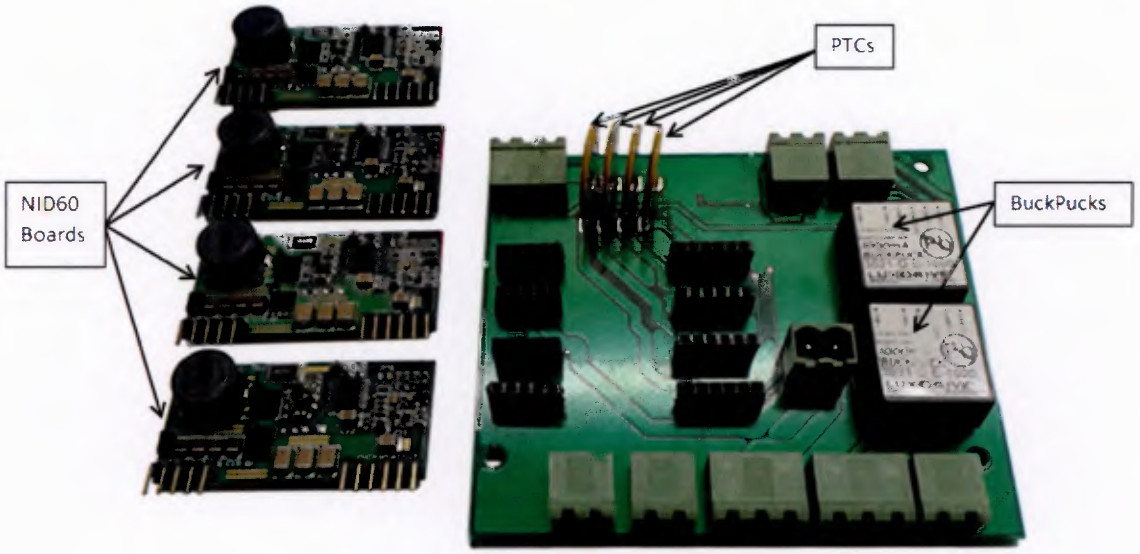

(a) The top PCB and the NID60 boards.

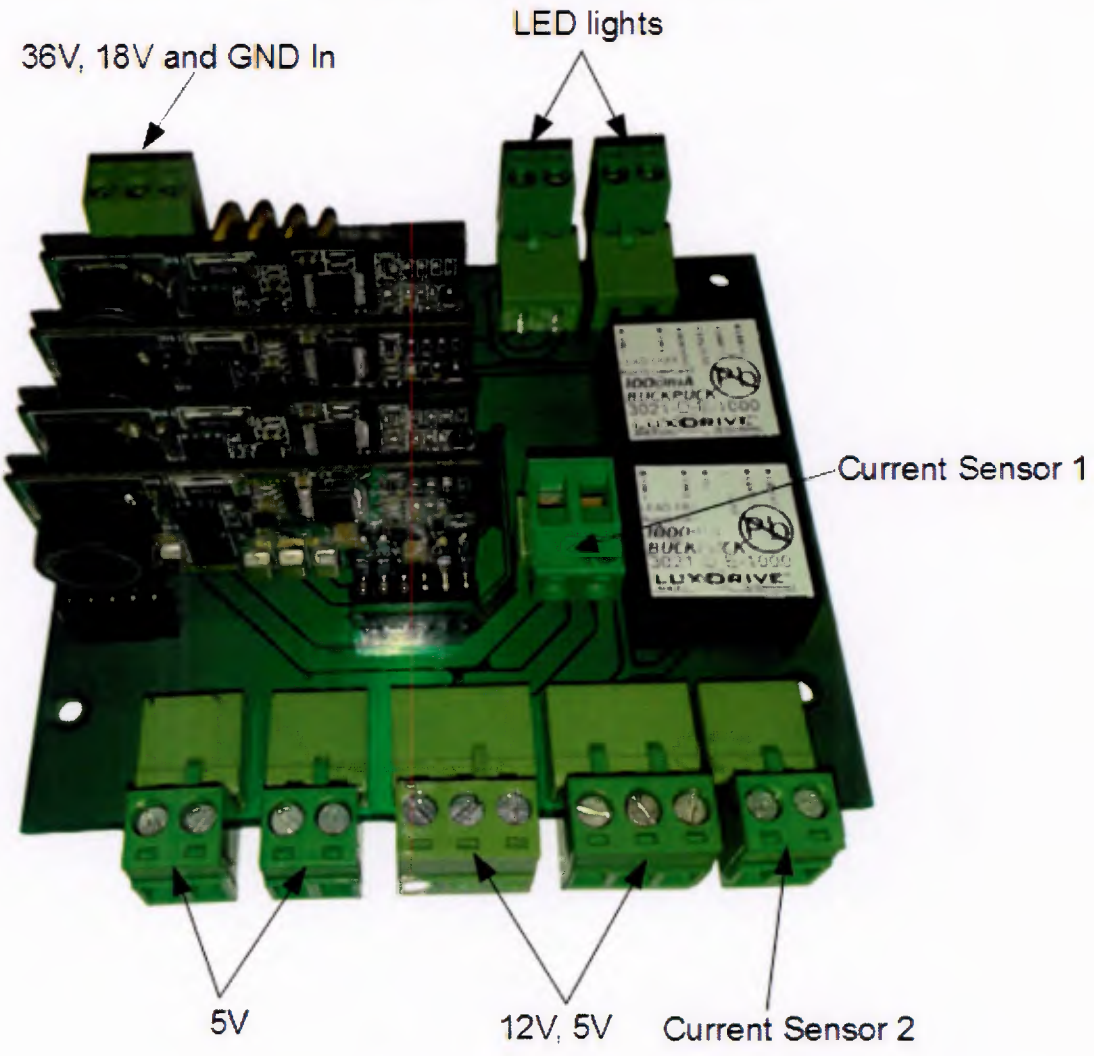

(b) The assembled top board.

Figure 5.10.: The regulator board.

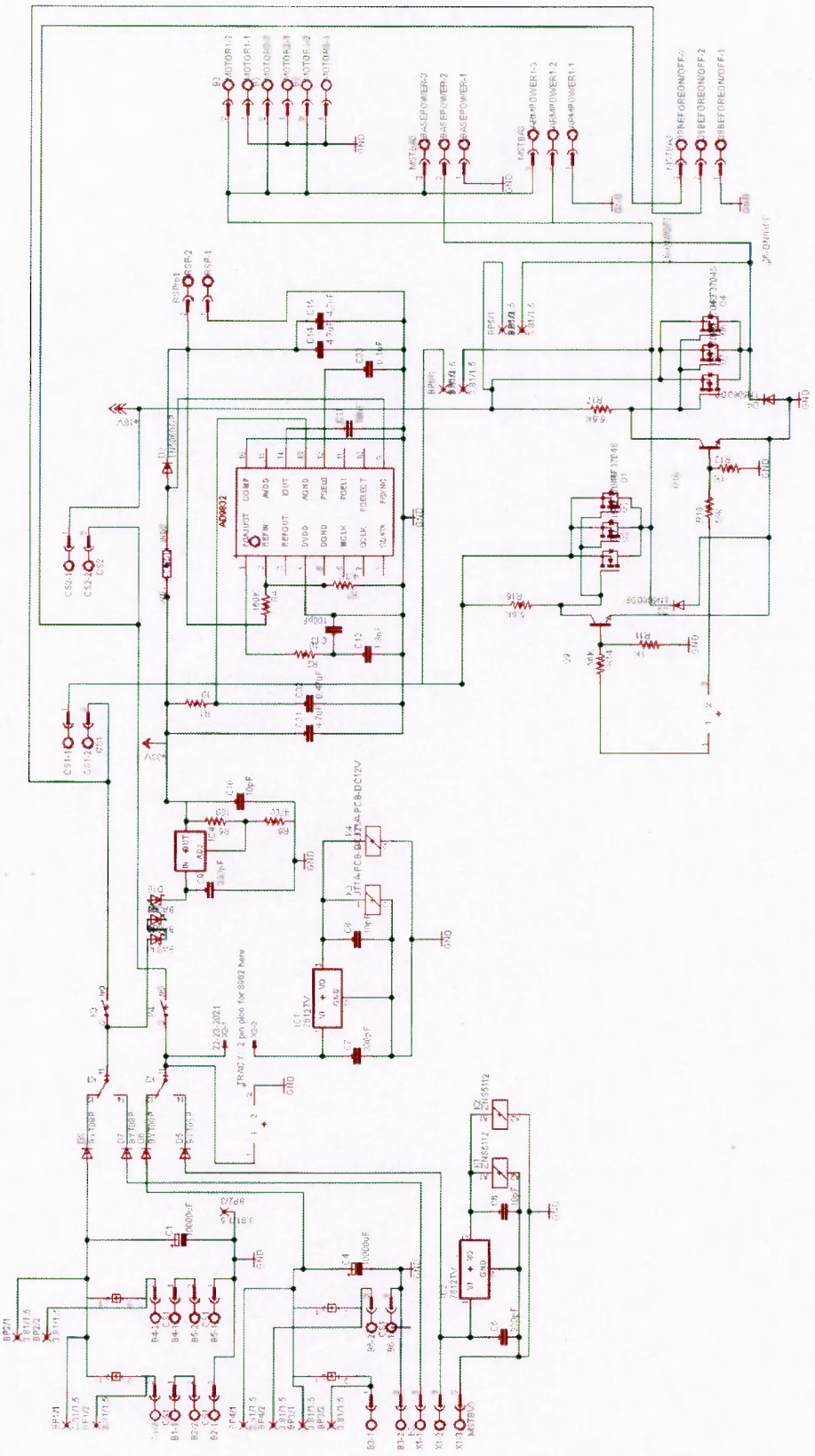

Figure 5.11.: The EAGLE CAD schematic of the power regulation board.

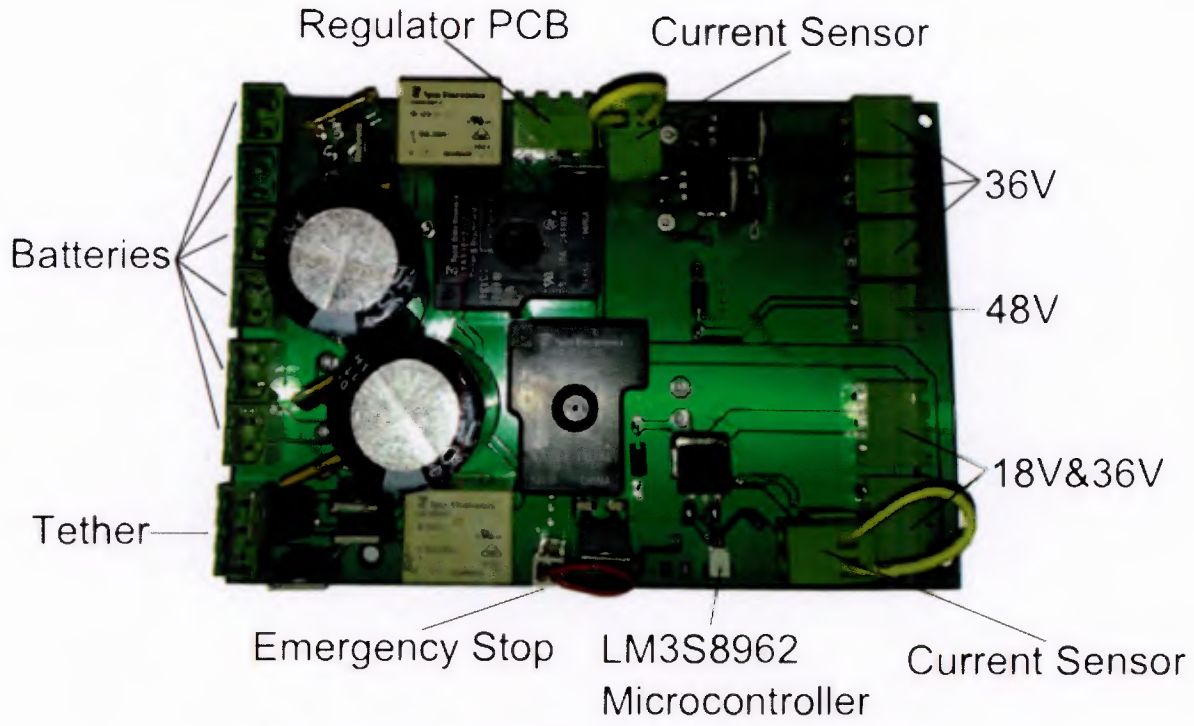

Figure 5.12.: The connections of the power board.

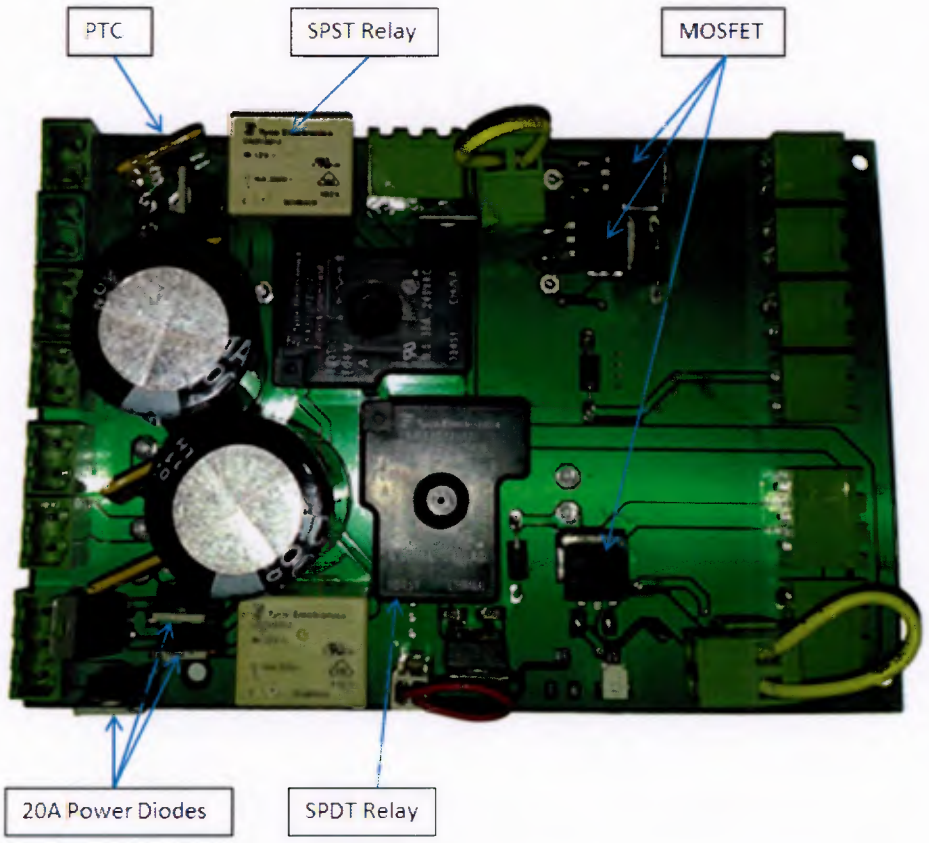

Figure 5.13.: The components of the power distribution board.

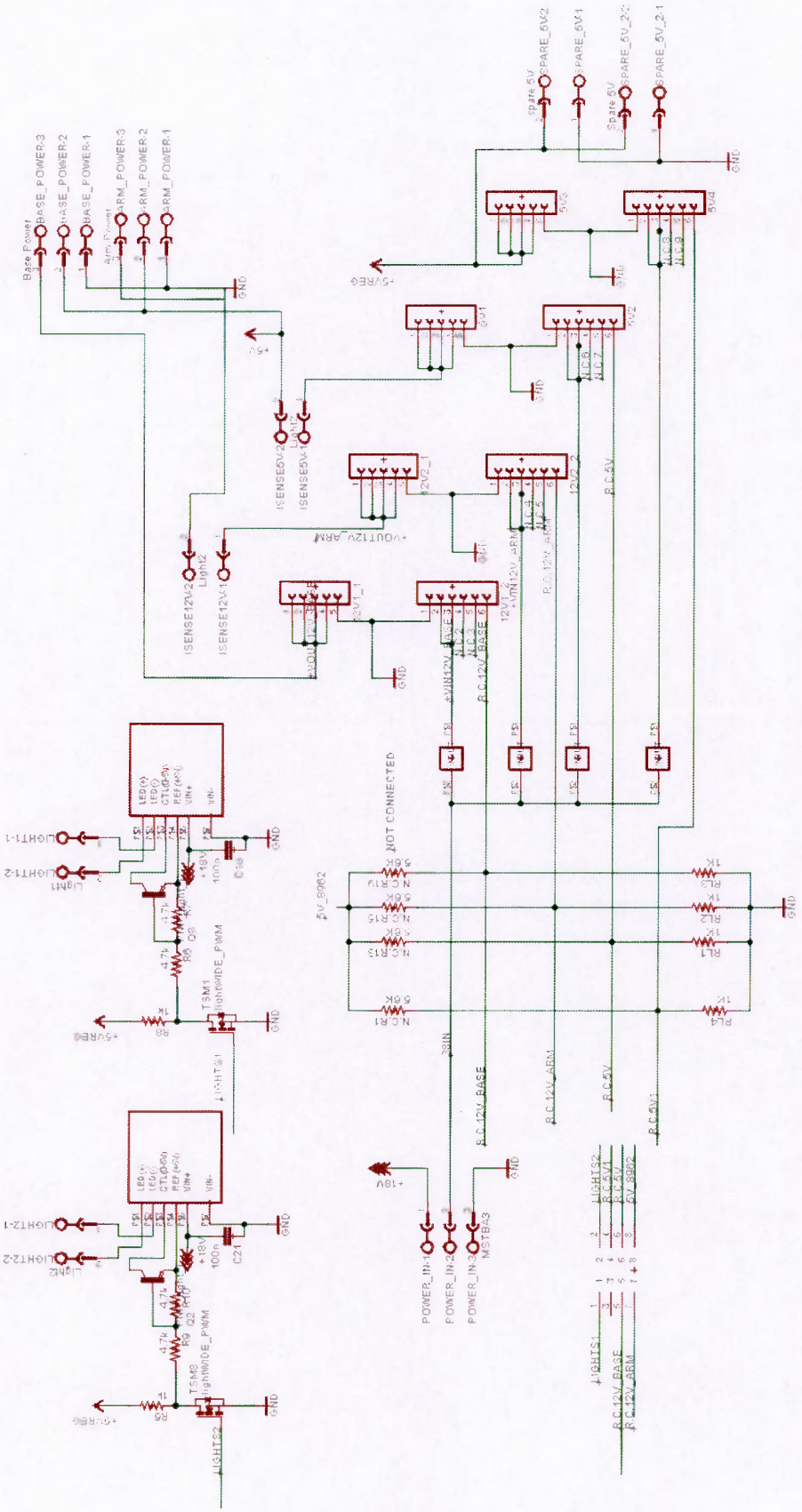

Figure 5.14.: The EAGLE CAD schematic of the power distribution board.

5.4. LM3S8962 Embedded Controller

The new microcontroller board needed to be versatile in order to be used for the power board as well as the actuation system and other systems throughout the robot. One of the main requirements for the board to be compatible with the **NI LabVIEW** ARM Embedded Module, since this software was intended to be used for all the control systems of **Ratel**.

The development of the microcontroller was done in collaboration with the chief scientific officer of **UCT's** mechanical engineering department Tracy Booysen and MSc students Michael Rieger and Bradley Springer. Over the course of a few weeks a total of three generations of the microcontroller board were produced, with each generation being an improved version of the previous iteration. While researching for an adequate processor, the Luminary Micro ARM Cortex-M3 LM3S8962 50MHz, 32-bit processor stood out, mainly for its compatibility with the **LabVIEW** ARM Embedded Module. The processor has a built in 3V **A**nalog to **D**igital **C**onverter (**ADC**) and its **I**nput/**O**utput (**IO**) pins are accessible on the board through Pico-Clasp connectors. Otherwise the board contains a RJ45 jack for Ethernet and two MAX3232 for RS232 serial communication. Included on the board was the DAC7554, a 10-bit **D**igital to **A**nalog **C**onverter (**DAC**), and quadrature encoder protection circuit consisting of Schottky diodes and resistors. The board was capable of using **I**nter-**I**ntegrated **C**ircuit (**I2C**) and **S**erial **P**eripheral **I**nterface (**SPI**). The Texas Instruments (**TI**) Stellarisware ICDI JTAG seen in Figure 5.15 and the Keil µVision development suite were used to program the LM3S8962 board. The board itself is depicted in Figure 5.16.

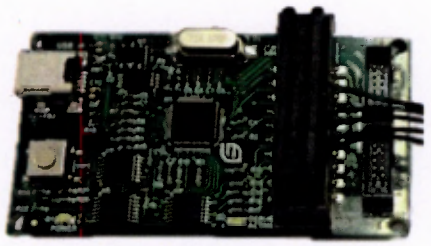

Figure 5.15.: The TI Stellarisware ICDI JTAG board used to program the LM3S8962.

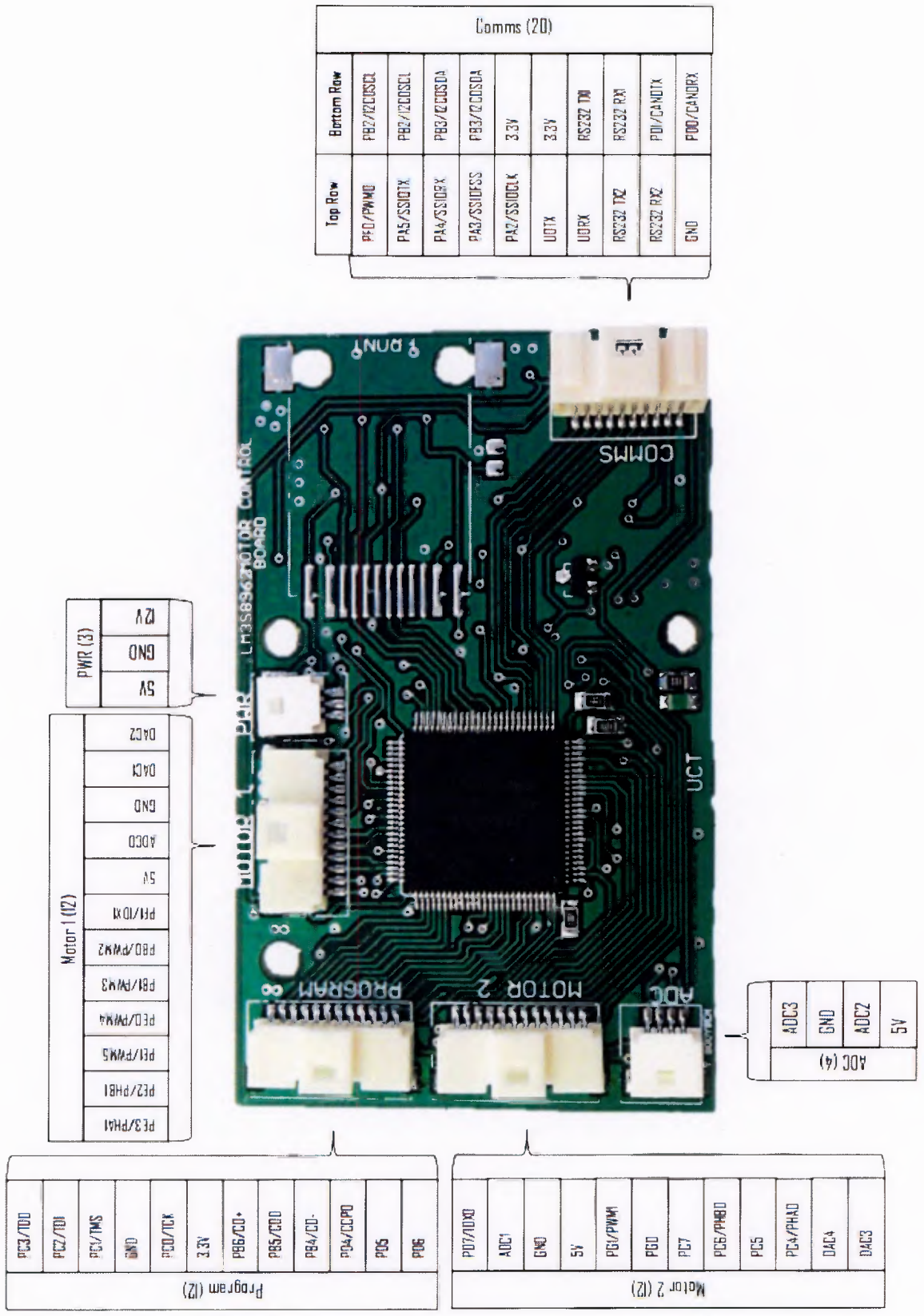

Figure 5.16.: The LM3S8962 microcontroller (photo courtesy of Michael Rieger).

5.5. Current Sensor Board

A current sensor circuit was not included in the power board itself. Since several systems resided on the platform and because the arm and the gripper were in need of a current sensing system, it was decided to have a single separate board that could meet all these requirements. This added the advantage of being able to swiftly interchange these board in case of a fault on one of them. The sensor boards were needed to monitor the batteries and verify their correct operation as well as to determine their **SOC** through coulomb counting.

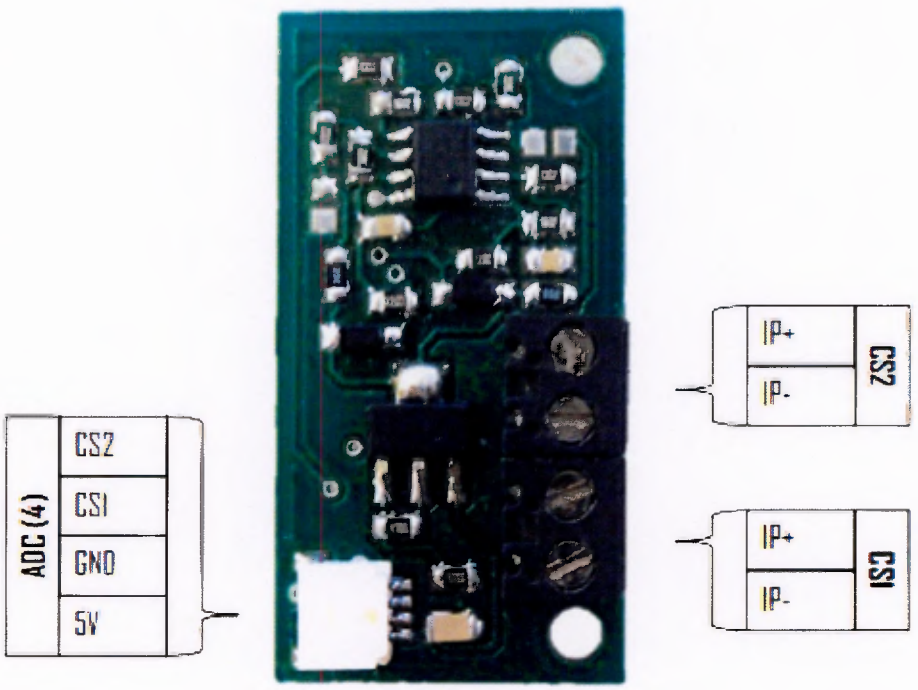

Figure 5.17.: The current sensor board [27].

A number of possible solutions were examined and ultimately a custom designed current sensor board, depicted in Figure 5.17, was developed by Michael Rieger. The Allergo ACS712 ±20A hall effect sensor was chosen to measure the current of the platform, because its implementation was non-intrusive and it was isolated from the rest of the system. The sensor worked in both the positive and negative regions and its output ranged from 0V-5V, which corresponded to readings ranging from -20A to +20A. A value of 2.5V indicated a current reading 0A. Since the sensor was intended to work in conjunction with the LM3S8962 board, its output signal was reduced to a maximum of 3V, so that it did not exceed the 3V value of the processor's built-in **ADC**. To accomplish this an **op**erational **amp**lifier (**opamp**) circuit was utilised to limit the output voltage. Each current sensor board contains two of these sensors.

5.6. Summary

Two power distribution **PCB** were designed to address the missing functionality of its predecessor, while adding new features to the system. The overall physical dimensions of the boards enabled them to be housed within the left sidepod. The evaluation and testing of the system can be found in Chapter 9. Once the power system was finalised, work on the platform's actuation system could begin. The development of this system is presented in the subsequent chapter.

6. Platform Actuation System

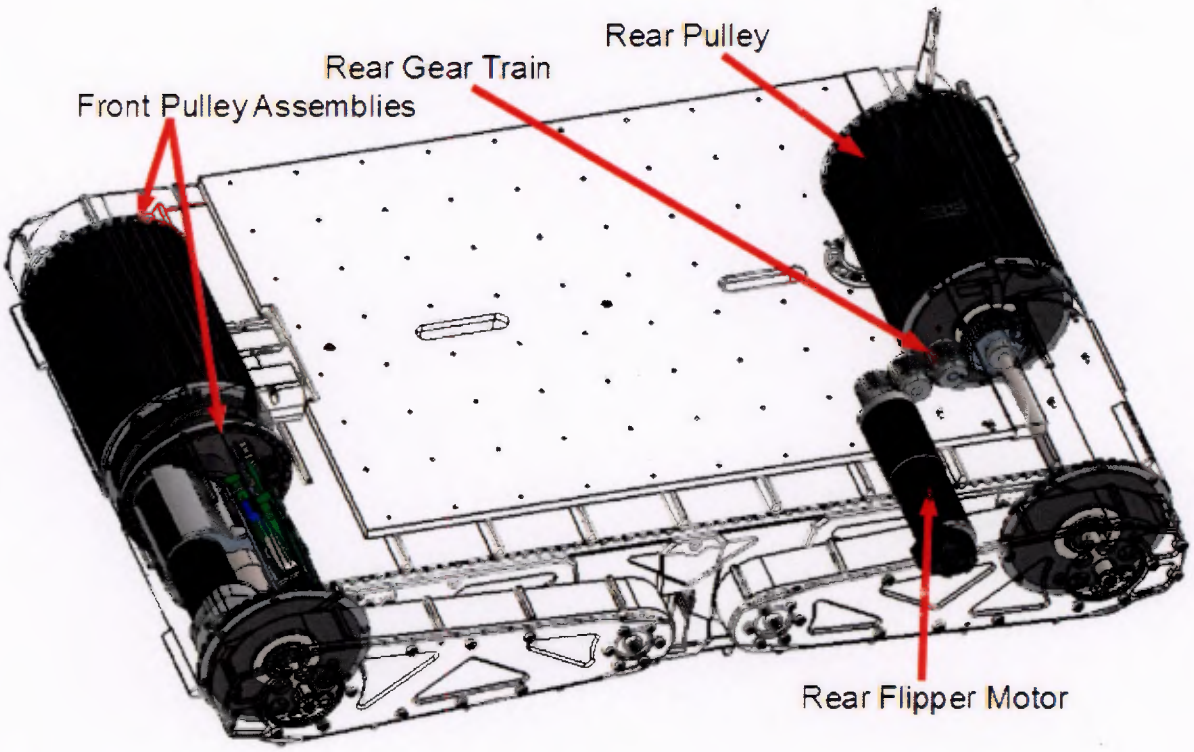

Figure 6.1.: The placement of the actuation system within the rescue robot platform.

The actuation system of the platform, highlighted in Figure 6.1, can be broken down into two major sections, namely the drive pulleys and the rear flipper actuation system. The front pulleys, one on each side of the spine, are responsible for moving the drive track and the front flipper of their respective side. The rear flipper actuation system on the other hand moves the two rear flippers in unison.

6.1. Platform Actuation Specific Specifications

The list of specifications in Table 6.1 is derived from the primary specifications contained in Table 3.1 of Chapter 3.

Table 6.1.: Platform Actuation Specific Specifications.

Location	Specification	Desired Value
Physical Specifications		
6.1.1	Dimensions of Motor Assembly	cylinder of ø 115.46mm and height of 187.80mm
6.1.2	Wiring Diameter	ø 12mm
Functional Specification		
6.1.3	Driving Speed	1.4 m/s
	Rotational speed of flippers	9 rpm
6.1.4	Improved Turning Capability	Yes
6.1.5	Motor and Gearbox	Maxon EC40 motor and a Maxon GP42C gearhead
6.1.6	Microcontroller	LM3S8962 Custom Board
6.1.7	Communications of the Control System	**I2C**
Electronic Specifications		
6.1.8	Flipper Position Feedback	Maxon Encoder HEDS 5540
6.1.9	Desired Flipper Positional Accuracy	1°
6.1.10	Limit Sensors for Flipper Motors	Yes
6.1.11	Current Sensor	40mA Resolution
6.1.12	Motor Controller	Maxon 4-Q-EC Amplifier DECV

6.1.1. Dimensions of Motor Assembly

The motor assembly and the control system are to be housed inside a cylindrical pulley, which has a diameter of 115.5mm and a height of 184.5mm. It has to be assured that the control subsystem does not come into contact with either the gears of the inside or the outside of the pulley. Figure 6.2 depicts the overall dimensions of a front pulley.

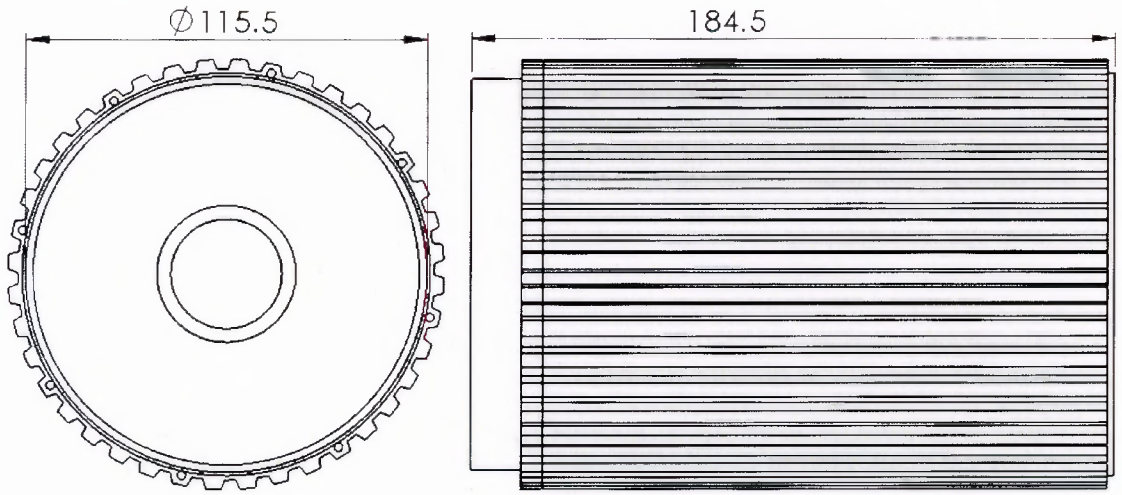

Figure 6.2.: The front pulley dimensions.

6.1.2. Wiring Diameter

The pulleys and motor assembly were designed with a circular pathway for wires that is 12mm in diameter, as can be seen in Figure 6.3. This value is the largest collective diameter of the wires that run from the body of the rescue robot platform to its pulleys.

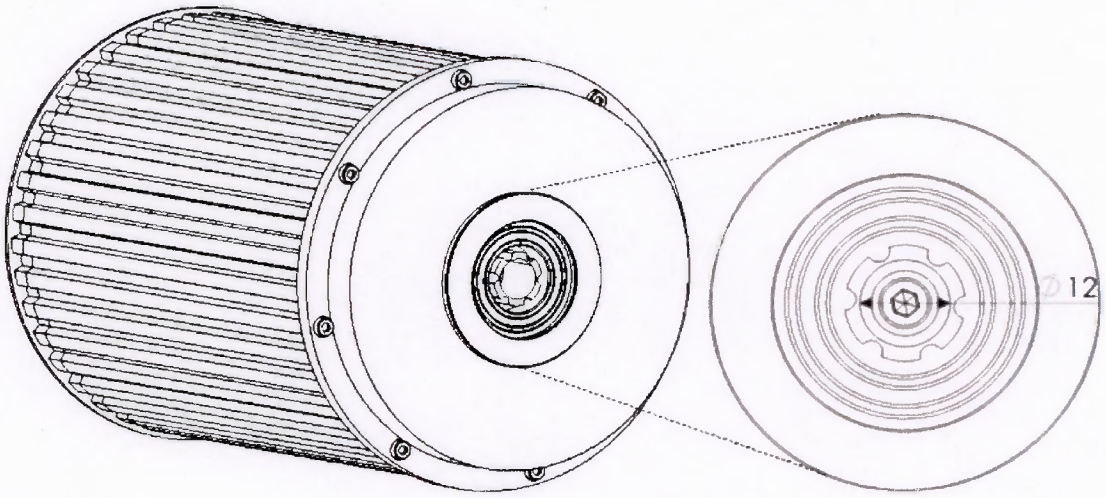

Figure 6.3.: The diameter of the channel through which the cables need to be fed through.

6.1.3. Driving Speed

In the previous development of the system a maximum driving speed of 1.4m/s was desired. This value was estimated to be the walking speed of an average adult and since the robot's function is to replace a human being, it should be able to move at least this fast.

6.1.4. Improved Turning Capability

When turning the platform, significant problems were revealed, which resulted in a decrease of the robots mobility. This imposed the need for the application of a method that would allow the robot to turn appropriately.

6.1.5. Motor and Gearbox

The robotic platform was designed to use the Maxon EC40 motor with an attached Maxon GP42C gearhead. Thus the entire actuation system has to include the capabilities and size of the devices.

6.1.6. Microcontroller

The LM3S8962 custom designed microcontroller board was desired for the control of the motors since it has all the required functionality, takes up a small footprint and because of its compatibility with the **LabVIEW** ARM Embedded Module.

6.1.7. Communications of the Control System

During the first stages of development, MSc student Peter Henson made the decision to use I2C as the main wire communications system throughout the **UGV**.

6.1.8. Flipper Position Feedback

The motors came with a Maxon Encoder HEDS 5540 attached. This optical encoder has 500 counts per turn and has 3 channels, namely channel A, channel B and an index pulse.

6.1.9. Desired Flipper Positional Accuracy

A positional accuracy of at least 1° was chosen.This value is easily accurate enough for the flipper positions and a difference of 1° between the desired value and the actual value would not be visible to the operator.

6.1.10. Limit Sensors for Flipper Motors

The Maxon Encoder HEDS 5540 is a relative optical encoder and it needs to be calibrated when the system is powered up.

6.1.11. Current Sensor

The current sensing integrated in the Maxon speed controllers was not suitable and thus an external current sensor that provides high resolution readings was required. The current values can be used to detect when the flippers are pushing against something and allow the operator to verify the correct operation of the pulley system.

6.1.12. Motor Controller

The Maxon 4-Q-EC Amplifier **DECV** was selected in the initial development of the system and thus the mechanical structure of the platform was design to accomodate this controller.

6.2. Previous Development of the Actuation System

All movement was actuated through a total of five 120W Maxon Brushless DC Motors. A Maxon planetary gearhead was used in conjunction with every motor. The gearing ratio for the driving and front flipper motors was 43:1 while that of the rear flipper motors was 113:1. The Maxon Encoder HEDS 5540, an optical, three channel rotary encoder, was attached to the back of every motor. The drive pulley assembly also included gearing and the rear flipper assembly included gearing and provide a further ratio of 1:2 for both tracks and the flippers.

The rear flippers were actuated by a single motor that was housed in the left sidepod. A light bridge in each drive pulley assembly was provided for the flippers and would send a pulse once every 360°. This was essential, because the encoders provide relative position readings only and thus need to be calibrated every time the platform is activated. No such functionality was provided for the rear flippers. The large width of the drive pulleys, is a direct result of an earlier decision, to implement wide tracks. This in turn allowed the motors for the tracks and front flippers to be housed within the pulleys. The motor assembly within the pulleys is illustrated in Figure 6.4.

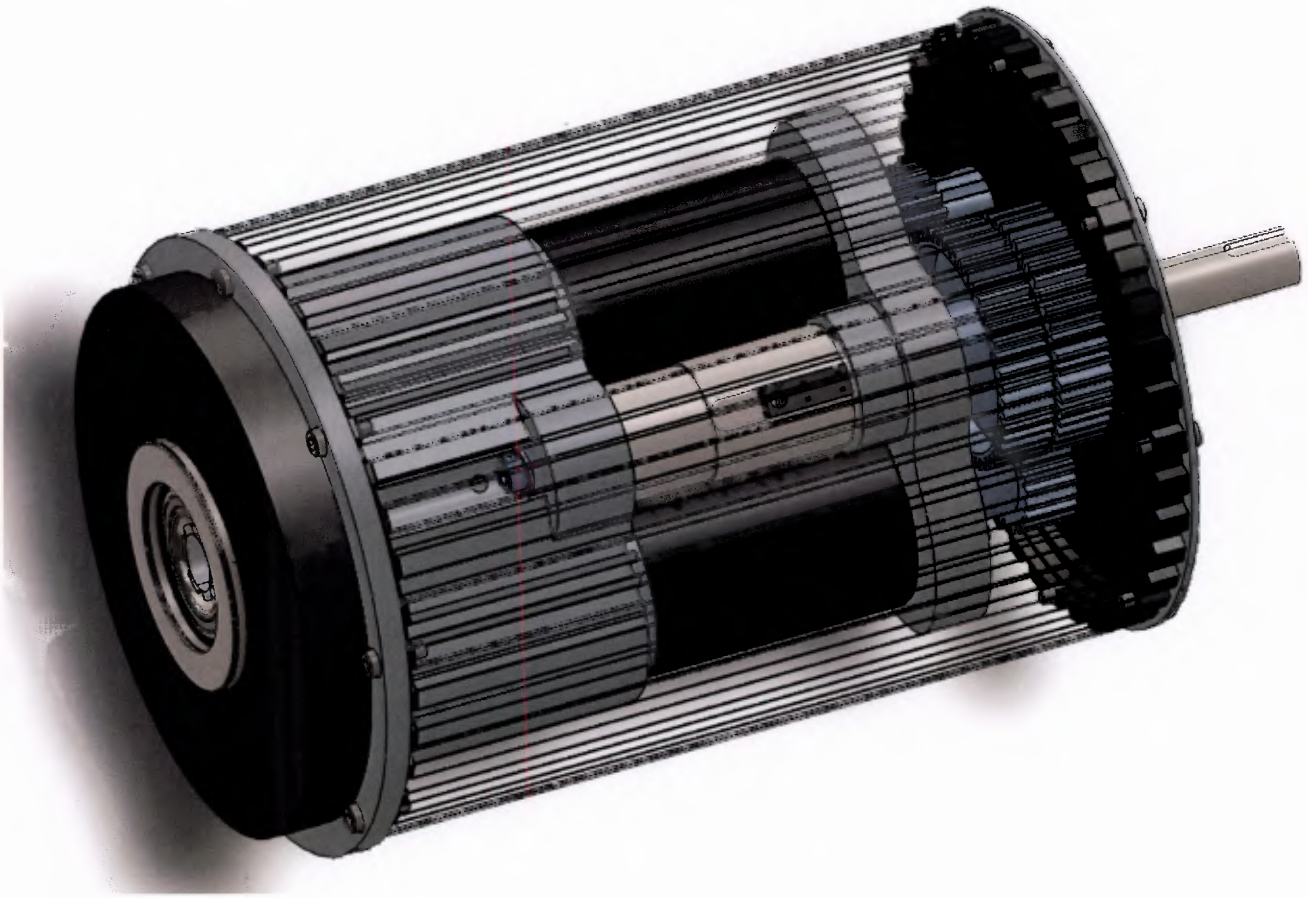

Figure 6.4.: The motor assembly designed by Eugene Dreyer.

6.3. Initial Configuration

The initial configuration of the drive pulleys was done in conjunction with MSc student Eugene Dreyer. Before attempting to design a fully functional actuation system, it was necessary to establish whether the mechanics of the driving systems were sound. An electronic system was configured to allow the verification of the mechanical aspects of the locomotion design. Useful insights about the system could be drawn from this initial development and allowed the further

development of the actuation system. The next sections will explore this initial system,after which the final design of the actuation system is presented.

6.3.1. Motor Controllers

MSc student Justin Pead developed a circuit board based on the Freescale GT16 that was used to control the platform's motors, was used to control the motors. The processor's 8 bit **D**igital to **A**nalog **C**onverter (**DAC**)had an output of 0V-5V, which corresponded to the motor speed range of 0-255. The **IO** pins on the microcontroller were used to enable/ disable the speed controller and to change direction of rotation. Signals were sent from a laptop to each board via a RS232 serial interface.

6.3.2. Maxon 4-Q-EC Amplifier DECV 50/5 Speed Controller

The Maxon 4-Q-EC Amplifier DECV (Digital EC Controller Voltage regulated) 50/5 is a 4-quadrant digital speed controller intended for the control of brushless **E**lectronic **C**ommutated (**EC**) motors of up to 250W. This device has a large input voltage range of 12-50V, which makes it compatible with a large range of power supplies. The controller is illustrated in the following Figure 6.5.

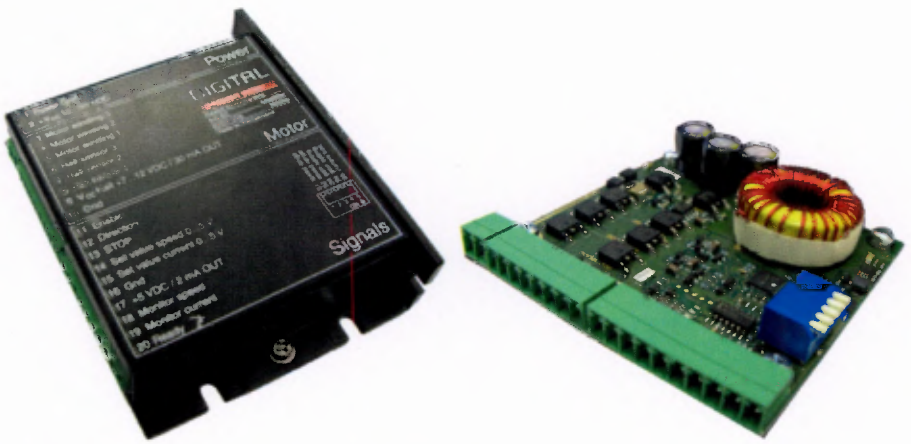

Figure 6.5.: The Maxon DECV 50/5 controller with and without its aluminium cover [11].

Both the speed range and the gain setting can be adjusted through a DIP switch. **IOs** in the form of detachable screw terminal strips allow for the control of specific settings, such as the speed and current limit of the motors by sending analog signals. Boolean signals were used to toggle the direction of rotation, the enable pin and the stop pin. The controller also outputs boolean data that allowed the verification of motor speed, in addition to the ready state of the controller itself.

During the design process of the platform the speed controllers were intended to be housed inside the sidepods and the wires from the controllers were meant to run along a channel to the motors inside the pulleys. During assembly its was realised that the channel was too small to accommodate all the wires and the size of the channel could not be increased. For

this reason the controllers were placed inside the drive pulleys. Each controller's cover was removed so that they could fit properly. Two speed controllers and the micro controller were accommodated within a single pulley. The advantage of this approach was twofold. Firstly the large weight of the motors made the platform front-heavy, which improves its mobility and secondly there is more space within the sidepods for additional equipment. The configuration of the drive pulley assembly with the Maxon speed controllers is depicted in the Figure 6.6.

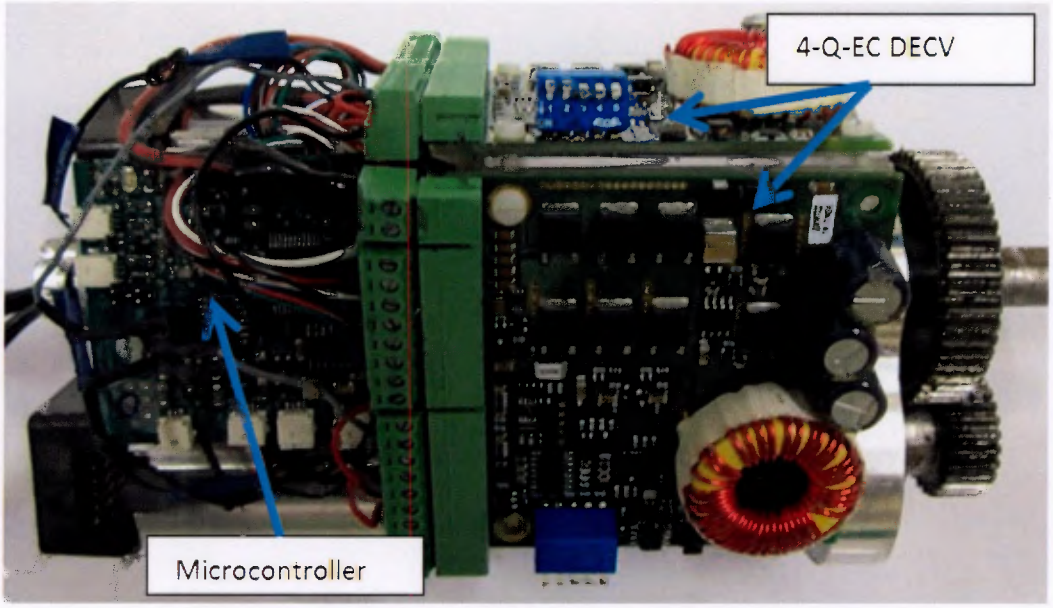

Figure 6.6.: Initial drive pulley configuration.

6.3.3. Initial Testing and conclusions

The proficiency of the locomotion system was tested and it was established that the system performed adequately, yet several problems came into light. Although the system was capable of driving straight in a suitable manner for most of the time, turning proved to be very difficult. The motors appeared to be too weak to turn the platform and the tracks would constantly be driven inwards, towards the centre spine or outwards, depending on the direction of turning. After driving the rescue robot platform around for a while, the motors lost their ability to actuate the tracks altogether. Thus before the establishment of a satisfactory control system could commence, the issues that prevented proper actuation had to be resolved. The discovery of the causes of the aforementioned problems and their solutions are presented in the subsequent section.

6.4. Electro-Mechanical Alterations to the Actuation System

During the initial assembly of the platform the first aspect to be tested was its driving proficiency. This section details the aspects of the drive pulleys that required further development in order facilitate adequate operation of the actuation subsystem.

6.4.1. Motor Power

Certain complications immediately became evident. Even though the motors were powerful enough to drive the platform in straight lines, they did not manage to allow the robot to turn on the spot or around a radius. This discovery lead to the application of motors with a higher gearing ratio. The new drive motors that were chosen had the gearing ratio of 126:1, while the new flipper motor gearheads had a ratio of 156:1. The addition of the new motors improved the driving performance, yet the locomotion problems persisted.

6.4.2. Journal Bearings

After a rigorous inspection and some more testing it was discovered that the motor assembly within the drive pulley was chafing against the centre pulley section. The amount the motor assembly would chafe against the pulley was dependant on the position the platform was in. Chafing occurred as a result of the motor assembly not being balanced with bearings correctly. The whole assembly was supported by a single bearing on one end while the other side was unsupported. A computer aided design (**CAD**) model of this configuration is illustrated in Figure 6.7. Mitigating this problem required an additional bearing on the opposite side of the inner pulley assembly. It turned out that no bearing of the right size could be sourced and thus a brass journal bearing was designed instead. Figure 6.8 illustrates the pulley assembly with the journal bearing.

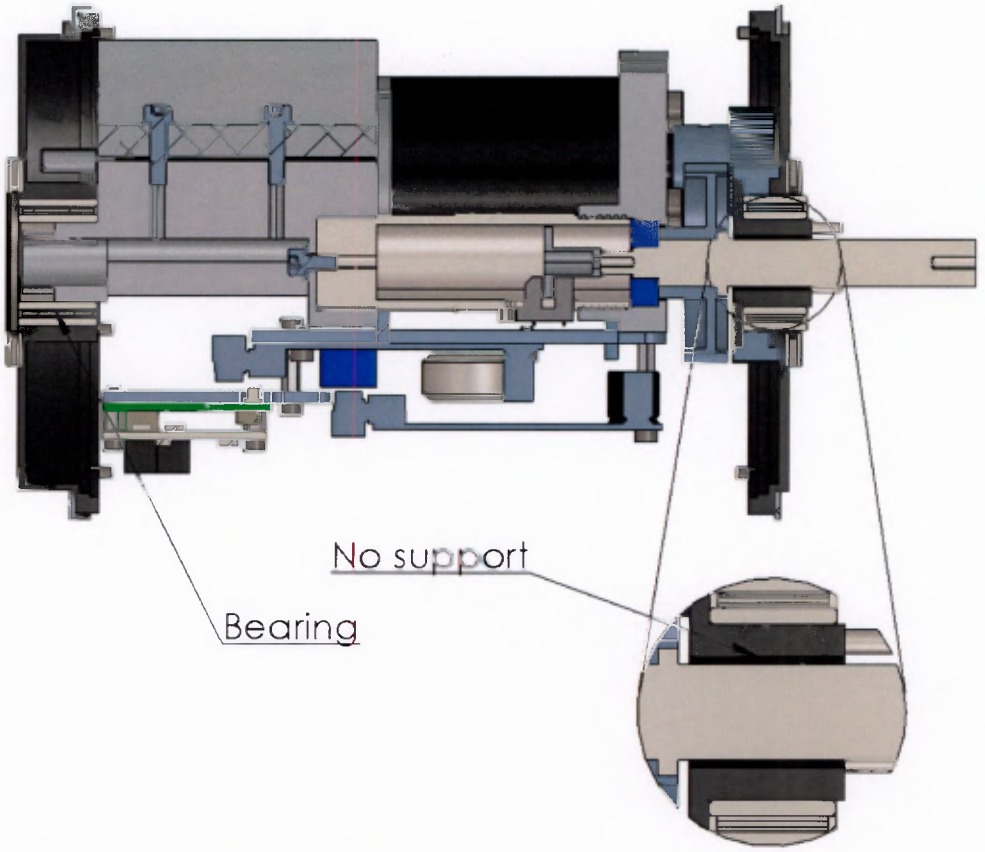

Figure 6.7.: The outer side of the pulley assembly was not supported.

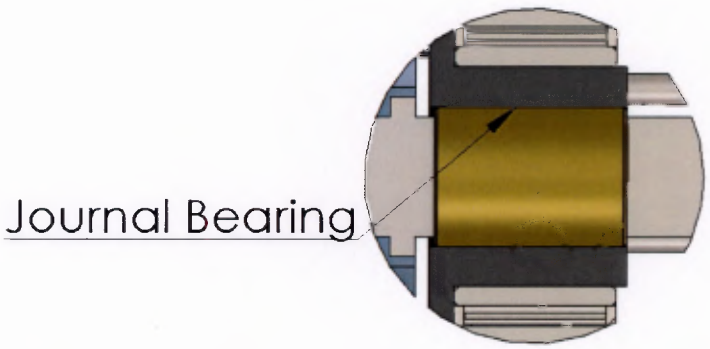

Figure 6.8.: A brass journal bearing added to the pulley assembly.

6.4.3. Turning

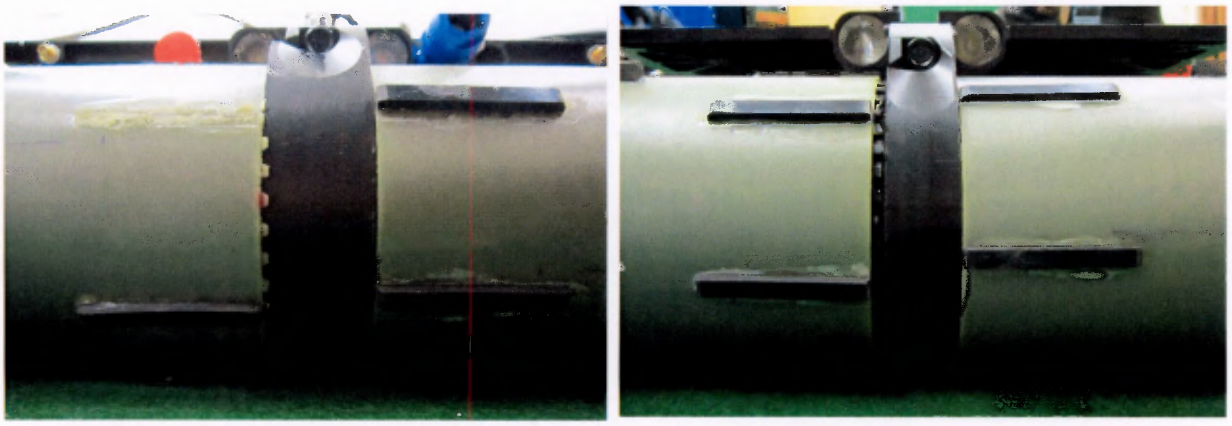

(a) The rear view of the tracks and spine.

(b) The front view of the tracks and spine.

Figure 6.9.: The spine biting into one of the belts during turning.

It was noticed that while turning on the spot or around a radius, the driving tracks would move laterally. They would either move outwards, away from the centre spine or inwards, towards it, depending on the direction in the platform was turning. A method that was previously attempted to mitigate this was the addition of pins to the pulley brackets. The pins prevented the tracks from moving outwards, however inwards movement still occurred during turning. Figure 6.9 illustrates how the spine would bite into the left track as a result turning right. A new way of preventing the tracks from moving this had to be developed. A pair of circular aluminium shoulders were developed that could be attached to the pulleys as seen in Figure 6.10. This was realised by removing material from the pulley covers so that the circular shoulders could be added to the assembly without rubbing against any section of the robot. The introduction of these shoulders had the added benefit that these components would rotate with the tracks and thus the relative velocity between the tracks and the shoulders was zero, which mean that there was no friction between them. Figure 6.11 portrays the fully assembled pulleys and tracks with this new configuration.

(a) A Solidworks render of one of the rear pulleys.

(b) A Solidworks render of one of the front pulleys.

Figure 6.10.: The modified pulleys .

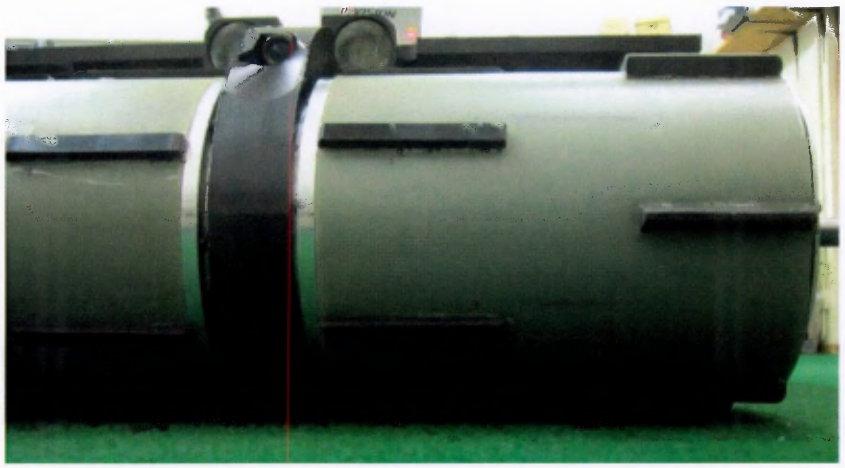

Figure 6.11.: The tracks are prevented from moving laterally by the circular shoulders on both sides.

6.5. Electronic System

Once the mechanical section of the actuation system performed adequately, work on the electronic section could commence. As mentioned earlier, the initial development of the electronic aspect of this system was mainly used to test the mechanics of the locomotion system. However, the final iteration of the system required additional functionality in order to allow for position control of the flippers and in order to provide overall system control.

The custom LM3S8962 board replaced the microcontroller that was initially used to control motion. This new board was more powerful and versatile than the previous one and allowed the quadrature signals of the motors to be interpreted. This facilitated the development of position control for the flippers. The four **DAC** outputs of the board were used to control the current limit and the speed of the motors through the two 4-Q-EC Amplifier **DECV** controllers. The **IO** pins were used to toggle the enable, direction and stop pins of the speed controllers. The current sensor board used in the power distribution system, as described in Section 5.17, was used to measure the current draw of each motor. Its values were sent to two **ADC** pins of the LM3S8962 board. The limit switch proved to be difficult to read with an **IO** pin and thus its value was read by a third **ADC** pin and compared to a predetermined value. The same set up was used to control the rear motor. The only differences are that only one motor had to be controlled and that the limit switch was not optical, but magnetic. A hall effect sensor was attached to the rear gear cover and a Neodymium magnet was placed onto the last gear of the rear gear train, as is depicted in Figure 6.12. A boolean low was sent to the microcontroller every time the magnet made its way past the hall effect sensor. The front LM3S8962 microcontroller boards received commands and sent data back through a RS232 serial interface, while the rear one did so through an Ethernet link. The communications layer of this system is further explored in Chapter 8. The new configuration was also designed in such a way that the microcontrollers could be programmed without having to take them out of the pulleys.

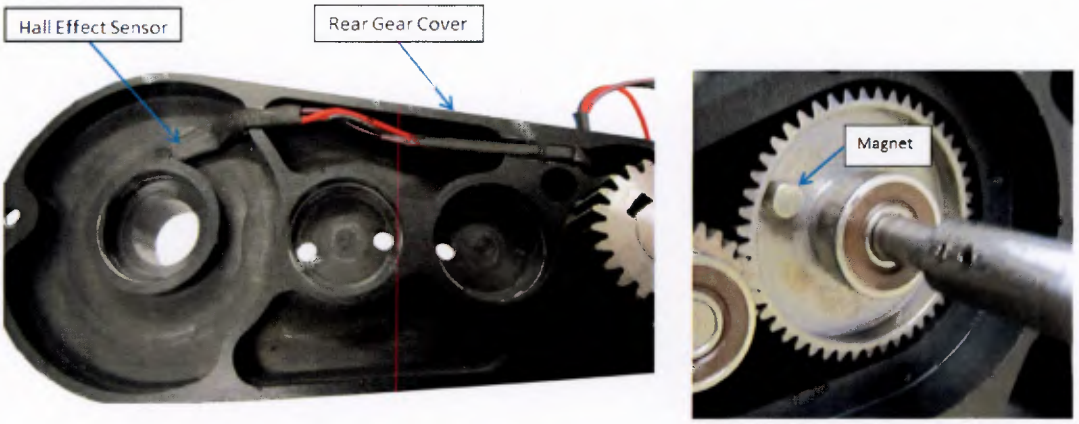

(a) The sensor on the rear gear train cover.

(b) The Neodynium magnet on the gear.

Figure 6.12.: The hall effect sensor and corresponding magnet on the gear.

With this new setup, the motor controllers were mounted differently. This was done, because initially the controllers would chafe against the inside of the pulley and this had the potential of destroying the controllers. The second mounting method ensured that no rubbing between any part of the inner assembly and any part of the pulley would occur. The new assembly can be seen in Figure 6.13 and an exploded view depicting the assembly is depicted in Figure 6.14. This is followed by a top view of the motor assembly in Figure 6.15 and Figure 6.16 portrays the actuation system of the rear flippers.

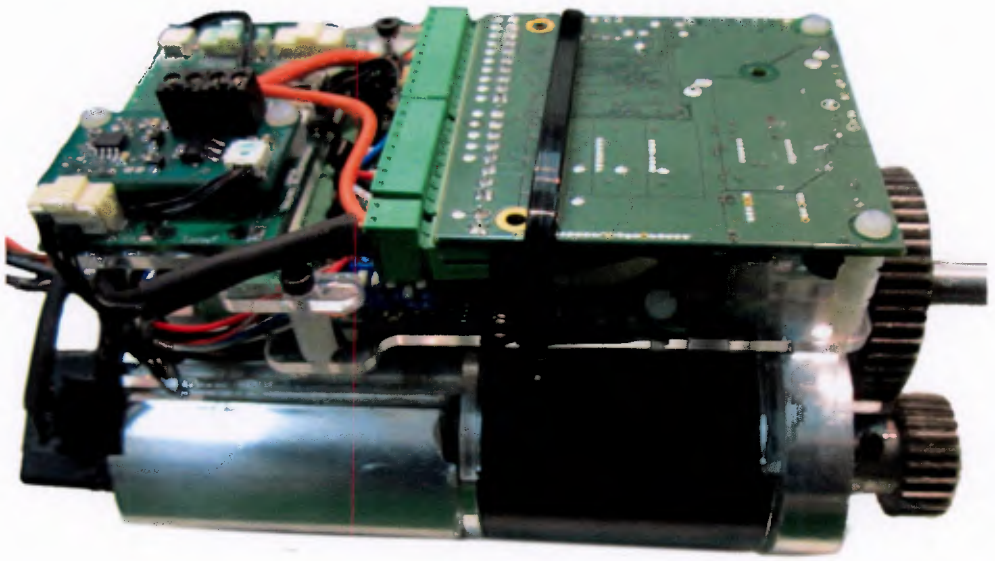

Figure 6.13.: The new motor front assembly.

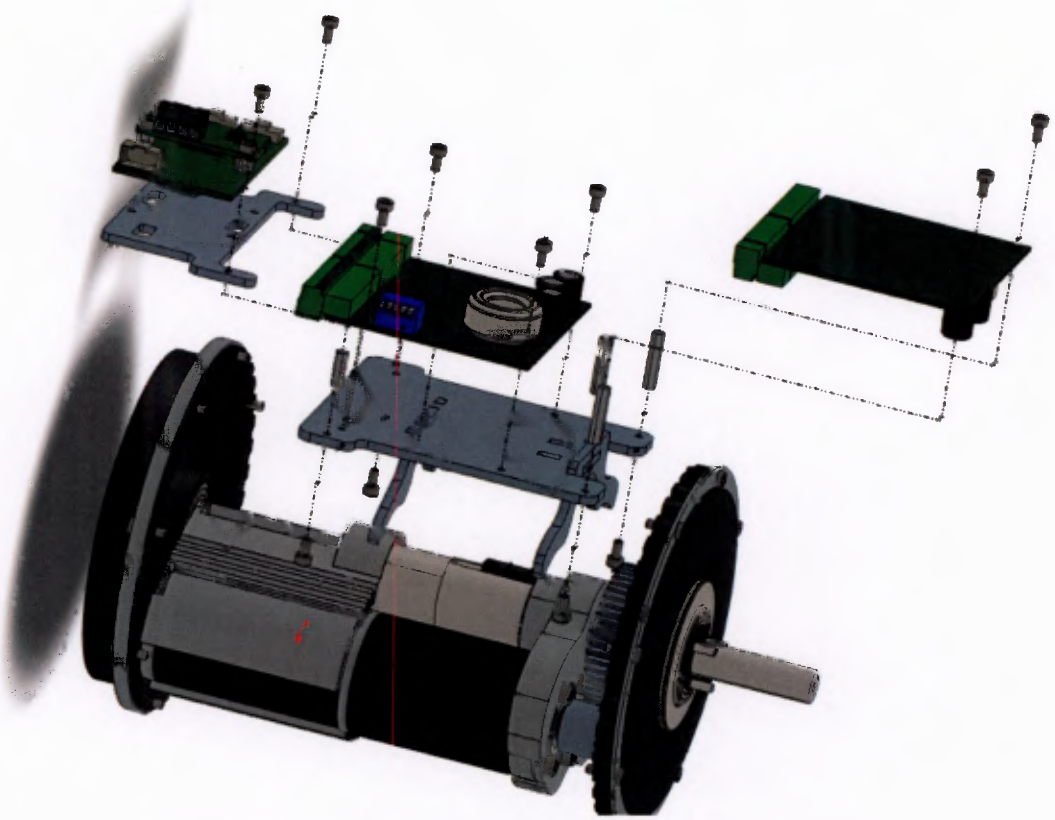

Figure 6.14.: Exploded view of the front pulley assembly.

Figure 6.15.: The top view of the pulley assembly.

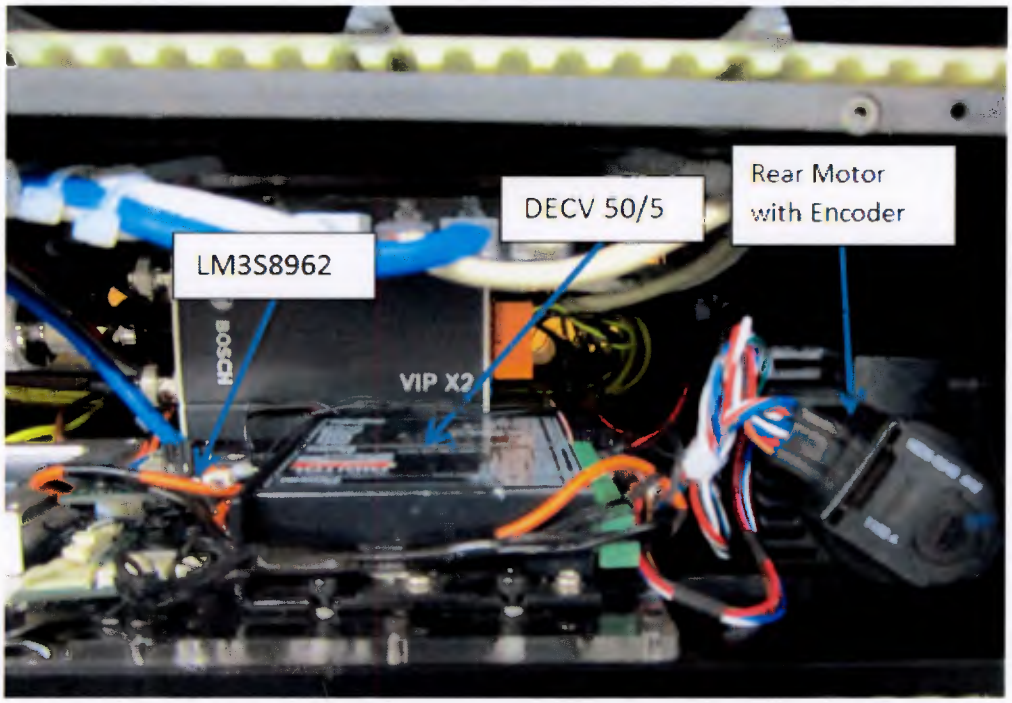

Figure 6.16.: The rear flipper actuation system.

The system met all the desired requirements and improved control over motion. However, complications did occur when attaching the pulleys to the rest of the robot. Even though most of the wires were very small in diameter, they were very difficult to fit in the channel of the spine. Figure 6.17 depicts the wires of the pulleys and the channel that they had to go through.

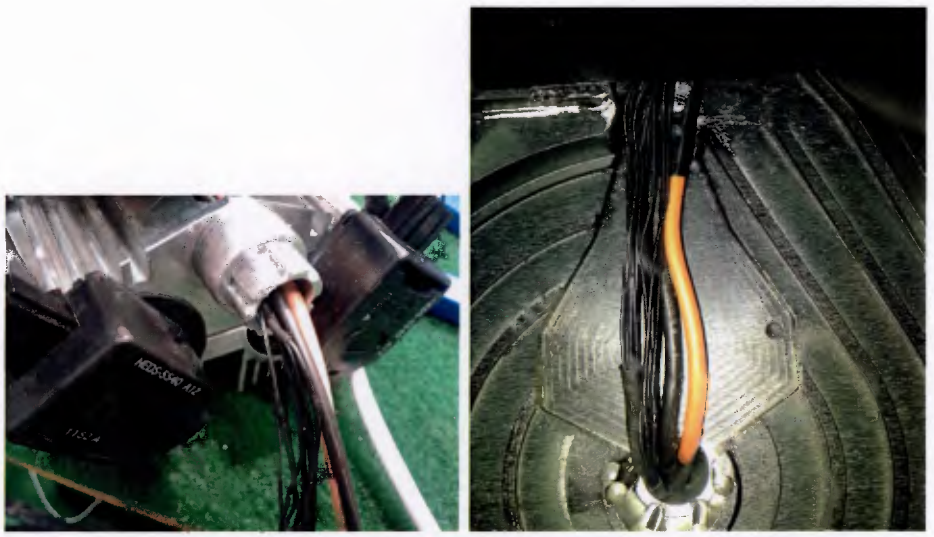

(a) Wires coming out of a pulley assembly. (b) Pulley wires being guided through the wire channel.

Figure 6.17.: Wires of a pulley.

6.6. Summary

Apart from the assembly complications induced by the small channel, the overall assembly and the features of the system met all the desired requirements. The next chapter will focus on the caterpillar track system and explain the modifications that were made in order to develop the system to a stage where it would allow the rescue robot to be competitive while traversing the complex arenas of **RoboCup Rescue**.

7. Caterpillar Tracks

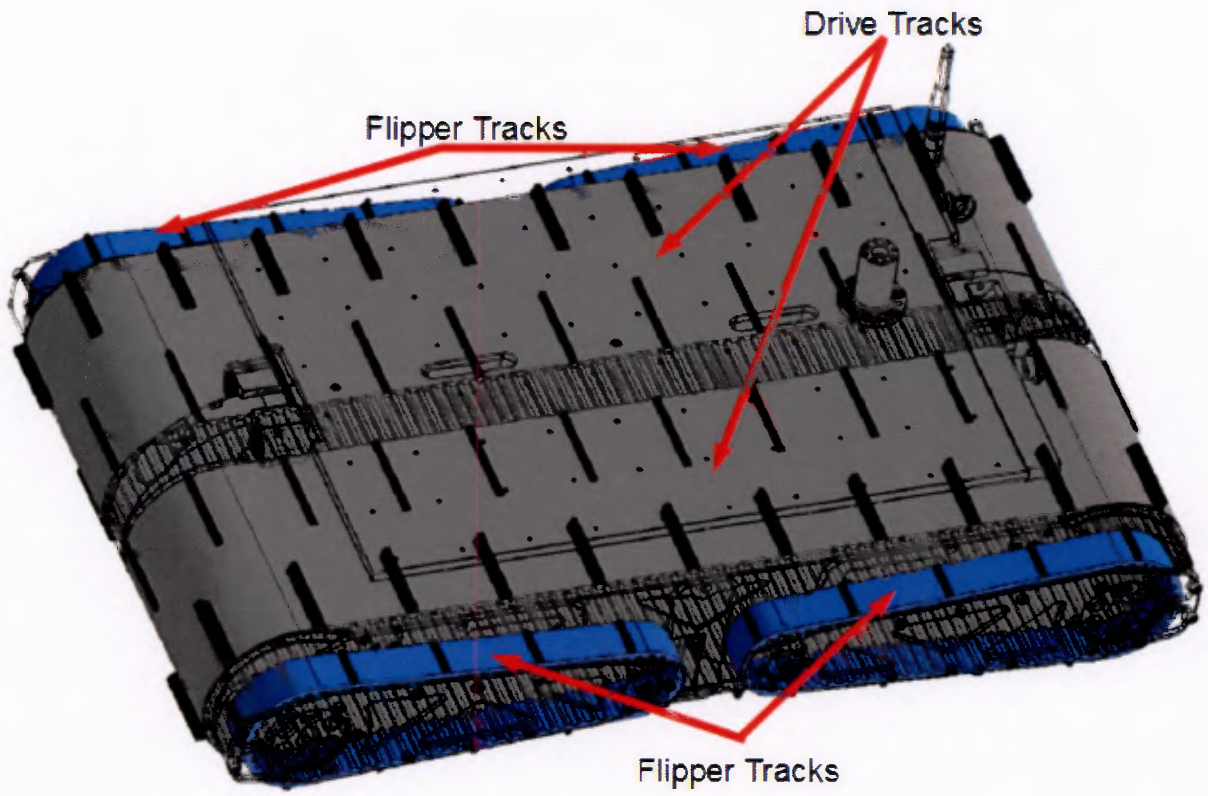

Figure 7.1.: The tracks of the platform.

The initial tracks of the robotic platform consisted of T10 **p**oly**u**rethane (**PU**) timing belts, obtained from "**BELT TORQUE (PTY) LTD**", and had teeth on a single side, with the smooth side making contact with the terrain of the environment. The two tracks were 175 mm wide and had 161 teeth, while the four timing belts, used as the flipper tracks, were 32 mm wide and contained 73 teeth. The circumferences were 1610 mm and 730mm for a track and a flipper track respectively. A steel mesh cast within the belts supplied structural reinforcement. Both a driving track and a flipper track are depicted in Figure 7.2 and 7.3 respectively. The platform with the tracks can be seen in Figure 7.4. After having performed several driving tests on both flat and inclined planes that consisted of smooth wooden floors, concrete floors and carpet, it came into light that the amount of traction from this configuration was insufficient and that a means of increasing said traction would have to be introduced. Conventional methods used by custom built and commercial tracked **UGVs** to attain desired traction were researched and it was decided that some kind of tread needed to be attached to the smooth

sides of the timing belts. The following sections will delve into the approaches that were taken in order to increase the platform's belt traction capabilities to desired levels.

Figure 7.2.: One of the two driving tracks in its initial application.

Figure 7.3.: One of the four flipper tracks in the previous development of the track system.

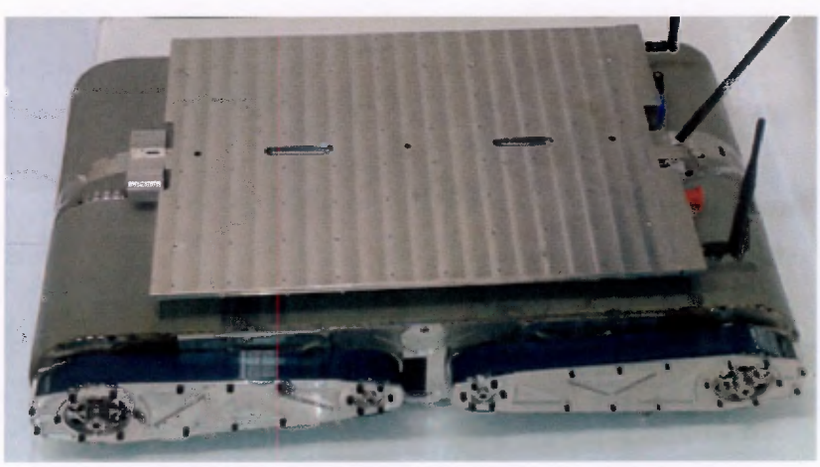

Figure 7.4.: The initial tracks mounted to the platform.

7.1. Material Selection

Tracks and their treads can be made from various materials ranging from steel, Polyvinyl chloride (**PVC**), rubber and a variety of other materials. When choosing the tread material the following performance traits were considered:

- Load Capacity
- Tear/ Cutting Resistance
- Abrasion and Wear Resistance
- Traction: The material's ability to grip the surface that it is operating on.
- Cushioning: Shock absorption while driving.
- Chemical Resistance: The ability to resist chemical changes
- Flexibility

The information from this section has derived from " Polyurethane and Rubber Tires: A Comparative Overview" [28]. The ease with which a tread (made from a particular material) could be attached to the tracks had to be taken into account as well. The two material's that stood out for their many desirable attributes in addition to being easily accessible were rubber and Thermoplastic Polyurethane (**TPU**). Both have their strengths and weaknesses, as well as some unique properties. This section will illustrate their properties and will present the reasons that lead to the final material choice.

Rubber enjoys a widespread use in many areas of the industry. Its flexibility and damping proficiency, in addition to being able to provide excellent traction on both dry and wet surfaces makes it a popular choice for tire manufacturers.

Belt manufacturers often choose **TPU** for their belts as it offers very high wear resistance and high tear resistance, among other things. Prevalent use of it has been seen in footwear, cable & wire, hose and tube, film and sheet and in other industrial sectors. Its proven performance traits made this material a very good candidate for the track feet.

Ultimately **TPU** was chosen because of the number of reasons listed below. Additional justifications for selecting **TPU** over rubber are contained within Table 7.1.:

1. The tearing resistance of **TPU** is superior to that of rubber and thus it withstands rough terrains and debris better. A rule of thumb about wear and abrasion resistance when it comes to tires is that **PU** tires will last four times longer than rubber tires under the same conditions. Additionally **PU** does very well under sliding abrasion, which is essential, seeing that tracked vehicles depend on sliding when they turn.
2. Sharp objects are found in debris sites and thus a suitable cutting as well as tearing resistance is needed for the feet. Comparatively **PU** can withstand such rough conditions better than rubber, as a result of its toughness. When it comes to tires, unlike rubber tires where a cut or tear will propagate, items that cause cuts or tears will get embedded in **PU** tires without causing any cuts or tears.
3. Polyurethane's rolling resistance is lower than that of rubber, which essentially means improved efficiency.

4. Even though rubber has superior shock absorption capabilities, **TPU** with an adequately low durometer value will provide adequate cushioning.
5. From a traction point of view rubber is superior. Making the right shore hardness choice in this area will, however, provide adequate traction for **TPU**.
6. Wet terrain conditions are likely in disaster sites and retaining sufficient traction is of utmost importance. Here rubber tires outperform **PU** tires, yet the **PU** tires still offer good performance.
7. The chemical resistance of the feet material cannot be overlooked. Since chemical spills fall under the category of **USAR** and because households and office buildings contain several chemicals, such as strong cleaning products, this characteristic can play an important role. It has been shown that solvents can diminish the tear strength of rubber tires, whereas **PU** tires are completely unaffected. **PU** is soluble in very harsh solvents.

Table 7.1.: Comparison between PU and Rubber tires [28].

Attributes of PU and Rubber		
	Rubber	**PU**
Load capacity	Good	Excellent
Tear Resistance	Fair	Excellent
Abrasion Resistance	Fair	Excellent
Traction	Excellent	Good
Cushioning	Excellent	Fair
Rolling Resistance	Good	Excellent
Floor Marking	Fair	Excellent
High Speed Operation	Excellent	Good
Outside Operation	Excellent	Fair
Inside Operation	Good	Excellent
Wet Floors	Excellent	Good

7.2. Shore Hardness

A pertinent consideration to make is that the terrain of a collapsed site will undoubtedly have numerous debris scattered all over. Traversing such an environment could cause the rescue robot to experience a significant amount of shock and the platform has no shock absorption capabilities. It would be desirable if the platform's tracks could provide some sort of cushioning, which is directly related to the durometer of the tread material. Higher durometer values will mean that the material is hard and offers less cushioning [28]. Therefore the shore hardness of the polymer of the tread should be hard enough to resist tearing and have an adequate load bearing capacity, yet to be soft enough to provide some shock absorption.

Moreover, the durometer value should be low enough to offer sufficient traction, even on smooth surfaces. An area that requires similar performance under somewhat related conditions is the car industry. Cars are capable of traversing various terrains without immediately ruining

their tires [28]. Automotive tires designed to allow cars to traverse various terrains, to be robust and have a long life. They have a shore hardness of approximately 70A [29] and for this reason it was desirable to have a shore hardness close to this value. Samples of polyurethane with that shore hardness in addition to shore hardnesses of 30A and 60A were obtained from various companies and the traction they provided, when tested on flat surfaces of pavement, carbon steel and various smooth and rough woods was tested and compared. It was established that the shore hardness that provided the most appropriate traction, yet still offered some form of cushioning was 60A.

7.3. Feet Profile

The size and shape of the timing belts, as well as the fully assembled robot's ability to fit through the 24" equilateral entry triangle, greatly influenced the overall size that the tread could have. The belts mainly bent between the teeth and the toothed sections stayed rather rigid. Therefore it was decided to attach feet only on the other side of the toothed sections. This particular configuration limited the maximum width a tread foot could have to the width of a tooth of the belt. The dimensions of the belt are illustrated in Figure 7.5.

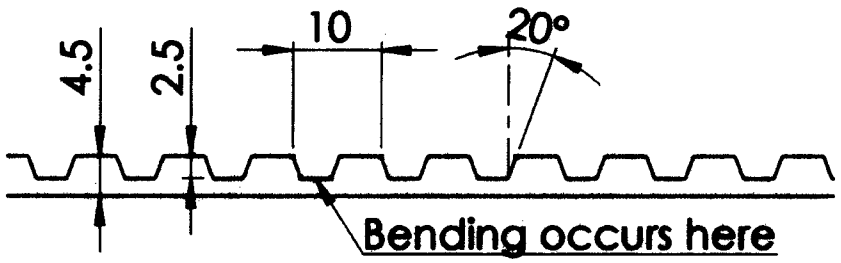

Figure 7.5.: Dimensions of a timing belt and joint area that facilitates the bending of the belt.

The profile of the track feet was initially envisioned to be round or curved, as depicted in Figure 7.6, as this would allow for smoother motion of the rescue robot than square feet could provide. Several companies were asked if they could produce such pieces of PU or at least cut a rectangular piece into a round or curved shapes and they either did not have the means to do so or it turned out that it would cost a substantial sum of money.

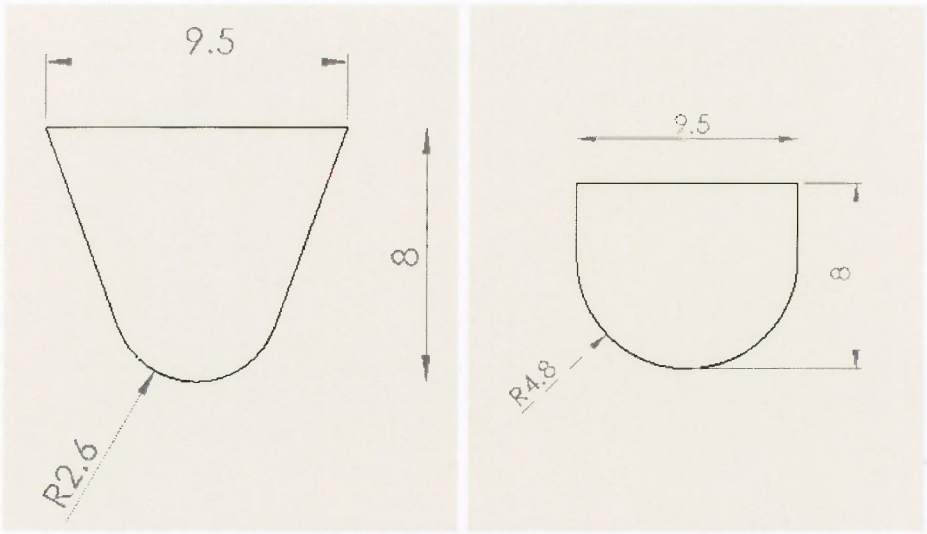

(a) Triangular profile with round apex. (b) Rectangular profile with round apex.

Figure 7.6.: Initial profile designs for the feet.

Thereafter it was attempted to manufacture teeth with this profile in-house, however, this soon proved highly impractical without having access to equipment that timing belt manufactures use. The closest shape to that of a curved profile that could be produced in a practical way was that of a trapezoid; the same shape as the timing belt's teeth. A concept of this track foot profile on a timing belt can be seen in the Figure 7.7. The angles of the corners were chosen to be 70°, the same as those of the track's teeth. This angle allowed for both the side of the foot that makes contact with the terrain and the side that would be attached to the track to have decent contact areas. A method of manufacturing the **TPU** components like this had to be developed, but before examining how this would be done, it was necessary to establish a suitable tread layout, because this would determine the number of required feet.

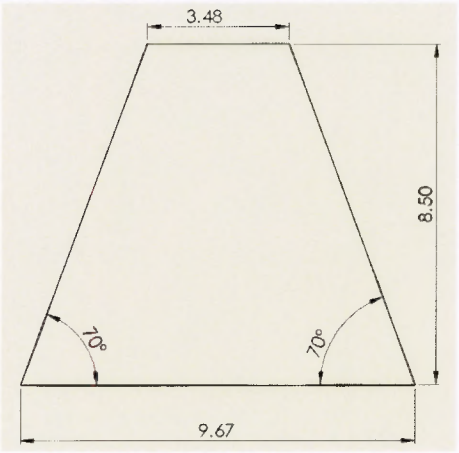

Figure 7.7.: The trapezoidal profile that was chosen for the track feet.

7.4. Layout

It was decided that the pattern should resemble the conventions used by other rescue robots that have wide tracks. After some research, as discussed in Chapter 2, it was discovered that **UGVs** with wide tracks commonly had patterns consisting of larger feet at the outermost sections of the tracks and shorter feet at the innermost sections. This configuration allowed the robot to move adequately while preventing debris from getting stuck in the undercarriage of the base. And additional benefit of such designs is that they greatly reduce the chances of beaching the platform on its underbelly.

For **Ratel** three distinct rows of teeth per driving track were chosen. The outermost row would have the largest feet were designed to be 8.0mm high, the middle row's 5.0mm and the innermost 3.0mm. Initially only the outermost and the innermost rows would be attached and the system would then be tested this way. The middle row would not be added, should the tracks perform adequately without it, so as to refrain from adding unnecessary weight to the tracks. The sizes were chosen in such a way that the feet could be as large as possible, while still allowing **Ratel** to have a cross sectional area smaller than that of an entry triangle. The heights of the three feet are depicted in Figure 7.9. As discussed earlier, the large timing belts have 161 teeth and are 1610mm in circumference. A uniform layout for the feet that would be attached would require uniform spacing between successive feet. The largest number that 1610 can be divided by and produce an integer is 70. Thus $1610 \div 70 = 23$ and therefore it was ultimately decided to have each one of the three tread rows to contain 23 teeth evenly spaced at 70mm. A section of a belt with the feet attached to it had been modelled and is depicted in Figure 7.8 and Figure 7.9. Even though 730, the circumference of a small belt, produces a non integer value of 10.42857 when divided by 70, the same spacing of 70mm can be used if only 10 feet were added.

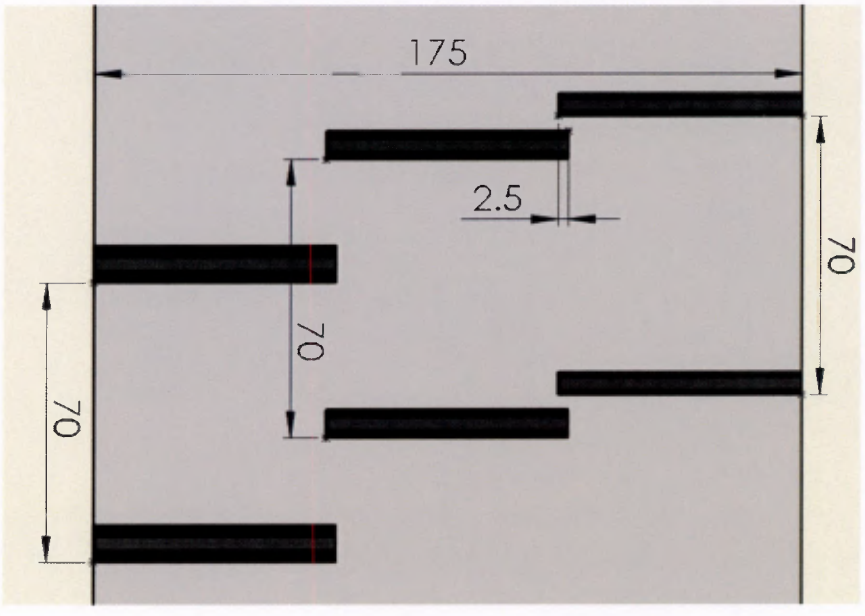

Figure 7.8.: The top view of the drive track's feet layout.

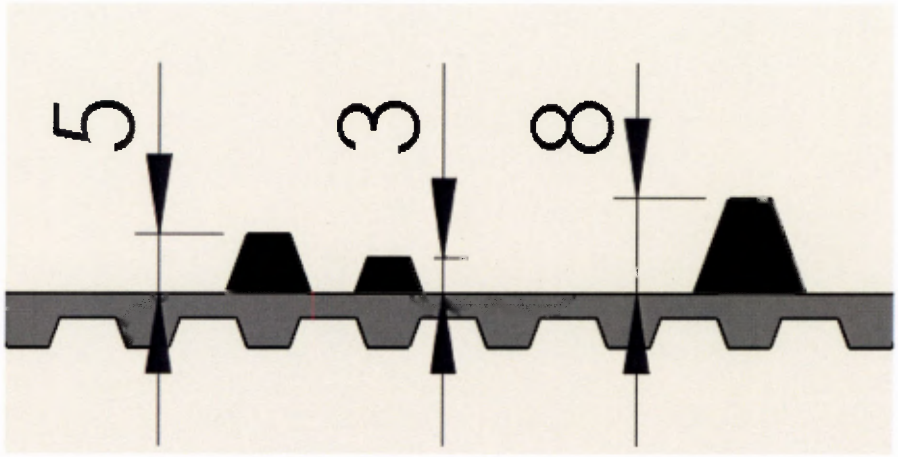

Figure 7.9.: The side view of the drive track's feet.

7.5. Manufacture of Feet

After the required dimensions were chosen, it was time to manufacture these components. Only three methods of producing the required dimensions of **TPU** were considered, due to the limited ways in which this particular task could be accomplished in the facilities of **UCT's** mechanical engineering workshop. The three methods were moulding, hot wire cutting and band saw cutting of feet.

7.5.1. Moulding

Moulding was considered, as this method would have permitted the creation of feet to specific dimensions. It had to be ensured that the final material could be attached to the tracks, possibly through solvent adhesive bonding. The search for a fitting material that could be moulded was unsuccessful and therefore this method abandoned.

7.5.2. Hot Wire Cutting

The second attempted method of producing feet was hot wire cutting. Initially the feasibility of how effective cutting **TPU** this way had to be established. Should this have proven to be an effective procedure, a rig would have been designed and constructed to cut feet into the required shape. The deciding factors were the finish of the cut surfaces and the amount of time it took to produce a tread foot.

Nichrome wire was attached to the leads of a power supply and the current limit and voltage were varied until the wire was hot enough to cut through the material. This procedure was repeated several times, with the numerous **TPU** samples that were collected from various vendors. Even though using this method the polymer could be cut quickly, easily and allowed one to produce intricate shapes, the finish of the cut material was very coarse, as can be seen in Figure 7.10. An additional disadvantage was the release of fumes detrimental to one's

health and therefore this too was considered and impractical method, especially because 178 feet would have to be manufactured this way.

Figure 7.10.: The rough surface finish as a result of hot wire cutting.

7.5.3. Band Saw

The final procedure for manufacturing that was analysed, was using a band saw to cut rectangular polyurethane sheets into the desired trapezoidal shapes. This method yielded a smooth and aesthetically pleasing finish and took little time to do. It was thus decided to produce the feet this way. The next two figures present **TPU** components after they had been cut with a band saw.

Figure 7.11.: The smooth surface as a result of a TPU component being cut by a band saw.

Figure 7.12.: A TPU sample cut with a band saw.

Four **TPU** sheets were ordered from **Specialised Mouldings**. For the large feet, the dimensions of the sheet were 8mm x 60mm x 300mm, while the dimensions for the small feet were 3mm x 60mm x 300mm. The sheet for the flipper feet had the dimensions of 3mm x 32mm x 300mm. With the intention of repeatedly cutting the feet in an efficient and accurate manner, a cutting jig had to be designed that would hold and position the sheets of polyurethane the same way each time for cutting procedure. The jig consisted of a base where a single polyurethane sheet would rest. Two L-shaped plates could be screwed onto the base and held a sheet in place on either side so as to stabilise it during cutting procedures. Even though the brackets stabilised a sheet, they still allowed the sheet to slide forward and backward. This configuration is depicted below in Figure 7.13. The brackets had two separate positions in which they could be attached to the base plate.

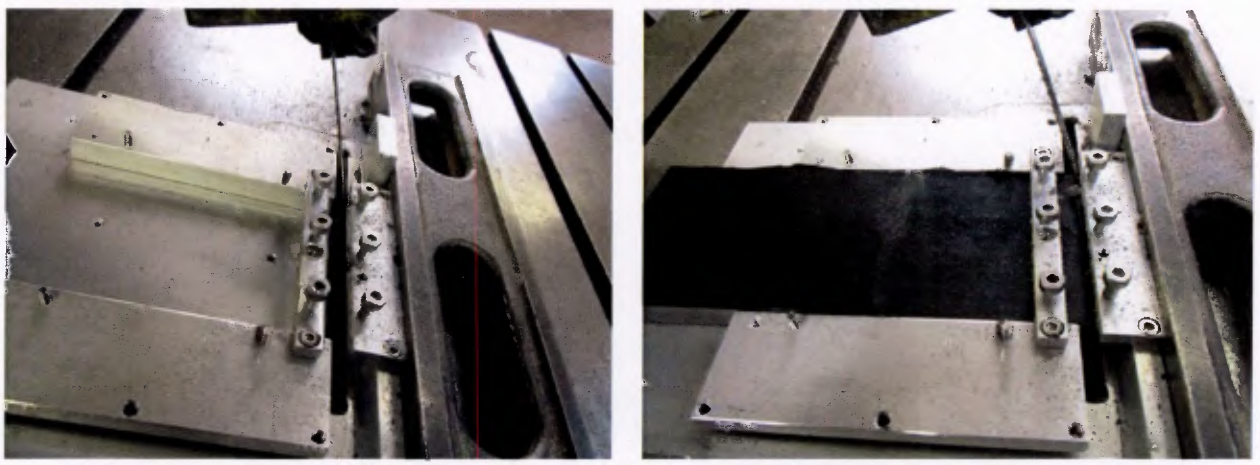

(a) Cutting jig on the band saw table.

(b) Large sheet clamped by the cutting jig.

Figure 7.13.: The cutting jig before and after the insertion of a TPU sheet.

The base plate was designed in such a way that the brackets would have three distinct configurations. The first configuration allowed the brackets to laterally stabilise a large sheet while track feet were being cut out of it, as can be seen in Figure 7.13. The second configuration had the brackets positioned 32mm apart from other, so that the flipper sheet would be laterally supported during cutting. The third and final configuration allowed them to support a sheet

from the top and laterally from a single side so that its width could be reduced with the band saw, as depicted in Figure 7.14.

Figure 7.14.: The third configuration of the cutting jig.

A small section held the end of each sheet with M3 screws, while a single side of the sheet rested against a shoulder that was angled at 70°. The band saw passed through a slit that was machined into the base of the cutting jig.

During cutting the rectangular sheets, one first had to have one side cut at a 70° angle so that this side could fit onto the angled shoulder of the base. This was achieved by tilting the band saw's cutting bed to 20° as shown in Figure7.15. Once the first side was done, the sheet was flipped and a tread was cut. Thereafter the sheet was flipped each time to cut a tread. Figure 7.16 depicts the final product that was produced using the band saw cutting method.

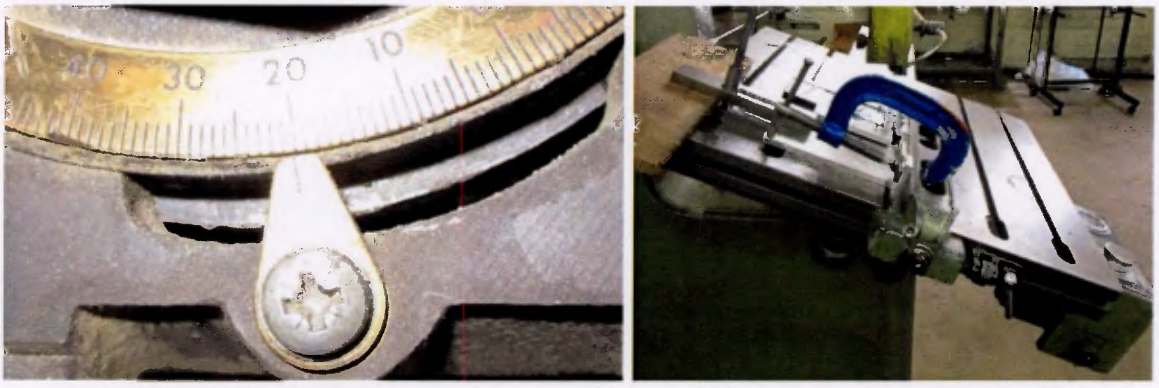

(a) the band saw's dial is set to 20°. (b) The band saw's bed at 20°.

Figure 7.15.: Cutting the sheets at the right angle.

Figure 7.16.: The produced feet.

7.6. Attaching Feet

After a method of economically and efficiently manufacturing the feet was discovered, work stated on finding a way of sufficiently attaching them onto the timing belts. The methods that were considered and used are described in the following sections.

7.6.1. Solvent Bonding

Solvent bonding was also tested because of this method's simplicity including the added advantages of being fast, economical and result in strong bond strength. **TPU** is a polar compound and is thus soluble in polar solvents [30].

7.6.1.1. Alcohols

Alcohols, such as ethanol and isopropanol can cause **TPU** to swell between 15%-30%, but do not fully dissolve the material [30]. Alcohol was applied to separate **TPU** sheets were then pressed together for an extended period of time. When examined, the sheets came apart when relatively little force was applied to move them apart. There was no visible evidence of tearing having taken place on the surface and thus it was concluded that no actual bonding took place, deeming alcohols insufficient for this task.

7.6.1.2. Ketones

Ketones such as **M**ethyl **E**thyl **K**etone (**MEK**), acetone and cyclohexanone and aliphatic esters such as ethyl acetate are supposed to be capable of partially dissolving **TPU**[30]. They were difficult to get a hold off and as such the only ketone that was tested on the **TPU**

components was acetone. It had no discernible effect on the material and did not lead to any form of bonding.

7.6.2. Esters

The organic compound ethyl acetate was the only ester that was tested for solvent bonding. Bonding was attempted by applying ethyl acetate on clean surfaces of two pieces of **TPU**. The surfaces with the ester were then pressed together and held tight with a G-clamp for 2 days. After this period of time had expired the G-clamp was removed and the bond was tested by prying it apart. Initially the components appeared to have been successfully bonded, but they came apart with more forceful prying. If a bond was actually formed, then the surface would have shown tearing, but there was no discernible change in the surface. It appears that ethyl acetate only managed to swell the **TPU**.

7.6.2.1. Polar Organic Solvents

TPU is soluble in highly polar organic compounds, such as **tetrahydrofuran (THF, C_4H_8O)**, **dimethylformamide (DMF, C_3H_7NO)** and **N-methylpyrrolidone (NMD, C_5H_9NO)**. This process can be explained through the chemical rule of thumb "like dissolves like" [30], which in essence states that solutes dissolve very well in solvents that have similar chemical structures to themselves.

The only solvent that could be attained for testing at the time for various reasons was the aprotic solvent **DMF**. The solvent was applied on clean surfaces of two **TPU** components. These components were then pressed together with a G-clamp and placed on a table in an open area. The clamp was left on for a predetermined period of time to allow the **DMF** to fully evaporate.

The compound was tested with various clamp pressures with several evaporation periods on a number of polyurethane timing belts. The temperature was also varied during later tests, to see if heat would make a difference in the solvent's evaporation time.

The timing belts that act as the tracks for the rescue robot, as well as the belts for bonding tests were attained from the from the same supplier that provided the T10 belts for the tracks.

This method proved to be successful and the bonds could not be broken, instead the parent material was torn when attempting to separate them while holding them with G-clamps and pliers. The effects of such attempts are depicted in the next figure.

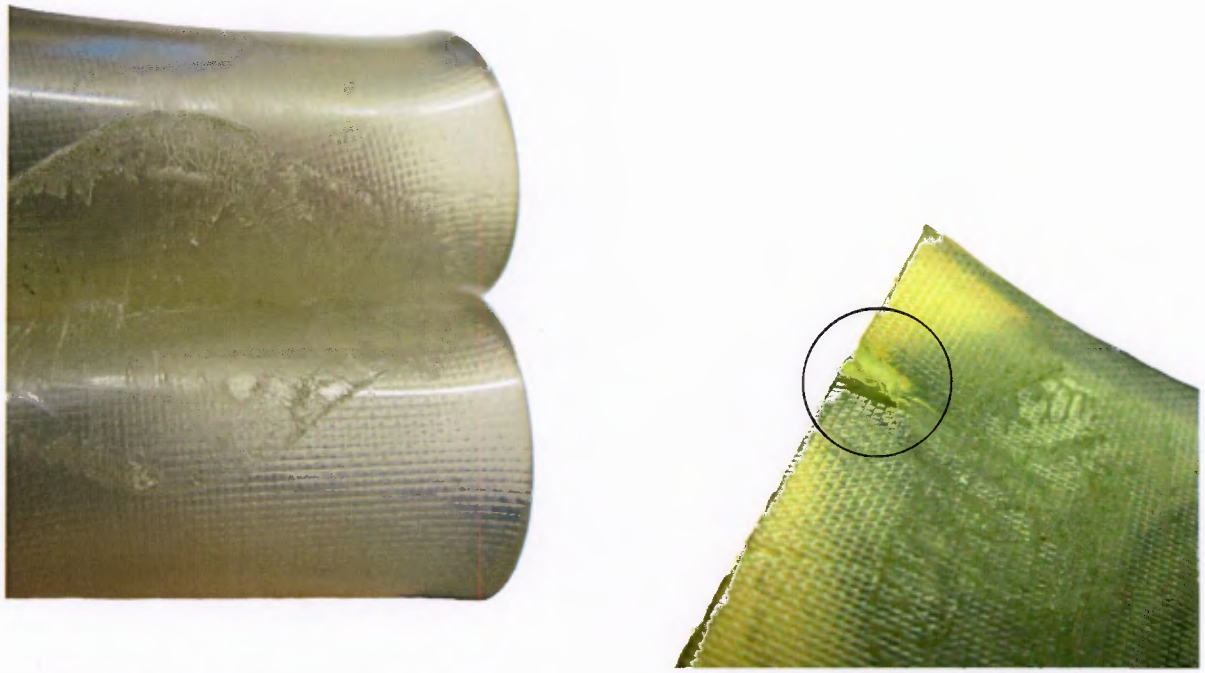

(a) The tearing that can be seen on the surface is an indication of successful bonding.

(b) The parent material ripped before the bonded section during a pull test.

Figure 7.17.: Evidence of successful and strong solvent bonding.

It was ultimately not chosen, because when it was finally tested on the tracks it took approximately four days before effective bonding was achieved. The reason for the time being longer than when it was tested with the other **TPU** components is that the belt was probably made from a different **TPU** grade.

7.6.3. Adhesive Bonding

Two different products were used for adhesive bonding, namely Bondstick and super glue. These products were chosen because Bondstick was designed to glue polymers together, whether the components were of the same material or not; super glue was chosen, because it is a very versatile agent.

7.6.3.1. Bondstick

The bonding using Bondstick procedure involved adding the bonding agent to the sections of the feet and the belt that were to be attached together. The components were then left alone for a while to allow the agent to solidify. After 30 minutes the glueing procedure was commenced. A hot air gun was used to apply heat onto the timing belt and the tread sections that had the glue on them. The tread was then carefully placed on the belt and aligned properly. Adequate pressure was placed on the tread for a while. This procedure was repeated

for the rest of the treads. Once the outermost row was completed the tracks were left to cure for three days before adding the second row.

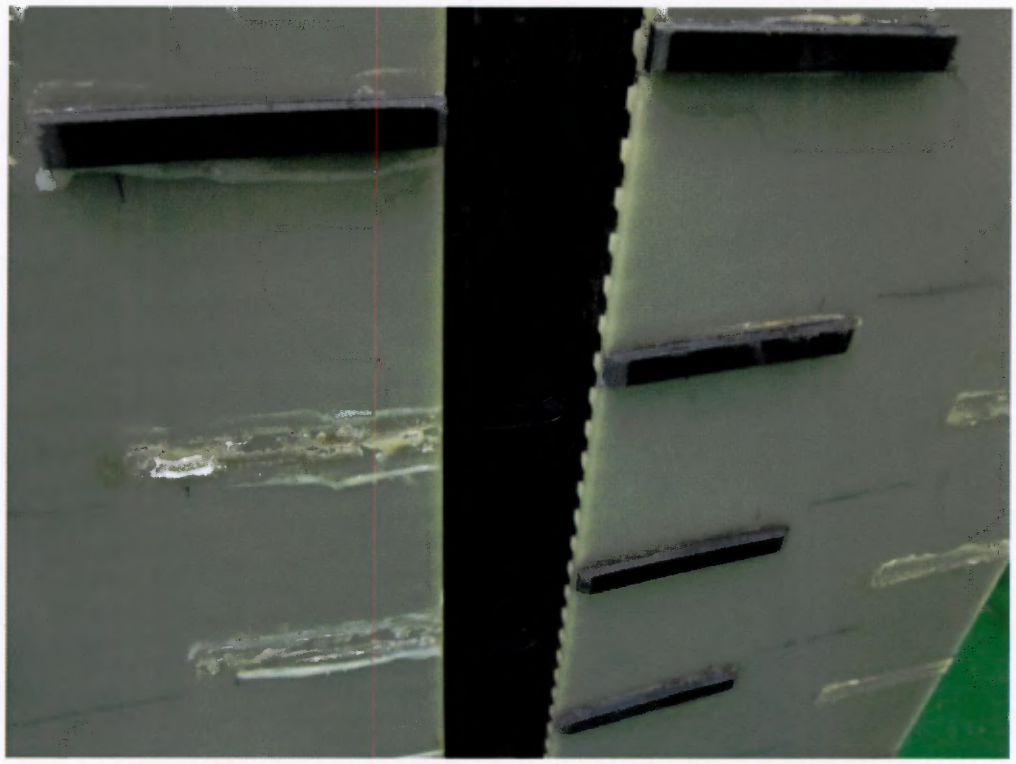

Figure 7.18.: Feet missing from drive tracks after some driving.

The bonds initially seemed to be reliable, but nearly all of them failed after driving the base for a while, especially when climbing stairs or pulling loads. Gradually more feet either became loose or fully detached from the tracks, as is illustrated in Figure 7.18. There was no tearing visible in the materials upon examining the surfaces were the bonds failed, which indicates that the glue was not adequate for the task.

7.6.3.2. Super Glue

After the glue from Bondstick was deemed insufficient it was decided to examine the glueing potential of super glue. This was done by removing the feet that were attached to the tracks using Bondstick glue and removing the remnants of the glue from both the tracks and the feet. Thereafter the super glue was placed on the feet, which were positioned properly and pressed against the tracks. Once all feet had been attached the tracks were left to cure for 3 hours. After testing the tracks by driving the platform around and making it climb stairs for several hours without having any feet detach, it was determined that super glue sufficiently attached the feet to the tracks.

An added benefit to using super glue instead of the glue from Bondstick was that no heat had to be added during bonding and the curing time was exceedingly shorter. The overall gluing procedure was simpler and the outcome was aesthetically more pleasing. In general, the gluing procedure was the simplest among all the methods that were used.

7.6.4. Bonding Jig

A jig was designed in order to allow the feet to be repeatedly glued at even spacing in a consistent manner. It consisted of two Aluminium components. One component was a rectangular, 23 mm thick plate that had teeth machined onto one side that had the same dimensions as those of the T10 timing belts. This was done, so that the belt could be held in place. A 6mm diameter dowel pin was inserted in each of the corners of the bottom plate. In order to lift the plate of the ground while a belt rested on it, four M8 hex bolts were screwed into the corners on the flat side of the plate. Screwing the bolts in further would lower the plate and screwing them out would have the opposite effect. Since the belts formed a loop, raising the plate was an easy method of allowing the belts to rest on it in an unobstructed way. The toothed plate can be seen in Figure 7.19.

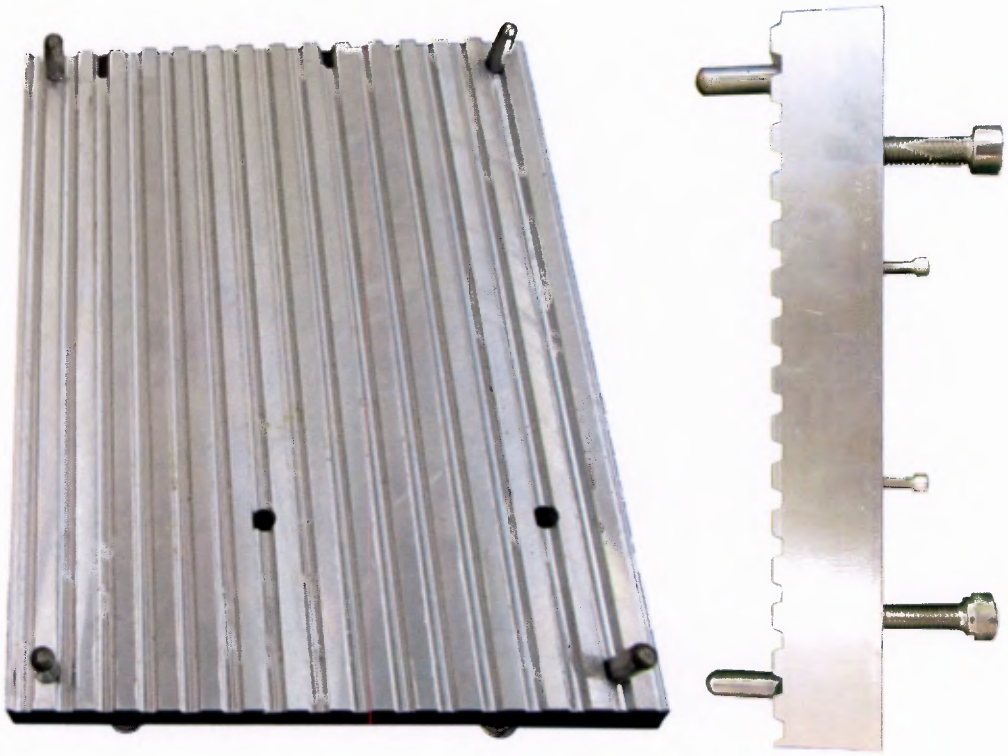

Figure 7.19.: The bottom plate of the clamping jig.

The second component was a 8mm thick plate that fit on top of the bottom plate and belt assembly. Four holes were in each corner of the top plate, corresponding to the positions of the dowel pins in the bottom plate. These were used to guide it onto the bottom plate. Three rows consisting of two rectangular holes that had the dimensions of the **TPU** feet that were to be glued onto the tracks were machined into the top section of the bonding jig. The holes in a single row were spaced 70mm apart, were used to precisely position the feet during gluing. Since it was desirable to be able to place the feet with one's fingers, grooves were machined around the holes to add space, as can be observed in Figure 7.20. The glueing sequence for a drive belt is depicted in Figure 7.21.

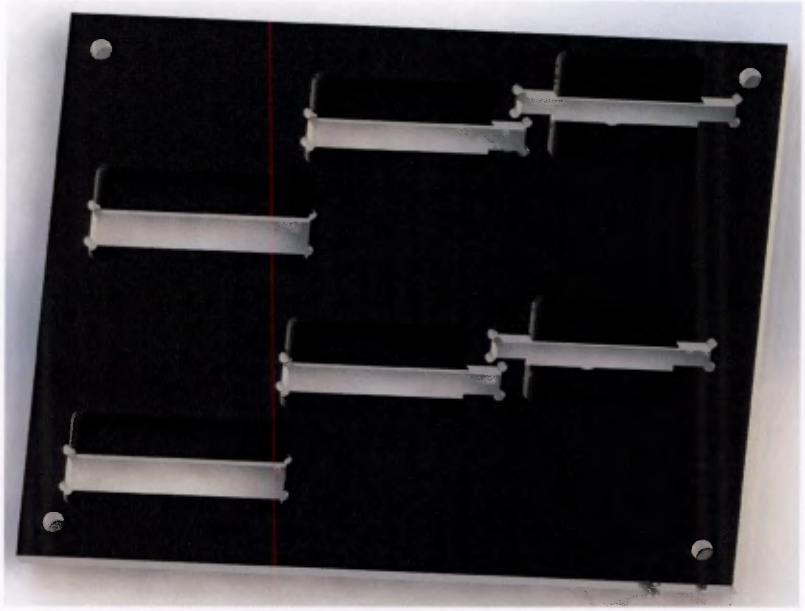

(a) A rendered CAD model of the top plate.

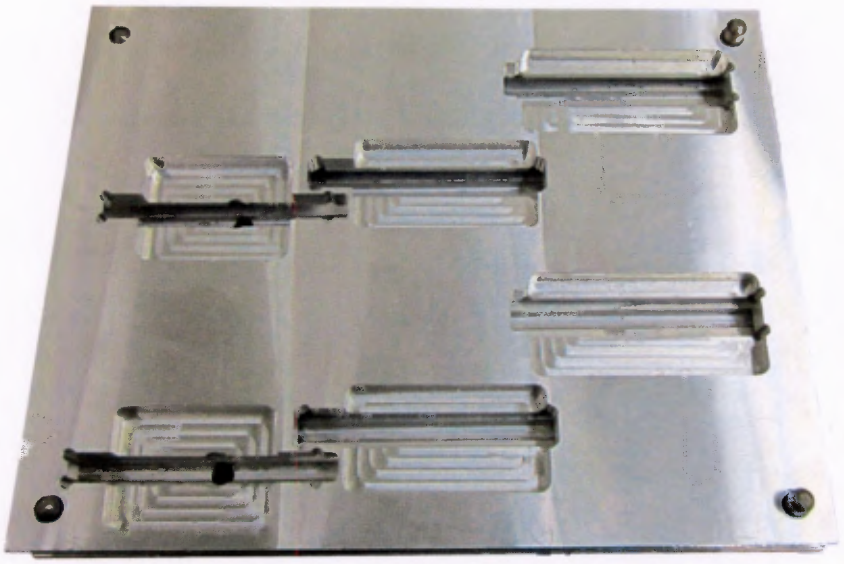

(b) The top view of the assembled clamping jig without a belt.

Figure 7.20.: The top clamping jig.

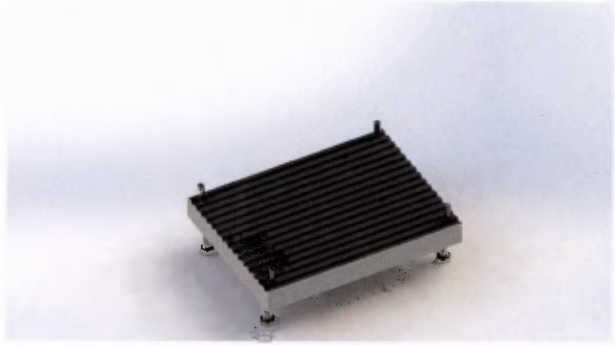

(a) Bottom Plate.

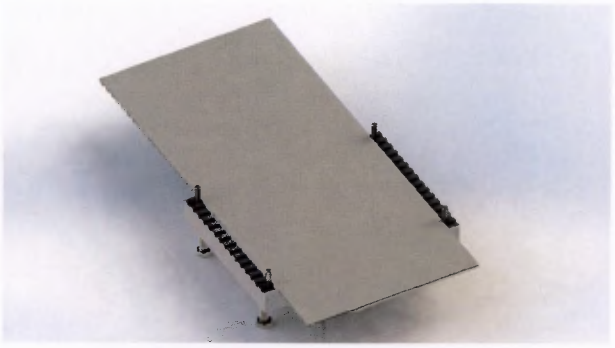

(b) A large belt is placed on the plate.

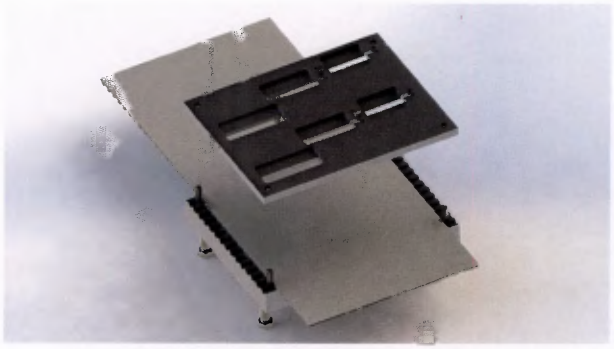

(c) The top plate is positioned.

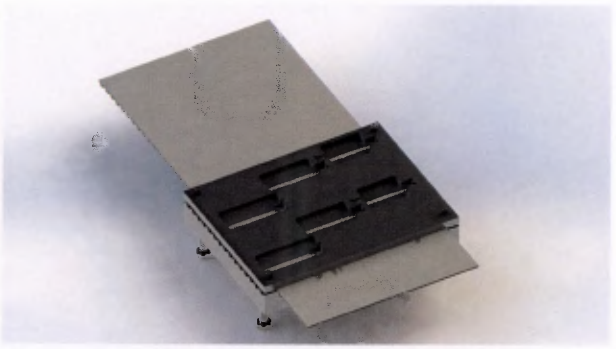

(d) The top plate is placed on to the belt.

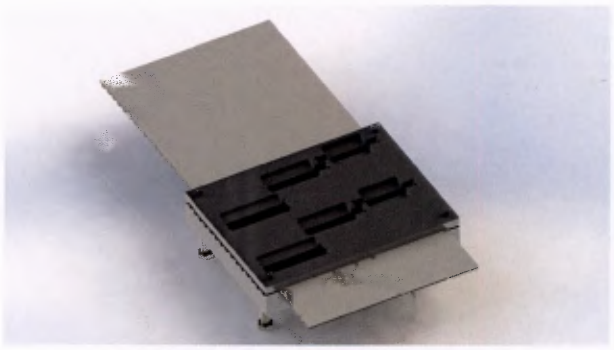

(e) The feet are glued onto the belt.

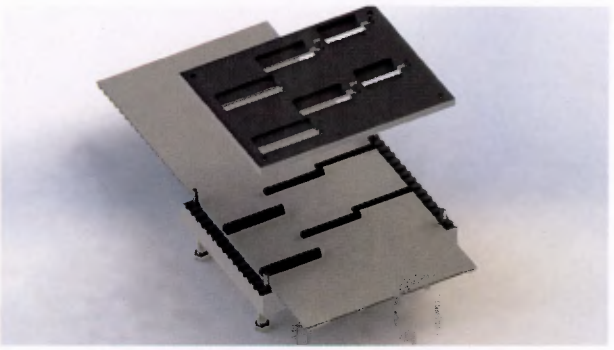

(f) The top plate is removed.

Figure 7.21.: Glueing sequence of a large belt.

The bonding jig was also used when gluing the flipper tracks. 6mm diameter steel dowel pins positioned 35 mm from the pins in the corners provided a 32mm gap for the flipper belts, as is illustrated in Figure 7.22. The same steps shown in Figure 7.21 are followed. The final tracks were thus produced by using the bonding jig and superglue to attach the tread to the timing belts. The final tracks can be seen in Figure 7.23.

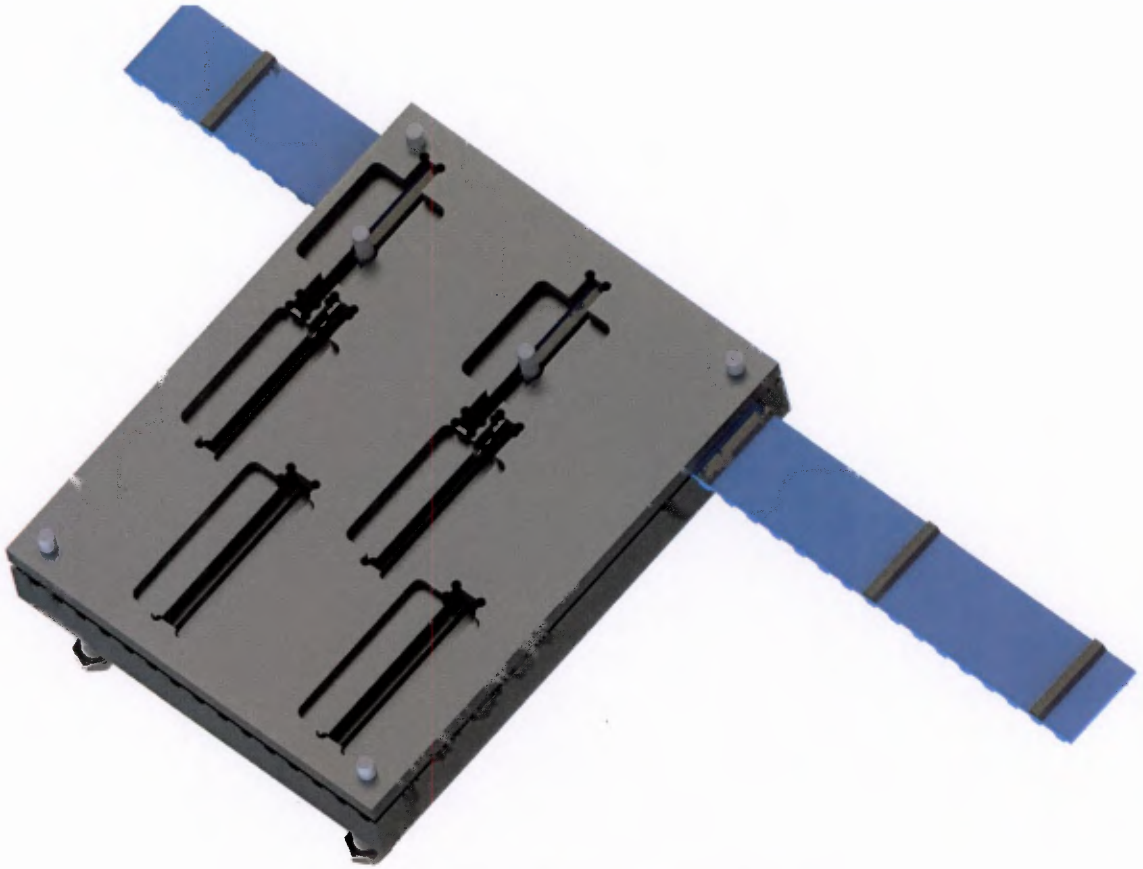

Figure 7.22.: Flipper belt feet glueing.

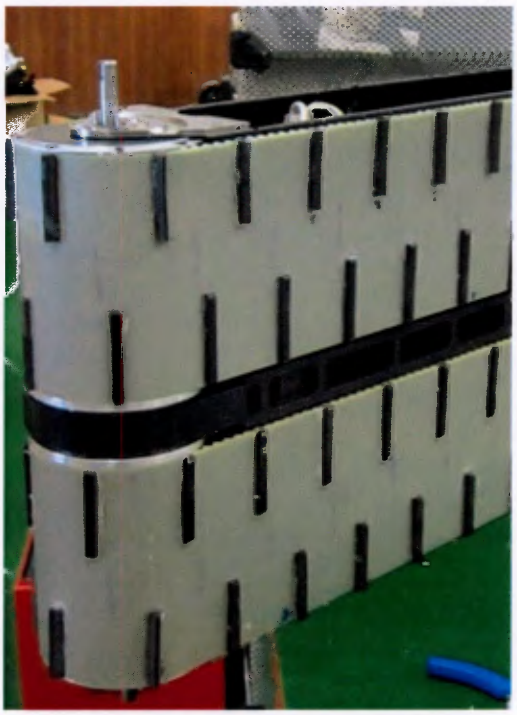

Figure 7.23.: The final tracks.

7.7. Summary

Through the use of the cutting jig track feet could be consistently produced to specific dimensions. This method proved to be fast and reliable and it added safety to the cutting operation, because the **TPU** sheets were not held by hand. Its configurations allowed the manufacture of the three different sized feet, without the need of additional components. The clamping jig enabled the gluing of track feet onto the timing belts in a consistent manner.

The subsequent section will examine the communications and control system that made the motion possible.

8. System Control and Communications

8.1. Software System Overview

The software system was greatly influenced by the need to provide a system capable of tele-operation. Even though many aspects overlap, the software and control system can be broken down into three distinct layers, namely the user interface layer, the communications layer and the control layer. An illustration of the the three layers can be seen in the next figure and a brief description of each layer follows in the subsequent sections. For a more detailed description of the upcoming section, see the commented code on the accompanying CD. The three layers can be seen in Figure 8.1.

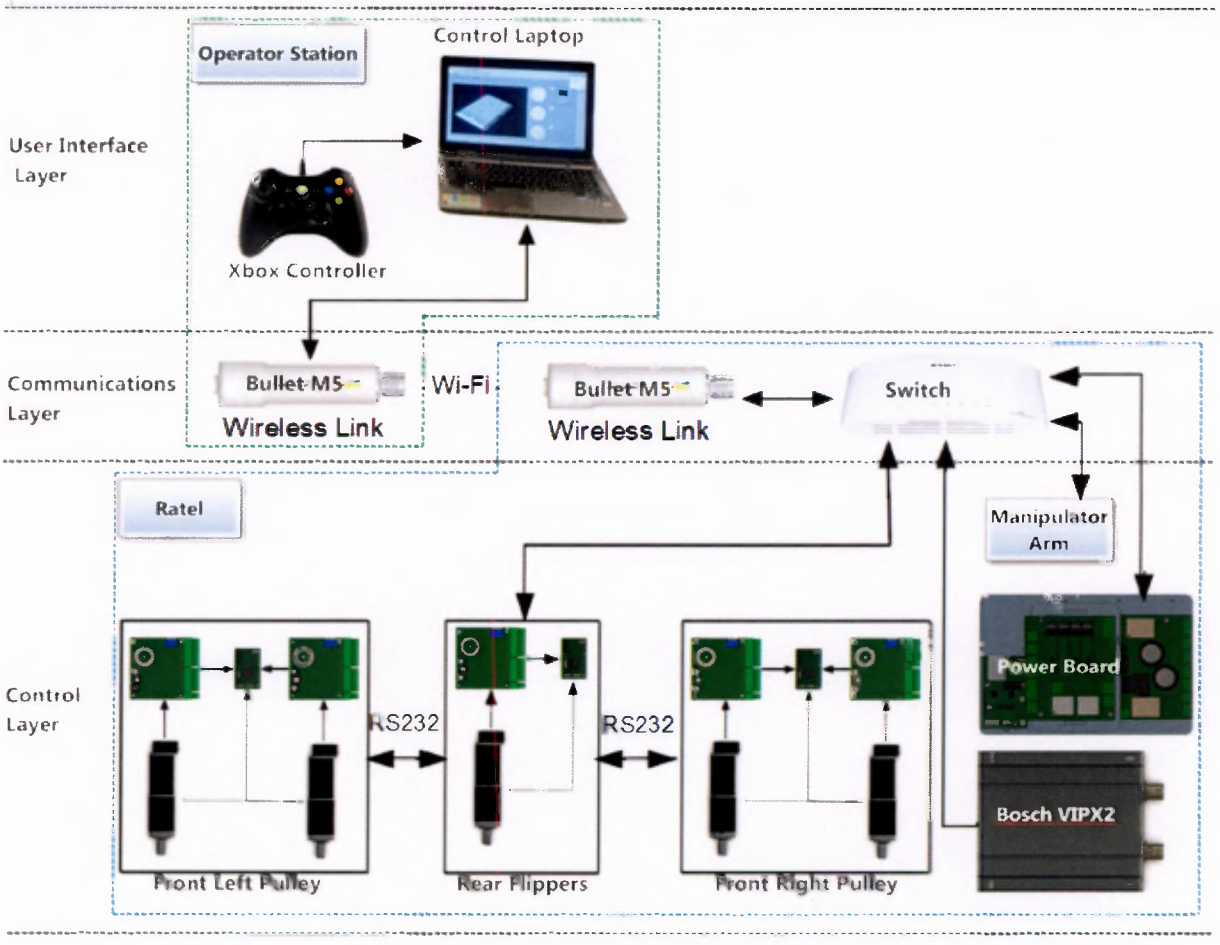

Figure 8.1.: Layout of the platform's communication structure.

8.1.1. The User Interface Layer

This user interface layer facilitates the interaction between the user and the robot. Paramount to the task is the operator's ability to effectively use the **UI**. The interface was designed to be intuitive, so that it required little time to learn how to use and understand it. Care was taken to create a clear, consistent and simple user interface that is fitting to the task. The following elements constitute the user interface layer:

1. An Xbox controller for game-like interaction with the platform
2. Real-time video feed from the front, rear and **HD** cameras
3. Current sensor information
4. Light bridge and hall effect sensor feedback to indicate the end-stop of the flippers
5. Pitch, Roll and Yaw of the **UGV** is provided graphically in the form of a model of the platform
6. 3-Axis acceleration data and temperature indicator
7. Lighting and power board controls as well as the battery **SOC** values
8. Speed setting and indicator for drive tracks and flippers
9. Calibration and control buttons
10. Indication of established communications link

The Interface is split across two 15.6" monitors. One screen displays the camera feeds, while the motion controls and other functionality are available on the second monitor. There is enough space on a single monitor to display all parts of the **UI**, but two monitors were chosen so that the video feed windows could be large on a screen that is dedicated to showing video feeds. The next four figures depict various aspects of the user interface.

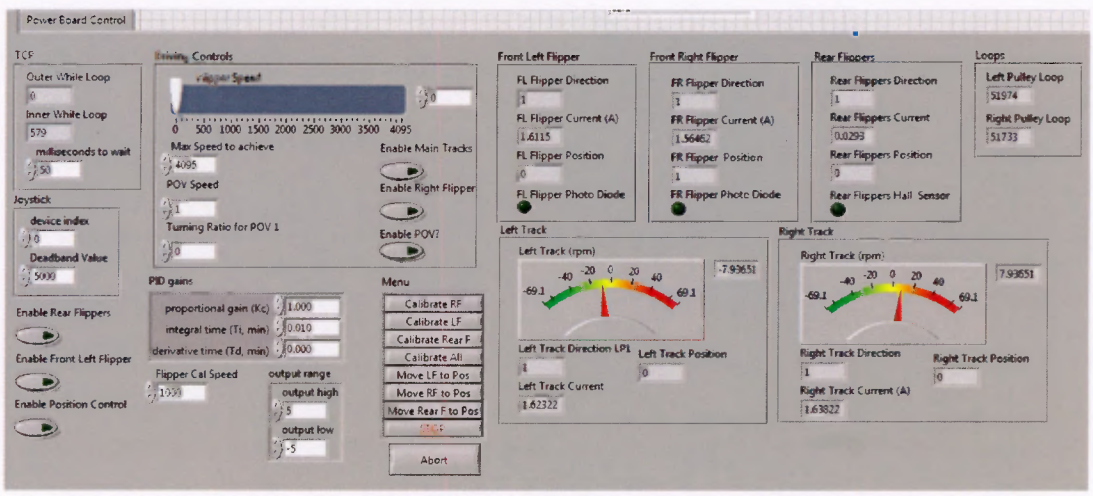

Figure 8.2.: Control tab of the platform.

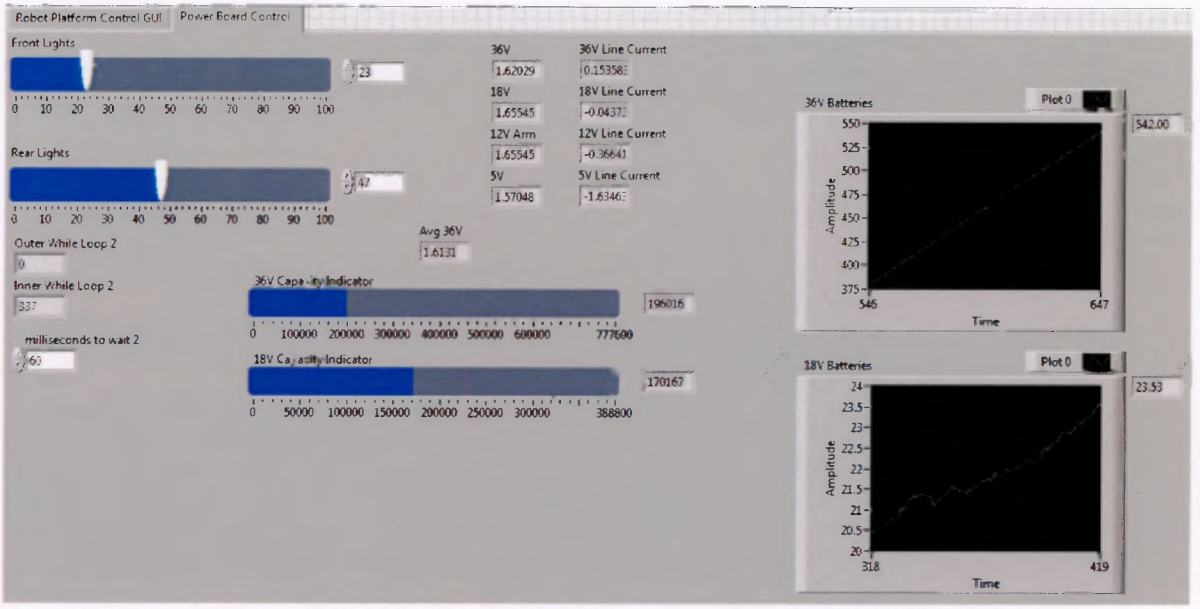

Figure 8.3.: Control tab of the power boards and lights.

Figure 8.4.: Front and rear camera feeds while driving.

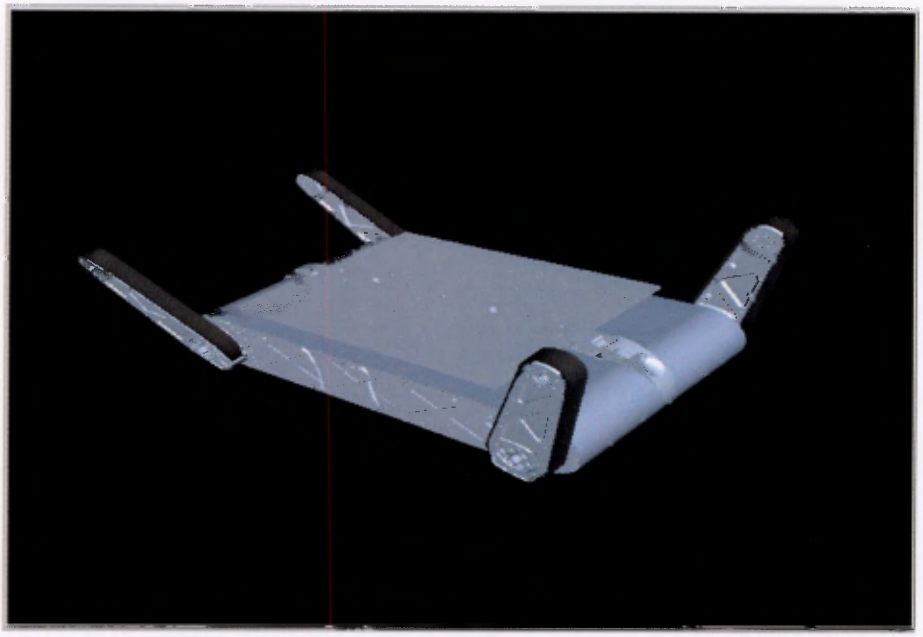

Figure 8.5.: The 3D model of the platform in **LabVIEW** produced with the Xsesns MTi.

All motion was controlled with an Xbox controller. One of the reasons why this controller was specifically chosen, was because it is ergonomic and would be comfortable to use for extended periods of time. It additionally had several buttons and two analogue sticks, which was considered useful should there be an expansion of the system. The controller and the function of each button are depicted in Figure 8.6.

Figure 8.6.: The Button Configuration of the Xbox Controller, modified from [31].

8.1.2. The Communications Layer

The bandwidth needs of the communications system were expected to be large, seeing that multiple video streams had to be supported and low latency was essential to ensure real-time teleoperation. Initially Ubiquiti RouterStation Pro wireless radios were used, but the wireless

link they produced was very unstable and unreliable. They were replaced by a pair of 600mW Ubiquiti Bullet M5 radios. The one on the operator station was configured as the station, while the other took on the role of the **a**ccess **p**oint (**AP**). As per **RoboCup Rescue** rules , the TCP/IP protocol used for wireless communication is 802.11a [10]. One of the wireless radios can be viewed in Figure 8.7. A closer look of a Bullet M5 radio can be seen in Figure 8.7.

Figure 8.7.: A Ubiquiti Bullet M5 wireless radio.

The laptop that runs the control station's code has a direct wireless link to a number of the robotic platform's subsystems. The links between the wireless radio on the **UGV** and its various electronic devices was achieved by connecting them all to the Ethernet plugs of the D-Link 5-port Desktop Gigabit switch. Initially a 5-port Trendnet 100 Megabit switch was used, but it turned out that it could not route the traffic properly and thus it was replaced by the D-link switch. Both switches are depicted in Figure 8.8. The following devices were connected to the switch and thus had a direct wireless connection to the operator station's laptop:

- The Bullet M5
- The LM3S8962 microcontroller that controls the rear flippers.
- The Bosch VIPX2 provides rear and front camera feeds.
- The LM3S8962 microcontroller controller that controls and communicates with the power distribution system.
- The manipulator arm assembly

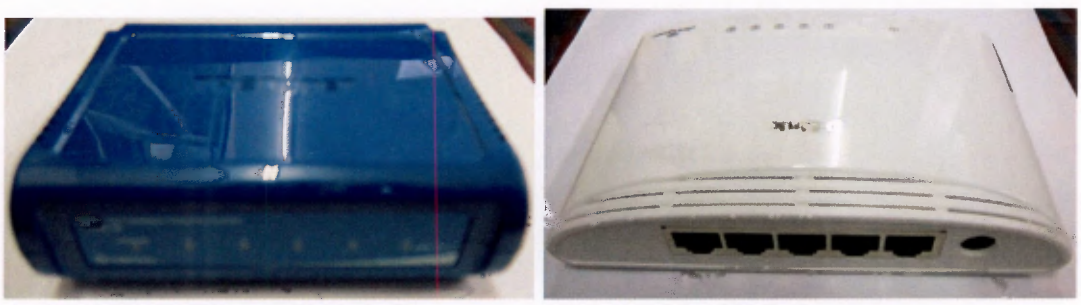

(a) The Trendnet switch. (b) The D-Link switch.

Figure 8.8.: The two switches.

This configuration is also depicted in Figure 8.1. During testing the manipulator arm was not always required and thus its slot on the switch went to a **HD** camera, that can be seen sitting on top of the platform in Figure 8.9.

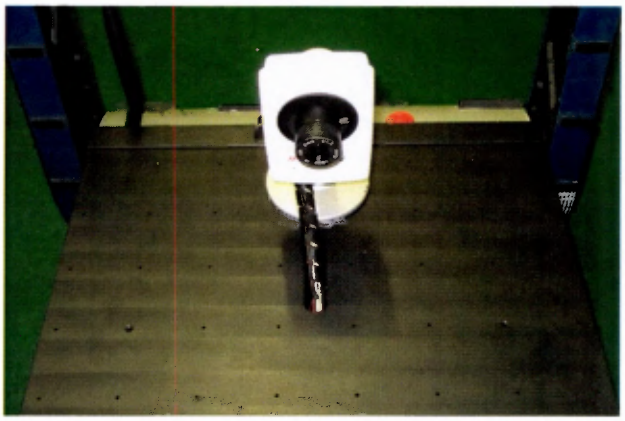

Figure 8.9.: The HD camera

As previously discussed, **I2C** had been chosen to be the primary communications protocol for all of the robot's wired communication and the task of accomplishing this was given to MSc student Bradley Springer. After rigorous testing, it was determined that this protocol was inadequate for the task. The protocol was not sufficiently robust as a result of inherent low voltage problems due to the length of the communication wires. Henceforward, the RS232 protocol replaced I2C. This serial protocol was chosen, because it proved to be significantly more stable. The protocol is asynchronous, and as a result **LabVIEW** code was written that implements **t**he **p**oint-to-**p**oint **p**rotocol (**PPP**) to ensure the correct transmission of data via the serial link.

The LM3S8962 microcontrollers of the drive pulleys are wired to the one governing the rear flippers via RS232. This allows a single Ethernet connection to be used to control all motion. The rear microcontroller receives a transmission of data from the control station. It divides the package into three sets of data, namely data for the rear flippers and data for two the front drives. The microcontroller then sends the appropriate control commands to the speed controller of the rear motor and transmits the rest of the data to the front drives via RS232. They in turn send the appropriate control commands to their respective speed controllers. While operating the robotic platform and using wired TCP/IP communications the platform was pigged and which indicated an average time of 3ms and a maximum time of also 3ms. When pinging the platform during wireless operation the average time was 3ms and the maximum time was 4ms. These values did not change even over the largest tested distance. This time indicated the amount of latency that was experienced. The link quality was constantly monitored using the software of the wireless radios and it was shown to be excellent. The following table shows the data packet that is sent to the rear flipper and via the wireless TCP/IP link. The table that follows shows the 35 data packet that is sent by the laptop. In the table, the booleans are the enable, stop and direction signals.

Table 8.1.: 35 Byte Packet sent from the Control Station to the Platform.

Byte Nr	1-4	5-7	8-11	12-14	15-18
	Left Track Speed	Left Track Booleans	Right Track Speed	Right Track Booleans	Left Flipper Speed
Byte Nr	18-21	22-25	26-28	29-32	32-35
	Left Flipper Booleans	Right Flipper Speed	Right Flipper Booleans	Rear Flipper Speed	Rear Flipper Booleans

During operation data collected by the front microcontrollers of the front pulleys is sent to the rear LM3S8962 controller, again via RS232. The rear controller makes a new data package out of the packet received from the front drives and out of the information about the rear flippers that it gets. The new data packet is then sent to the control station via Ethernet and is interpreted there. Table 8.2 portrays the 91 byte data packet that the operator station received from the LM3S8962 of the rear flippers.

Table 8.2.: The 91 Byte Packet received from the Platform.

Byte Nr	1-40	41-48	49-50	51-54	55-58	59-62	63-66
	All Current Readings	Loop Iterations	Front Flipper LEDs	Left Flipper Direction	Left Flipper Position	Left Track Direction	Left Track Position
Byte Nr	67-70	71-74	75-78	79-82	83	84-87	88-91
	Right Flipper Direction	Right Flipper Direction	Right Flipper Direction	Right Flipper Direction	Rear Flipper Hall Signal	Rear Flipper Direction	Rear Flipper Position

Data to and from the microcontroller that control the power distribution only involves Ethernet. Table 8.3 shows the data packet that it receives from the PC. The PC receives a 36 byte string that makes up the current readings of the four voltage lines of the power board.

Table 8.3.: The 6 Byte Data Package that the Power Board's Microcontroller receives.

Byte Nr	1	2	3	4	5	6
	Toggle 36V Line	Toggle 18V Line	Toggle 12V Line	Toggle 5V Line	Front Lights PWM	Rear Lights PWM

8.1.3. The Control Layer

The system was designed to be flexible and thus versatility was provided in several ways. The speed, stop and enable of each flipper could be controlled separately or together. The front flippers could also move in unison at the push of a button. The speed, stop enable and direction of the drive tracks could also be individually controlled if desired. The maximum speed values of flippers and drive pulleys could be set, while still retaining the maximum physical range of the joystick's motion. Even though every aspect of the motion system could be tuned to the

user's personal liking, the default settings were set in such a way that the user would have adequate control over every aspect. The front lights and the rear lights could be individually set and their power ranged from 0-255, with 0 indicating 0% brightness and 255 indicating 100% brightness. Data recording was also included at the press of a button and the roll, pitch and yaw as well as all current readings could be recorded in a spreadsheet along with the time.

All control occurs on the laptop and the LM3S8962 microcontrollers only transfer data and set values on their **IOs**. Programming a microcontroller took a few minutes and not having them take care of the control allowed one to alter the control code on the laptop on the fly. An additional advantage of this is that the controllers had do less work to do. For safety, the embedded controllers had been programmed to stop all motors should the wireless connection disappear.

The tracks only require speed control, while the flippers require both position and speed control. As previously discussed, the Maxon DECV 50/5 controllers take care of the speed control. They are not capable of providing position control and thus this aspect of the control system had to be done with **LabVIEW**. Position control was achieved by altering the speed, direction and stop signals of the microcontrollers. **LabVIEW** contains sophisticated control algorithms, such as **PID** and fuzzy logic, which were used to attain position control. After rigorous testing it was established that a simple proportional position control system suffices. For additional information about the performance of this system refer to chapter 9.

8.1.4. Software Structure

The software structure of the code running on the embedded controller is straight forward; it receives the data and then used it to control the motors. The speed controllers were not designed for position control. This was adequate for the drive motors, seeing that only their speeds needed to be controlled. The flipper on the other hand required to achieve and maintain certain rotational positions. This was accomplished by calculating how large the difference between the desired set position and the actual position was. The motor was then activated to move towards the desired position. If the difference was large, then the motor speed was large. The motor speed would decrease as the actual position was nearing the desired position. Once the actual position was within a pre-set range, the motor would stop rotating. If the motor was moved from that position, the control software would note the direction in which it was moved and quickly move in the opposite direction, until the difference between the set and the actual position was once again within the pre-selected range.

As previously discussed, the control station is responsible for the all the control that takes place. As a result of the large number of tasks that the control station is given, the code tends to be complex. For this reason **LabVIEW's** state machine design pattern was implemented. The "Moore machine" model is used and this allows **LabVIEW** to implement decision making algorithms.

In this implementation of the state machine architecture each state runs, until the user changes something. Each state can lead to one or many states, depending on the exact input. Thus different user actions have specific actions, which improves the user interface. The basic standard machine element is depicted in Figure 8.10. An overview of the control station's state machine architecture is portrayed in Figure 8.12 and Figure 8.11 illustrates a section of

the control code where the state machine architecture as well as the different states can be seen in a drop down menu.

The control code that is implemented through the state machine design pattern runs in parallel with the communications program. This enables both tasks to take the amount of time they require to complete without interfering and possibly slowing each other down. Local variables are used to send the control values from the state machine section of the code to the communications section.

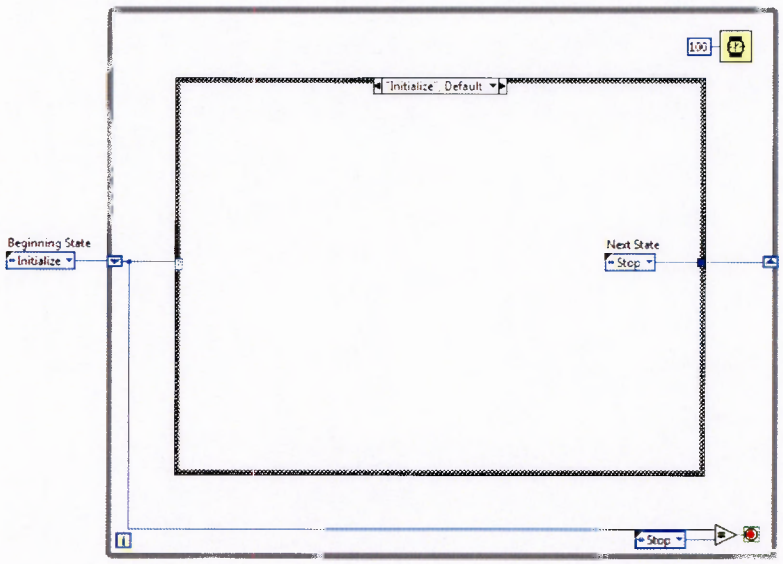

Figure 8.10.: A Standard State Machine Algorithm in LabVIEW.

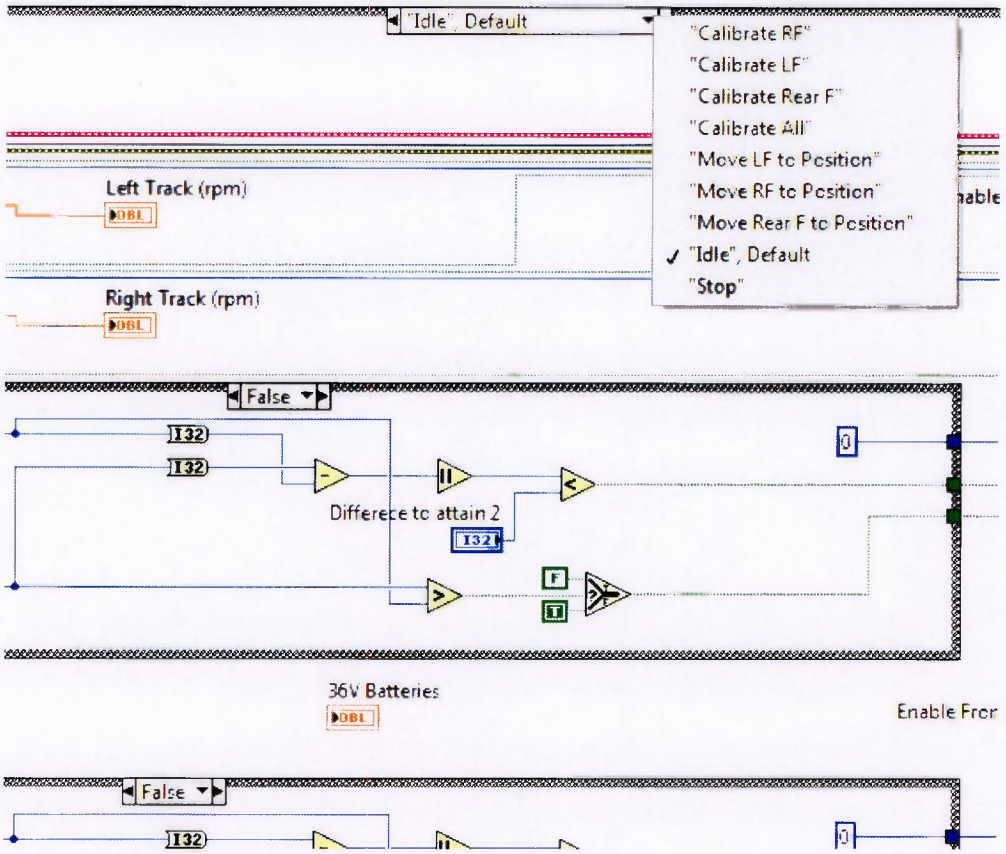

Figure 8.11.: The state machine of the control code.

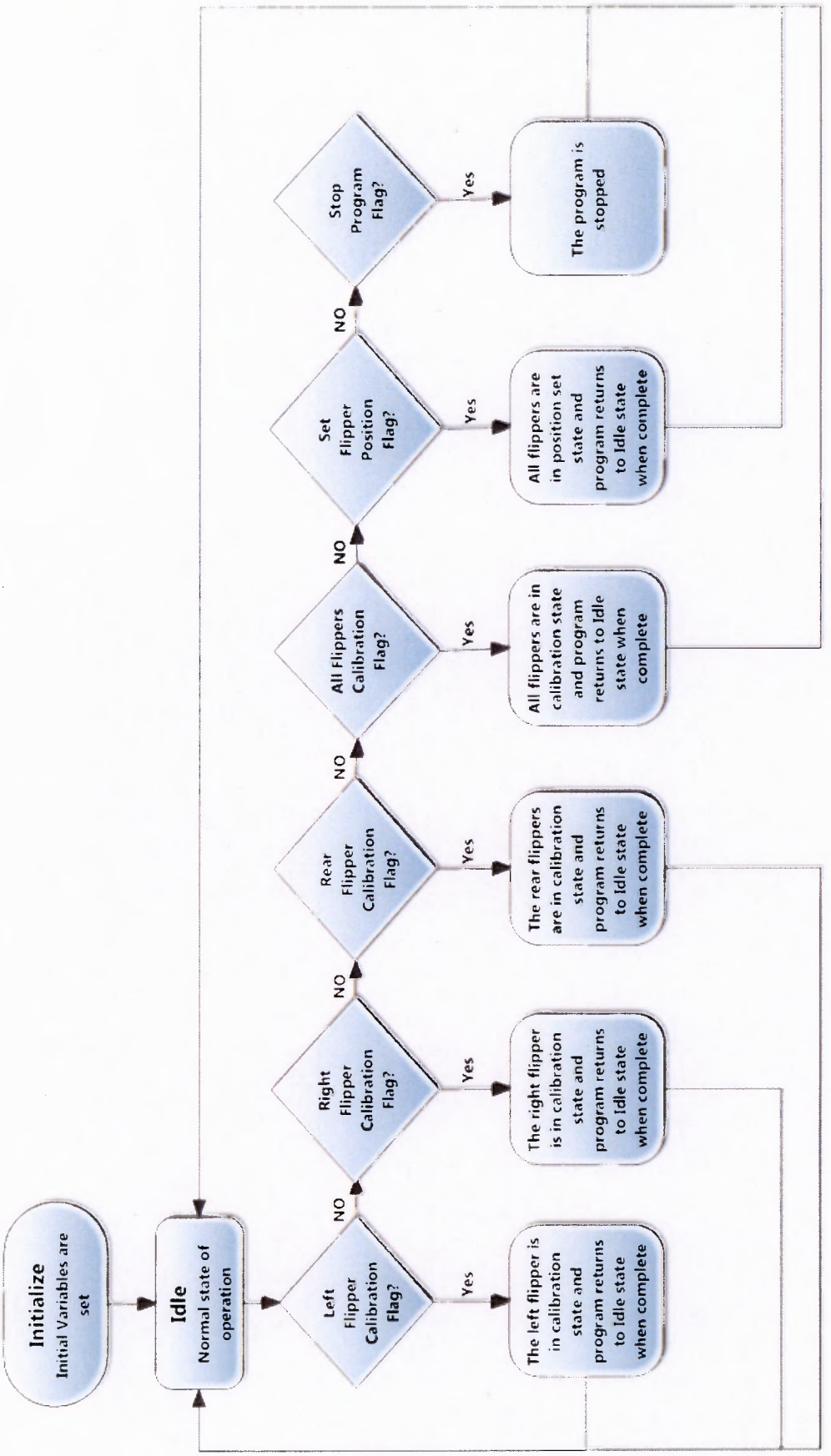

Figure 8.12.: Overview of the state machine design pattern.

8.1.5. Summary

Wireless communication was enabled through the implementation of Ubiquiti Bullet M5 radios. Wired communication between the embedded controllers was realised through the use of the RS232 serial link. Control of the system was left in the hands of the control station's laptop. The underlying structure of the software that runs on it is the state machine design pattern. A simple proportional control method for the flipper position was determined to be sufficient for tasks at hand. The following chapter will present the testing of the rescue robot's subsystems.

9. Testing and Results

The specifications that were set in Chapters 5, 6, 7 and 8 governed the design and development of the various systems of the robotic platform. These specifications can be verified by testing the performance traits of the systems of the robotic platform in structured environments. This will also gauge the capabilities of the platform as a whole.

9.1. Overall System Tests

9.1.1. System Weight

The weight related specifications set in the platform's previous development governed the further development of the overall system. The robot was specified to weigh less than 20kg and during the modifications to its various subsystems this value of weight was kept in mind and thus an effort was made to keep the the weight of components added to the system down. This specific test is used to evaluate whether the weight specification of the robot was accomplished and to illustrate the amount of weight contributed by individual components and sub subsystems.

9.1.1.1. Test Procedure.

The setup up of this test consisted of placing the Sasco Africa WP-PW30 scale on an even and flat surface. Individual components were weighed and the overall weight of assembled subsystems was established afterwards. The weight of all mechanical components as well as the electromechanical and electronic components was determined. Figure 9.1 illustrates how the weight of the top section of the right sidepod was determined.

Figure 9.1.: The assembled top plate of the right sidepod being weighed.

9.1.1.2. Results

The total mass of the fully assembled platform, including all fasteners and electronic components, was 42.160kg, which is more than twice the set specification of 20kg. The mechanical subsystems that are the primary weight contributors are displayed in the pie chart in Figure 9.2. Table 9.1 contains the masses of the individual component of the platform.

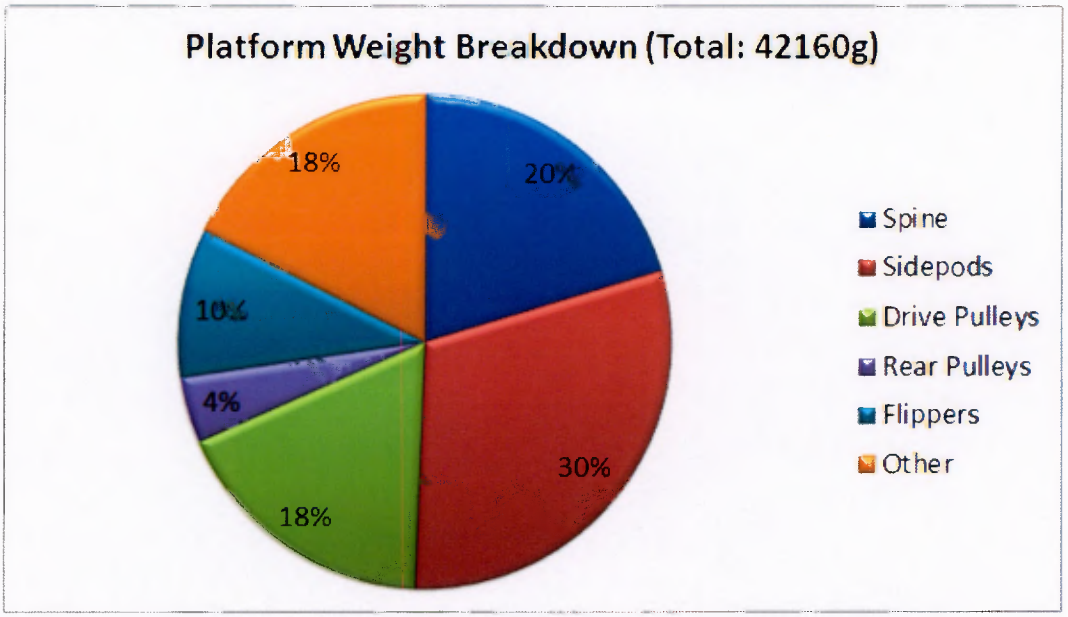

Figure 9.2.: The major mass contributors of the platform.

Table 9.1.: The weights of the components in grams.

Component	Quantity	Unit Weight (g)	Total Weight (g)
Spine			**8591**
Centre Spine	1	4960	4960
Sidepod Support Rails	4	40	160
Mount Plate	1	1870	1870
Mount Plate Rear Support	1	170	170
Light Housing Inner	4	20	80
Light Housing Outer	4	20	80
LED Mount	4	10	80
Camera Cover	2	6	12
Fan	1	90	90
Arm to Base Interface	1	240	240
Front Cable Cover	1	9	9
Rear Gear Cover	1	130	130
Rear Shaft Cover	1	60	60
Rear Flipper Drive Gear	1	50	50

Component	Quantity	Unit Weight (g)	Total Weight (g)
Rear Motor Clamp	1	90	90
Sidepod Side Cover	2	355	710
Rear Flipper Idler Gear	2	60	60
Rear Flipper Gear	1	70	70
Rear Flipper Drive Shaft	1	40	40
Rear Flipper Drive Idler Shaft	2	15	30
Rear Flipper Shaft	2	60	120
Rear Flipper Coupling	2	100	200
SKF608	6	10	60
Sidepods			**12749**
Sidepod Bottom	2	1090	2180
Sidepod Top	2	940	1880
Sidepod Upright	3	467	1401
Rear Motor Mount	1	430	430
Track Tension Bar	6	120	720
Track tension Bar Holders	6	3	18
Outside Hub Support	4	200	800
Slider Clamp	12	5	60
Battery Ejector Plate	4	20	80
Batteries	6	610	3660
Battery Guide Plate and Contact Holder	2	360	720
Drive Pulleys	**2**	**3740**	**7480**
Pulley	2	610	1220
Front Pulley Inside Cover	2	140	280
Front Pulley Outside Cover	2	100	200
Outside Center	2	20	40
Motor Mount 1	2	210	420
Motor Mount 2	2	60	120
Motor Mount 3	2	90	180
Motor Mount Connect	2	140	280
Rear Pulleys	**2**	**910**	**1820**
Rear Pulley Inside Cover	2	110	220
Rear Pulley Outside Cover	2	140	280
Pulley	2	610	1220
Small Pulley Hub	4	10	40
Small Pulley Nut	10	4	40
Small Pulley Shaft	4	5	20
Flippers	**4**	**1030**	**4120**
Flipper Inside Plate	4	190	760
Flipper Arm Plate	4	120	480
Flipper Pulley	4	90	360
Flipper Small Pulley	4	90	360

Component	Quantity	Unit Weight (g)	Total Weight (g)
Rear Motor Clamp	1	90	90
Sidepod Side Cover	2	355	710
Flipper Track Support	8	40	320
Flipper Arm Hub	4	70	280
Small Pulley Hub	4	10	40
Small Pulley Nut	10	4	40
Small Pulley Shaft	4	5	20
Flipper Tensioner	8	7.5	60
Flipper Rear Brace	4	15	60
Flipper Track	4	210	840
Flipper Pulley Bearing	4	80	320
Flipper Shaft Bearing	4	60	240
Other			**7400**
Drive Tracks	2	1400	2800
Maxon Motors	5	860	4300
Maxon Motor Controllers (With Cover)	1	180	180
Maxon Motor Controllers (Without Cover)	4	30	120
Sum/Total	**188**		**37640**
Fully assembled rescue robot platform			**42160**

9.1.2. Idle Power Consumption of the Overall System

During wireless teleoperation the rescue robot is powered from six 18V 3.0Ah batteries and determining the platform's power efficiency is essential. The following tests involved measuring the current draw of each system at the voltages that they ran at when the platform was operational.

9.1.2.1. Test Procedure

During the tests the platform was not being driven, but the current consumption of each electronic system was measured individually using a handheld multimeter. This was done by only having the systems to be tested switched on. The power consumption of the motors, while motion occurred, was not included, seeing that the values there would vary significantly, depending on factors such as speed of motion, terrain and task being performed.

9.1.2.2. Test Results

The test results for the overall power consumption when there was no motion is depicted in Figure 9.3 below. The maximum overall power consumption was 54.66W and it can be seen that the lights use up the most power at 40% while they are set at maximum brightness. Other than that the second component that requires a lot of power was the Bosch VIPX2, which

contributes 22% to the overall consumption. All other components use 10% of the power or less.

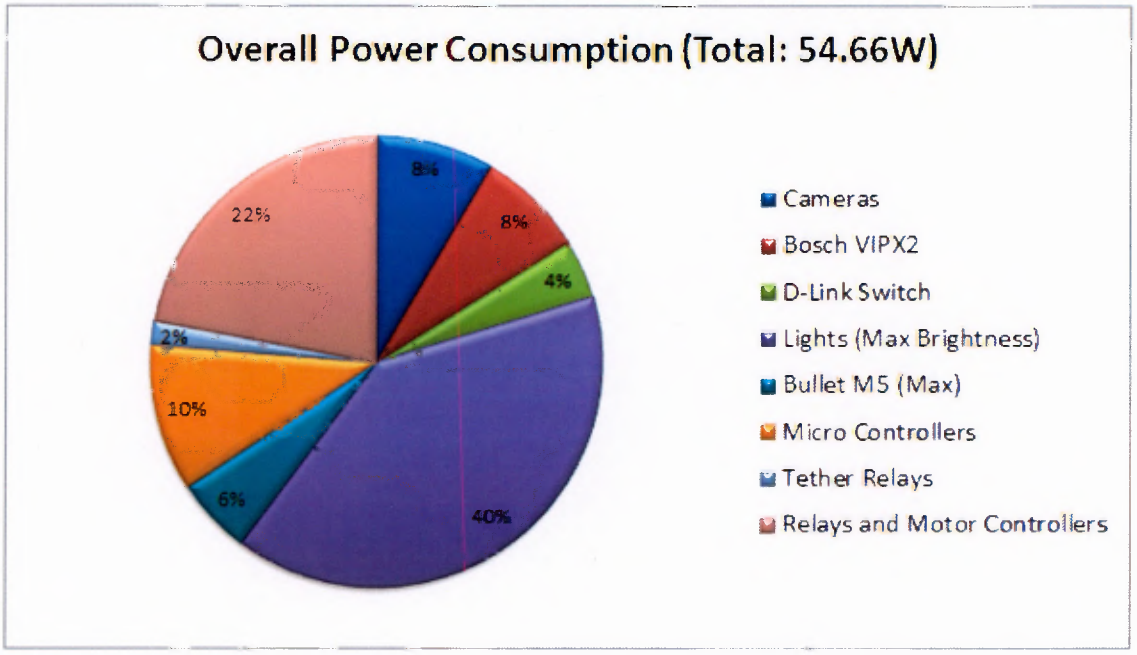

Figure 9.3.: Power consumption during no motion.

9.2. Flipper Tests

The mobility tests include the flippers and the main drive system. The tests were performed in order to establish the proficiency of the feet on the tracks, the drive electronics as well as the modifications made to the locomotion system.

9.2.1. Flipper Speed and Current Tests

One of the specifications was that the flippers should have a maximum speed of at least 9rpm. This performance trait is important, since directly influences the usability of the platform and thus it should be tested.

9.2.1.1. Test Procedure

A **LabVIEW** program was specifically written for this test. The program would set the rotational speed of a flipper. The flipper would then be activated and once it triggered its limit switch, a timer in the program was started. The flipper would rotate until it triggered the limit switch once again, resulting in the timer being stopped. This was repeated three times for a single speed value. The entire procedure was done for a range of incrementally increasing **DAC** values for all flippers. The current drawn from the flipper motors was recorded.

9.2.1.2. Results

Figures 9.4, 9.5, 9.6 and 9.7 portray line charts than illustrate the relationship between the **DAC** value and the actual speed in rpm of the right flipper, the left flipper, the rear flippers and all the flippers respectively. A trend line can be seen in the first three charts, as well as its accompanying straight line equation. Figure 9.7 shows that the three line charts defer from each other only slightly for the same **DAC** input value range. The results show that the maximum angular speed of the flippers was reached and that the flippers are capable of rotating at a speed 2.46 times the specified maximum speed of 9rpm. It can also be seen that the motor speeds reach an upper limit at high DAC values. This was caused by the speed and ramp setting of the speed controller. The controller is essentially trying to make the motor turn faster than the motor is capable of. A different speed and ramp setting could have caused a motor to plateau at a lower DAC value.

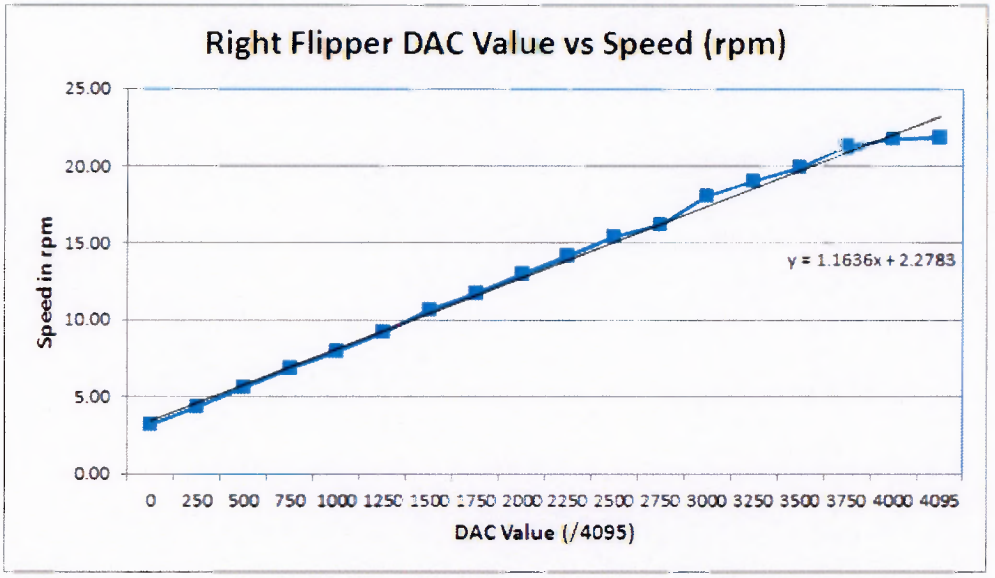

Figure 9.4.: Line Chart displaying DAC Value versus Speed of the Right Flipper.

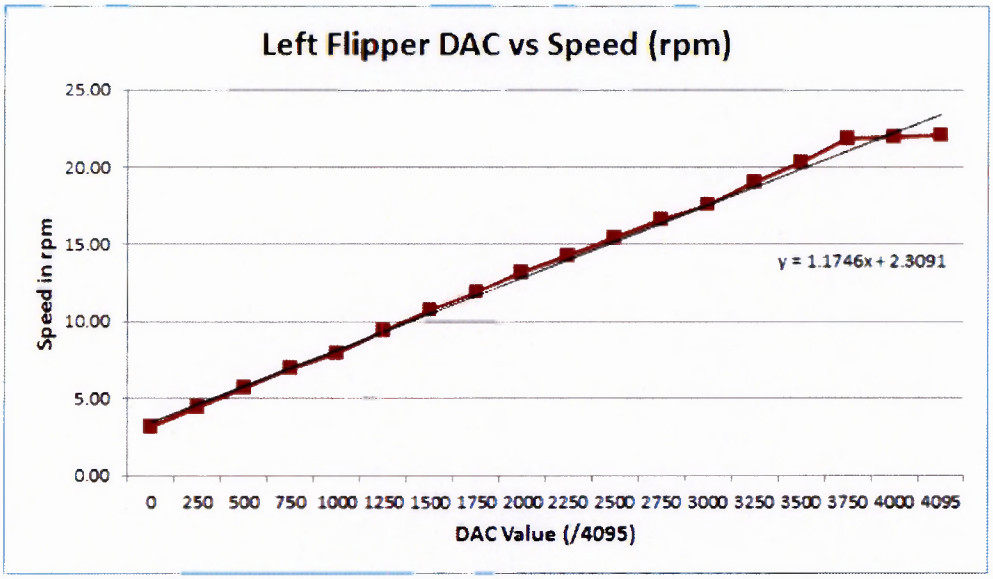

Figure 9.5.: Line Chart displaying DAC Value versus Speed of the left flipper

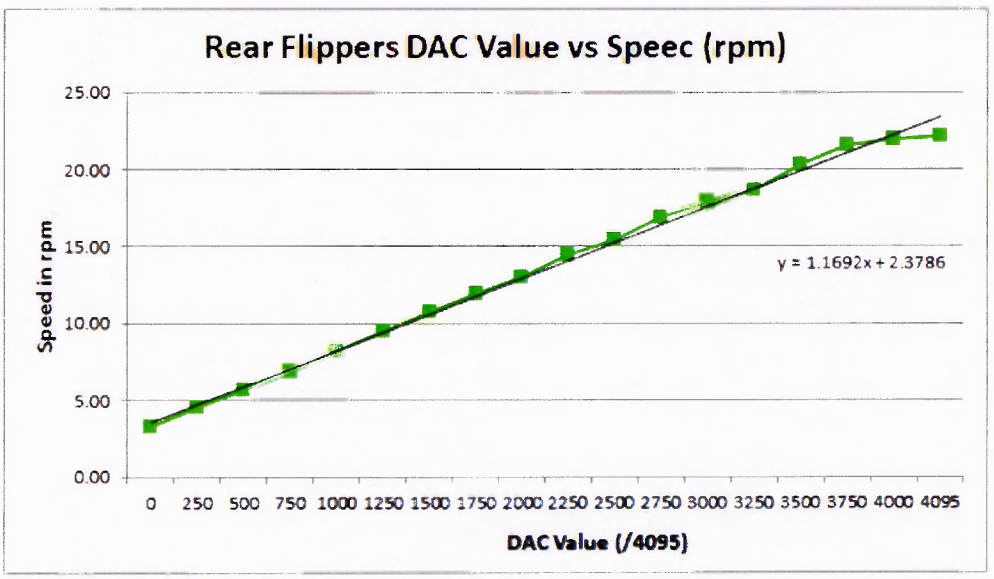

Figure 9.6.: Line chart displaying DAC value versus speed of the rear flippers.

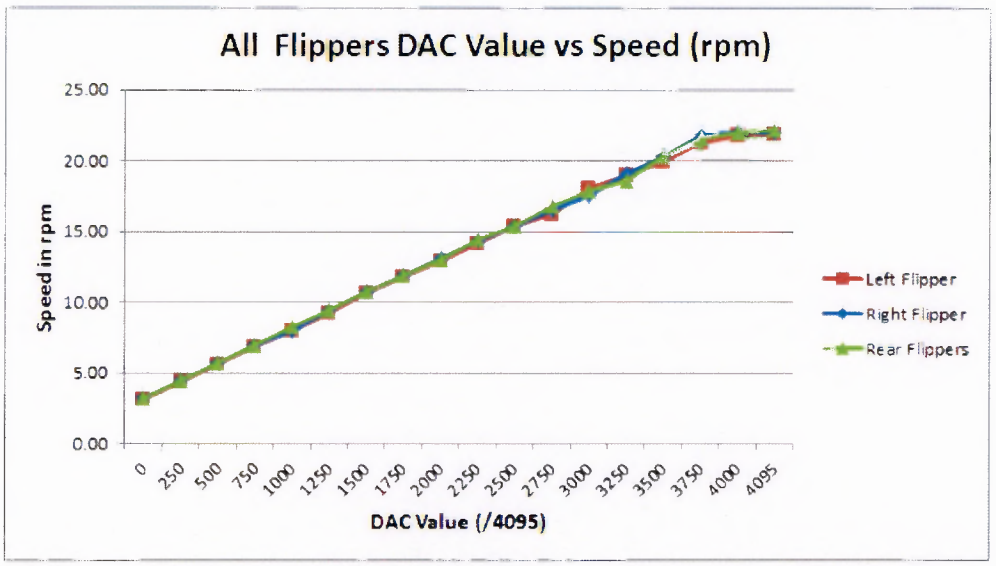

Figure 9.7.: Line chart displaying an overlay of DAC value versus speed of all flippers.

Figures 9.8, 9.9 and 9.10 illustrate the current that was drawn by the flippers during the test. It should be noted that the right flipper draws significantly more current than the other flippers for the same current. This discrepancy likely came into being, because the right flipper shaft was bent from a fall that occurred previously. The difference between these current values can be seen more clearly in Figure 9.11.

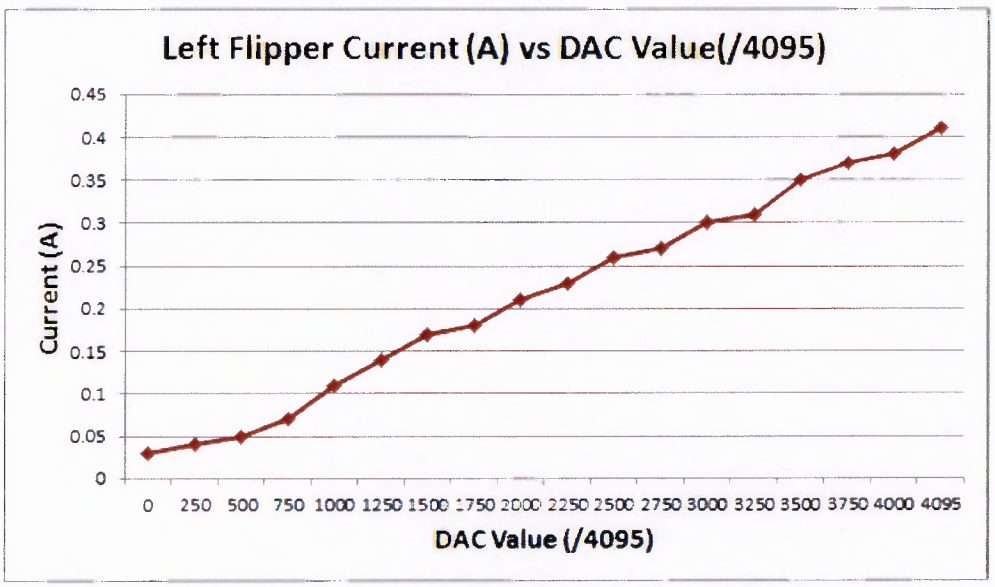

Figure 9.8.: The left flipper current readings for the specified speeds settings.

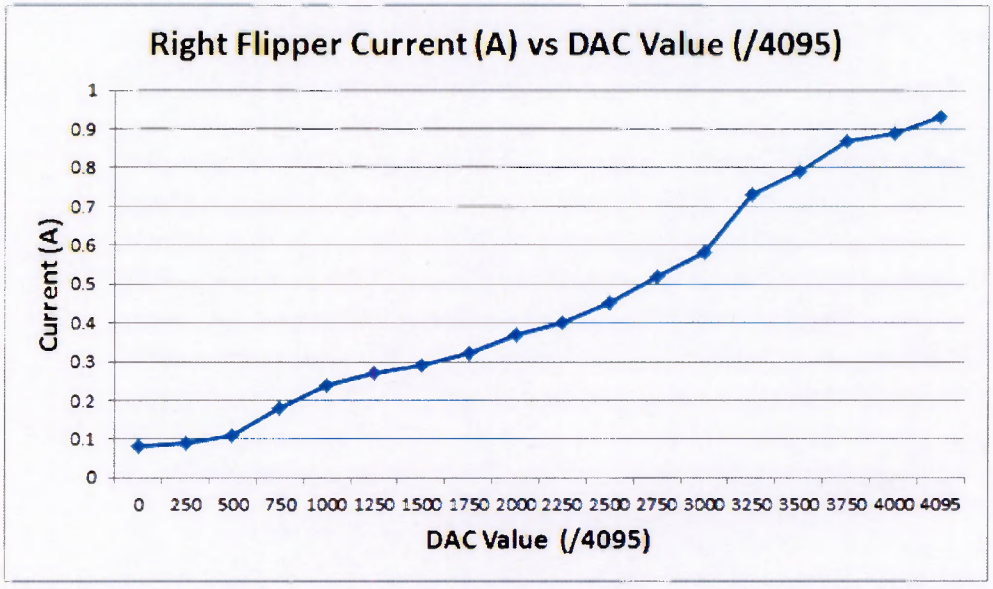

Figure 9.9.: The right flipper current readings for the specified speeds settings.

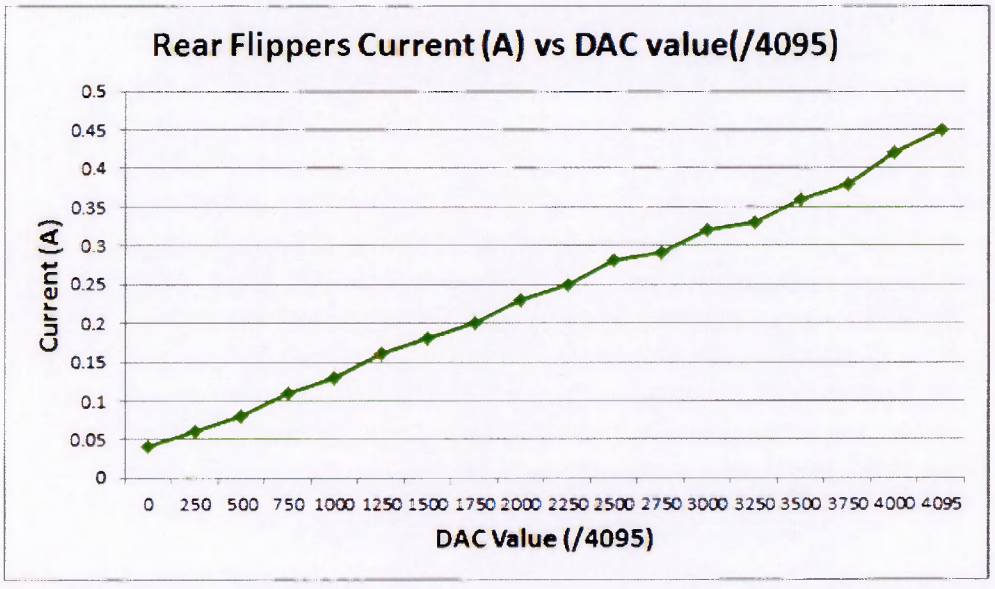

Figure 9.10.: The current readings of the rear flippers for the specified speeds settings.

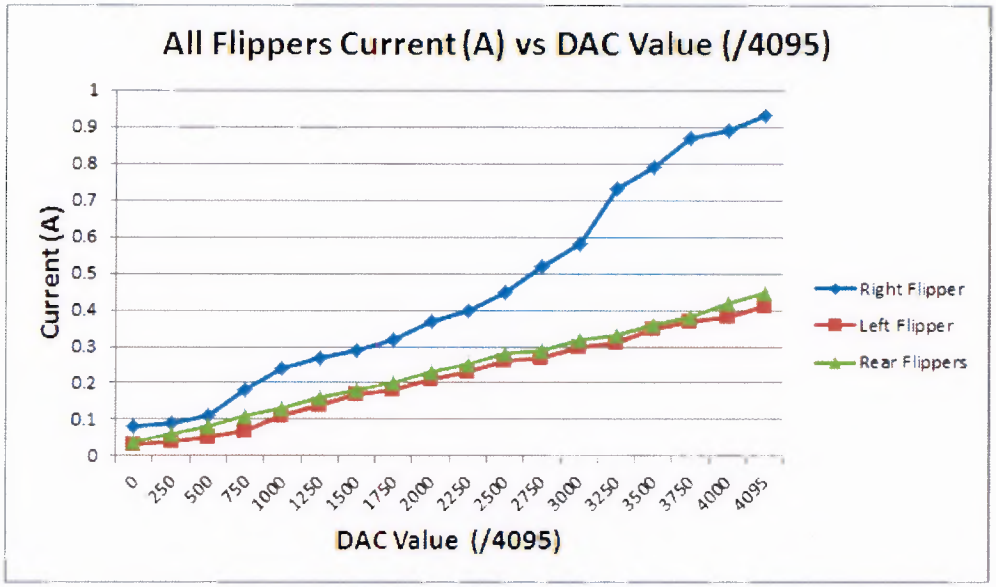

Figure 9.11.: An overlay of the current readings of all flippers at the specified speeds.

9.2.2. Flipper Backlash Test

9.2.2.1. Test Procedure

The backlash of the flippers was first inspected by hand, in order to establish whether it was practical to measure the backlash using a gauge. If the backlash was relatively small a gauge would be used to measure it accurately. If it turned out that the backlash was too large a simple protractor would be used to measure it.

9.2.2.2. Results

It tuned out that the backlash was significant for all flippers. A protractor was used ad the backlash for the rear flippers was determined to be 30°, as can be seen in Figures 9.12 and 9.13. The backlash of the right flipper and the left flipper were 20° and 22° respectively.

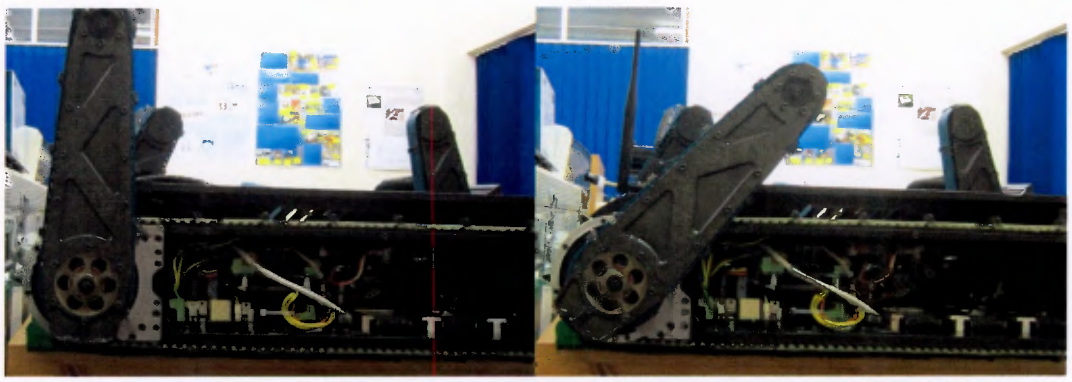

Figure 9.12.: Rear flipper backlash.

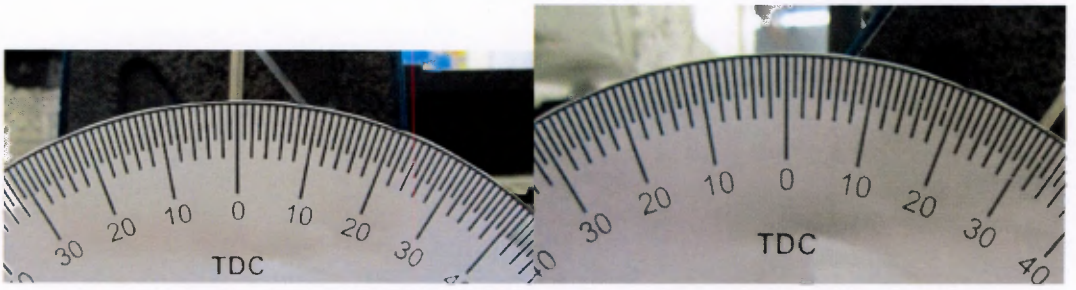

Figure 9.13.: Rear flipper backlash measurement using a protractor.

9.2.3. Flipper Position Control Tests

Position control plays an essential part when controlling the flippers and this testing the platforms capabilities in this area was warranted. The aim of this test was to establish the position control's capability of accurately setting flippers at desired positions.

9.2.3.1. Test Procedure

The procedure for this test was developed by MSc student Michael Rieger. A laser pointer was attached to each flipper and allowed for the evaluation of the positional accuracy of the control system that was implemented. A set of marking were drawn on a white board indicating angles of 0°, 5°, 10° and 15°. The laser pointer on the flipper was positioned 3400mm from the white board. The test was commenced by calibrating the flipper to 0° and positioning it so that the laser pointer pointed directly on the 0° mark when the flipper was horizontal. Due to the large amount of backlash inherent in the flipper, each time a test was performed; it had to be ensured that the flipper was at one of its maximum backlash positions. Forcing the flipper at a maximum of its backlash allowed for the testing of the accuracy of the control system. This could also be considered to be a test of the flipper shaft, because this component did not suffer from the large amount of backlash as the flippers. The flipper was then set to one of the angles mentioned above and the difference between the mark on the whiteboard and the laser pointer was recorded. This procedure was repeated three times for each flipper. Figure 9.14 illustrates the setup of the test.

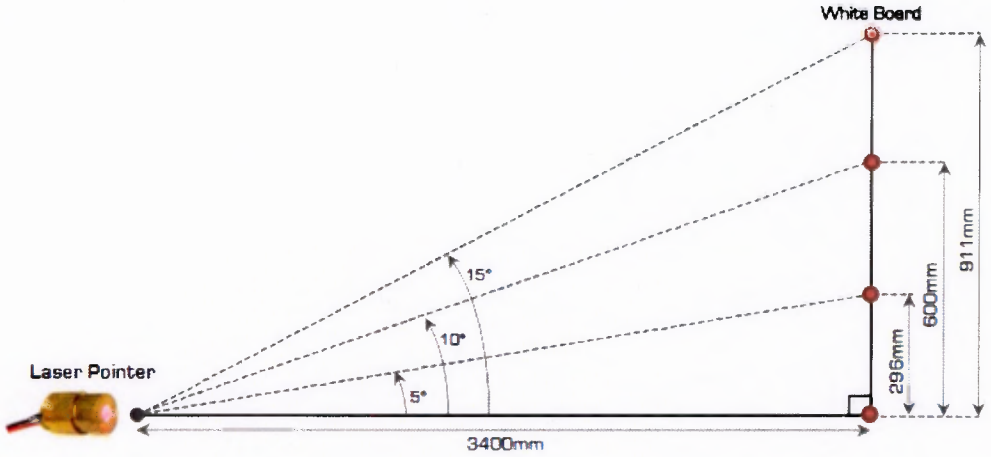

Figure 9.14.: The setup of the position control test, modified from [27].

9.2.3.2. Results

The minimum error that occurred was measured to be 64.4mm while the largest one was approximately 87mm. The angular discrepancies between set position and achieved position were:

Maximum Position Error $= tan^{-1}(\frac{64.4}{3400}) = 1.085°$

Minimum Position Error $= tan^{-1}(\frac{87}{3400}) = 1.466°$

The maximum error was 1.466°, the minimum error was 1.085° and the average error was calculated to be 1.28°. The positional accuracy was chosen in the specifications to be 1°, which was not achieved. However a maximum error of 1.28° will not be noticed by an operator. More accurate position control could have been achieved, were it not for the large flipper backlash.

9.3. Camera Tests

USAR responders are highly dependent on cameras to visually inspect the environment.

9.3.1. Test Procedures

EIA 1956 Resolution Target Test

The **E**lectronic **I**ndustries **A**ssociation (**EIA**) 1956 resolution target, seen in Figure 9.15, was used to determine the resolution of the cameras [32]. The chart was designed to be used on television systems and contains pie and linear wedge shapes that have 200 to 1000 **T**ele-**V**ision **L**ines (**TVL**) [32]. It additionally has 10 step density tables, measurement bars as well as edge definition points and is usually used to determine the limiting horizontal resolution. The test was performed at a distance of 36.5mm so that the edge of the camera view would just touch the edges of the resolution chart's borders and a snapshot of the image was taken. The four

sets of linear wedge patterns around the centre of the chart were visually inspected and once they started to unite and become indistinguishable from one another, the number next to that position represents the resolution of the entire image.

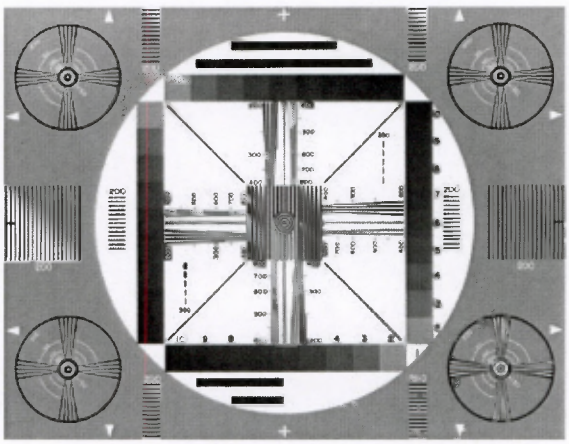

Figure 9.15.: The EIA 1956 Resolution Chart [32].

Snellen Chart Test

Conventionally during a Snellen eye chart test the distance from which one would view the chart is obtained by measuring the height of the letter "A" and then multiply this value by $\frac{6}{88}$[33]. The chart was printed on an A4 page which resulted in the letter having a height of 72.5mm and in calculated distance being 4.94m. However, this distance proved to be too far for the camera front and rear cameras, therefore the test was also done at a distance of 0.8m and a snapshot of the viewed image was taken each time. The **HD** camera took snapshots for both distances. A Snellen eye chart such as the one depicted in Figure 9.16 was used.

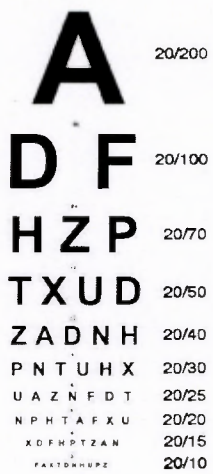

Figure 9.16.: A Snellen eye chart [33].

Distortion Grid Test

Distortion is any deviation from the rectilinear image. A distortion grid test was performed the camera lens distortion parameters. Even though distortion can be irregular, the two types

of distortion that occur most commonly are pincushion distortion and barrel distortion [34]. A rectilinear projection as well as the two types of distortion can be seen in Figure 9.17. The tests were carried out at a distance that would allow the borders distortion grid to touch the edges of the camera view, which turned out to be at a distance of 365mm from the cameras.

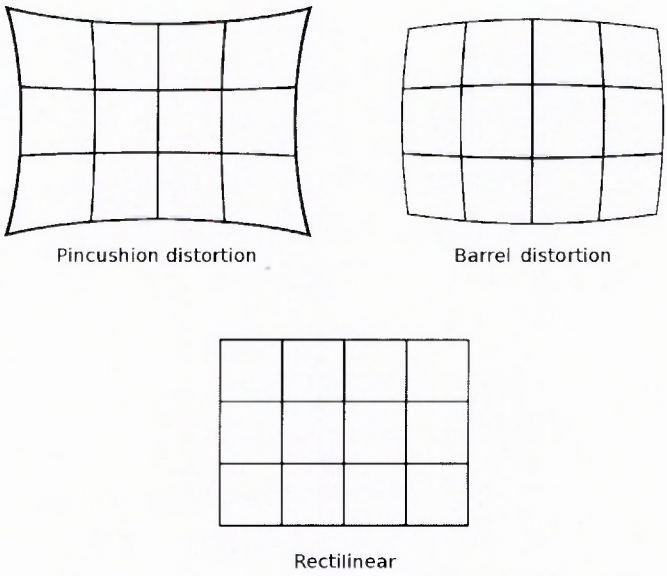

Figure 9.17.: Two main types of distortion [34].

9.3.2. Results

EIA 1956 Resolution Target

The three snapshots taken for the cameras are illustrated by Figure 9.18 and Figure 9.19. The tests for the front and rear cameras were done at 365mm from the chart, while the one for the **HD** camera was done at a distance of 625mm from the chart. This was done to ensure that as much of the sheet as possible could be seen on the cameras. The lines of both the front and rear cameras became indistinguishable just after the 300 increment line was reached and thus their vertical resolutions were determined to be 300 lines. The wedge lines in the snapshot of the resolution chart by the **HD** camera stated to blur into one at between lines 700 and 800 and therefore its resolution was determined to be approximately 750. 300 and 750 were the horizontal resolutions of the cameras. These values were less than the 640 and the 1280 horizontal resolutions that the two smaller and the HD camera were are supposed to have respectively. A number of reasons could have caused this difference, such as poor lighting.

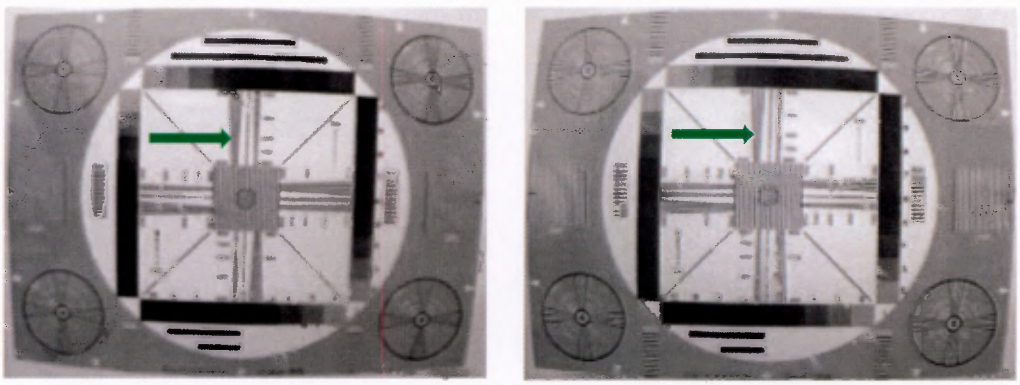

(a) The snapshot by the front camera indicates a resolution of approximately 300 lines.

(b) The snapshot by the rear camera indicates a resolution of approximately 300 lines.

Figure 9.18.: Snapshots of the EIA resolution chart by the front and rear camera.

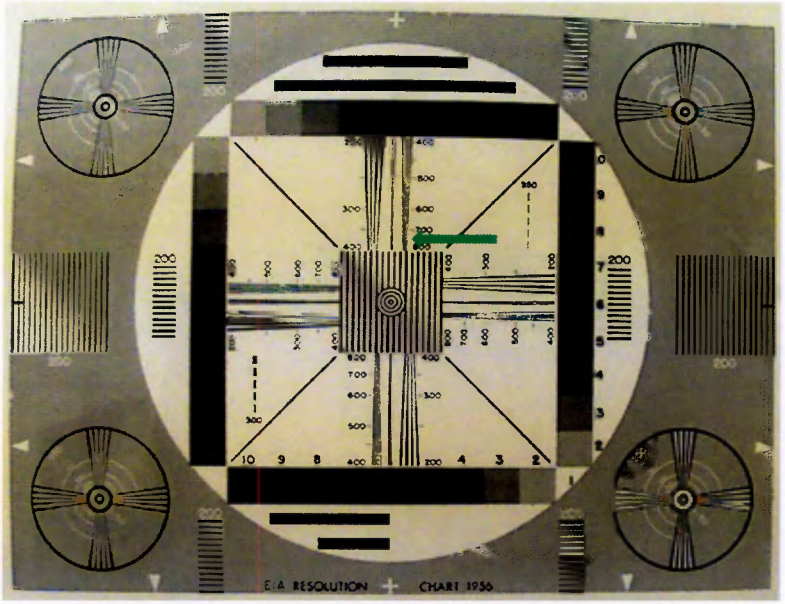

Figure 9.19.: The snapshot by the front camera indicates a resolution of approximately 750 lines.

Snellen Chart

Figure 9.20 illustrates the snapshots taken by each camera at a distance of 0.8m from the cameras. As seen in the images, the first six lines of the front and the rear camera **(A|DF|HZP|TXUD|ZADNH|PNTUHX)** could be read. It was significantly more difficult to read the seventh line and the letters of any lines after that could not be recognised. All lines of the **HD** camera could be read properly. Seeing that 0.8m is not the right distance for this test, an actual value for visual acuity could not be determined.

(a) The front camera. (b) The rear camera. (c) the HD camera.

Figure 9.20.: The snapshots of the cameras during the visual acuity tests at a distance of 0.8m from the Snellen chart.

Below in Figure 9.21 and Figure is are the snapshots that were taken by the **HD** camera at the distance of 4.94m. The first three lines **(A|DF|HZP|TXUD)** could be read properly and thus its visual acuity was 20/50.

Figure 9.21.: A normal snapshot of the HD camera viewing the Snellen chart at a distance of 4.94m.

Figure 9.22.: A snapshot of zoomed in image of the Snellen chart at a distance of 4.94m.

Distortion Grid

The results of the distortion grid test are shown in Figures 9.23 and 9.24. The green rectangle in each image represents a rectilinear box. By comparing the horizontal and the vertical lines of the distortion grids and the green rectangles it was determined that the barrel distortion caused by the **HD** camera was mild, while the barrel distortion caused by the lenses of the front and rear cameras was quite severe. This is however expected, seeing that the front and rear cameras were fitted with fisheye lenses.

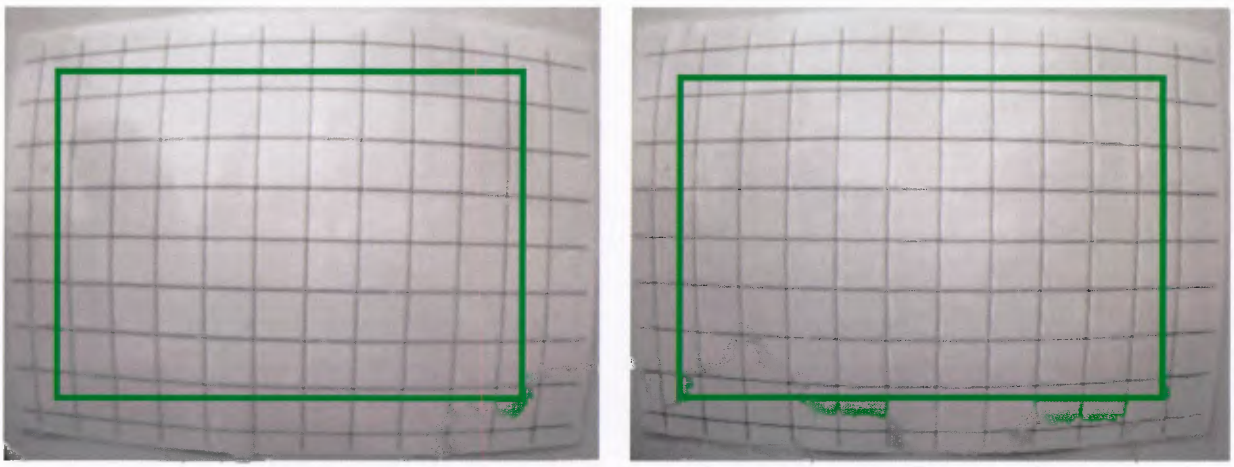

(a) A snapshot of the distortion grid of the front camera. (b) A snapshot of the distortion grid of the rear camera.

Figure 9.23.: Distortion of the front and rear cameras.

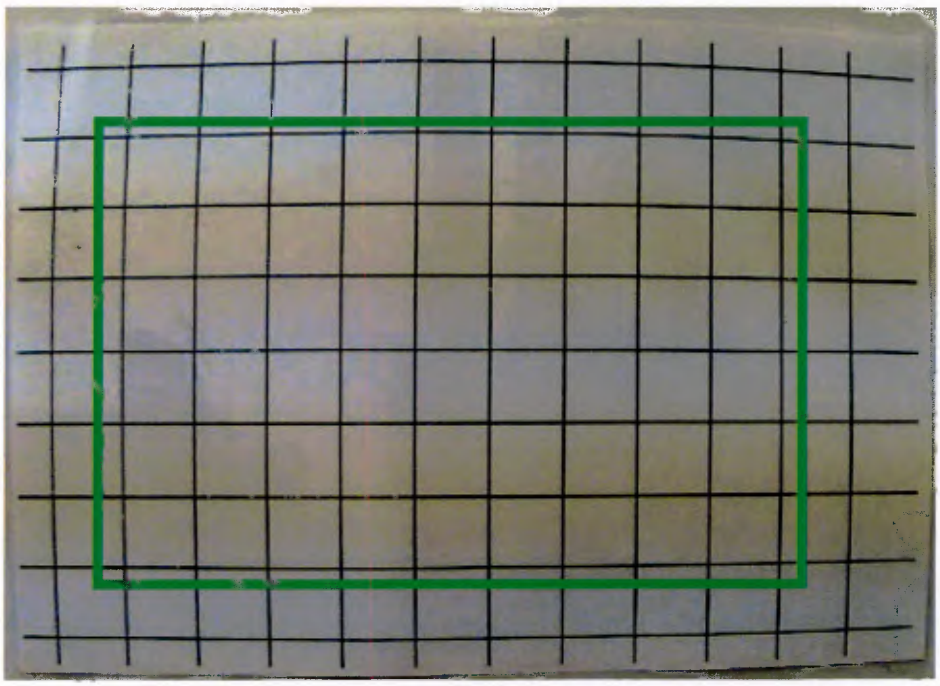

Figure 9.24.: A snapshot of the distortion grid taken by the HD camera.

9.4. Camera Data Throughput Tests

When deployed on a mission, the rescue robot would be operated wirelessly. Several systems, especially the video feed are required to function in real time, the wireless connection may be limited due to obstacles between the operator station and the rescue robot or because of range. It is therefore imperative to asses the data throughput of the cameras and ensure that it was within reasonable limits.

9.4.1. Tests Procedure

The front cameras were switched on and connected to the Bosch VIPX2. The data was then transmitted over the Bullet M5 wireless link to the operator station's laptop. On the laptop the bandwidth was recorded when the camera was not connected to the Bosch VIPX2, when it was connected and there was no motion in front of it and finally when it was connected and there was a large amount of motion in front of it. The test was repeated for the rear camera as well. A similar procedure was used for the HD camera, except that the Ethernet cable was pulled out to determine the bandwidth when it was not connected, since it does not use the Bosch VIPX2.

9.4.2. Results

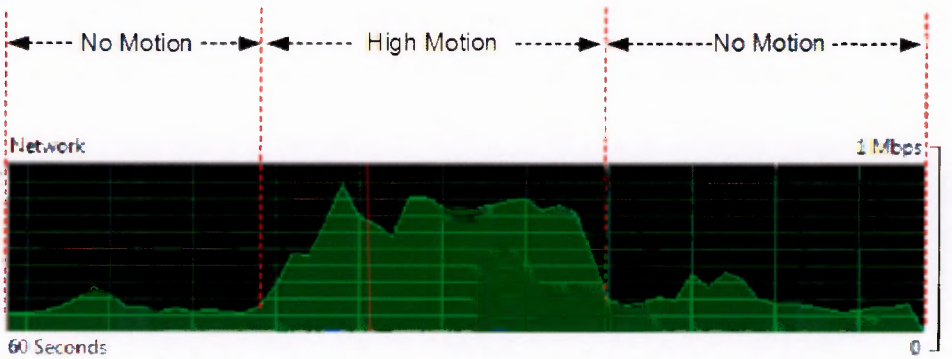

Figure 9.25.: Data throughput of the front camera.

As can be seen in Figure 9.25, the front camera uses a maximum of 400Kbps, when there is no motion in front of it. This value peaks at 900Kbps when a large amount of motion occurs in front of it. The rear camera had virtually identical results and the HD camera used 3.1Mbps when there was no motion and 7Mbps when there was a high amount of motion. These values are within the tolerable amount of the data throughput for the system and thus all video streams and other sensor data, as well as commands sent to the robot occur in real time.

9.5. Lighting Test

During **USAR** rescue robots can be deployed in environments that are dark. Sufficient light in such environments is vital for the intended operation of the cameras. During the manipulation of its environment, **Ratel's** platform does have artificial lighting on the sensor payload and on the gripper. On the other hand, while manoeuvring light is required to enhance camera quality during unfavourable lighting conditions.

9.5.1. Test Procedure

A LM-8000 light meter was attached to a plywood sheet, which was rested against a wall. The platform was placed in front of the sheet in such a way that the lights were always 1m away from the light meter. The setup, seen in Figure 9.26 below, also had the lights be at the same height as the sensor. All tests were performed in the dark. Initially the brightness level in the dark room was measured and verified to be 0 lx. Thereafter the brightness of the front lights was increased incrementally in steps of 5% of the maximum brightness. The brightness reading for every brightness setting was recorded. After the whole brightness range was tested, the platform was turned around so that the rear lights faced the light meter at a distance of 1m and the whole test procedure was repeated.

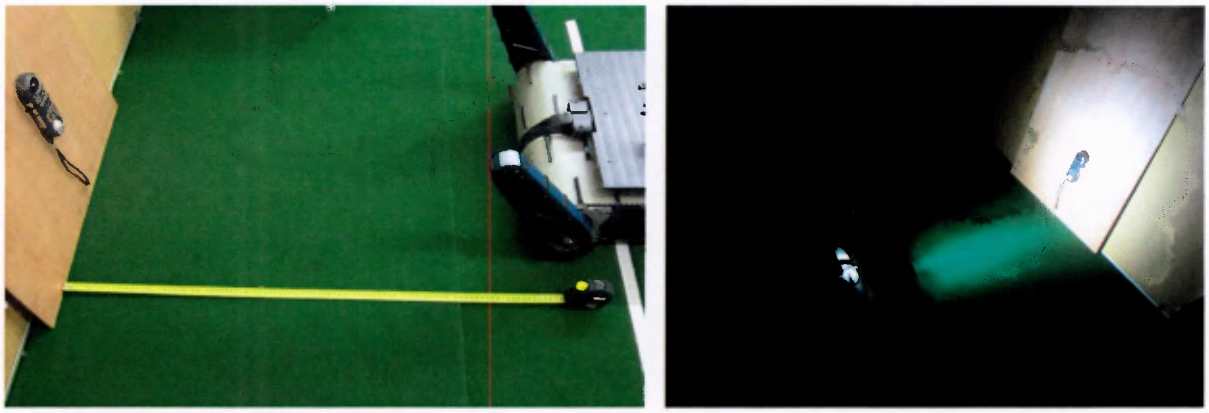

(a) The light testing setup showing the didtance between the sensor and the platform's lights.

(b) The testing in the dark.

Figure 9.26.: The light test setup.

The second aspect of the test was to gauge the performance of the lights over different distances. The front lights of the platform were set to maximum brightness and their brightness level was measured at a distance of 0.5m from the light meter. Thereafter the distance was increased by 0.5m until 5m was reached. The brightness reading was recorded for each incremental distance and the entire procedure was repeated for the rear lights.

9.5.2. Results

The results for the test that measured the brightness of the lights as the **PWM** value was incrementally increased are depicted in Figure 9.27 below. It can be seen that the values do not form a straight line as would usually be expected. It can be observed that the rear lights are brighter the front lights and that they become comparatively brighter as the **PWM** value is increased.

Figure 9.28 illustrates the amount of current that is drawn by the lights for several **PWM** values. It can be seen that the current values for both sets are almost identical and that these values increase with increasing **PWM** values in a proportional manner. Since the lights are powered by the platform's 18V line it can be deduced that he maximum power requirements for the front and rear lights are 14.22W and 14.4W respectively.

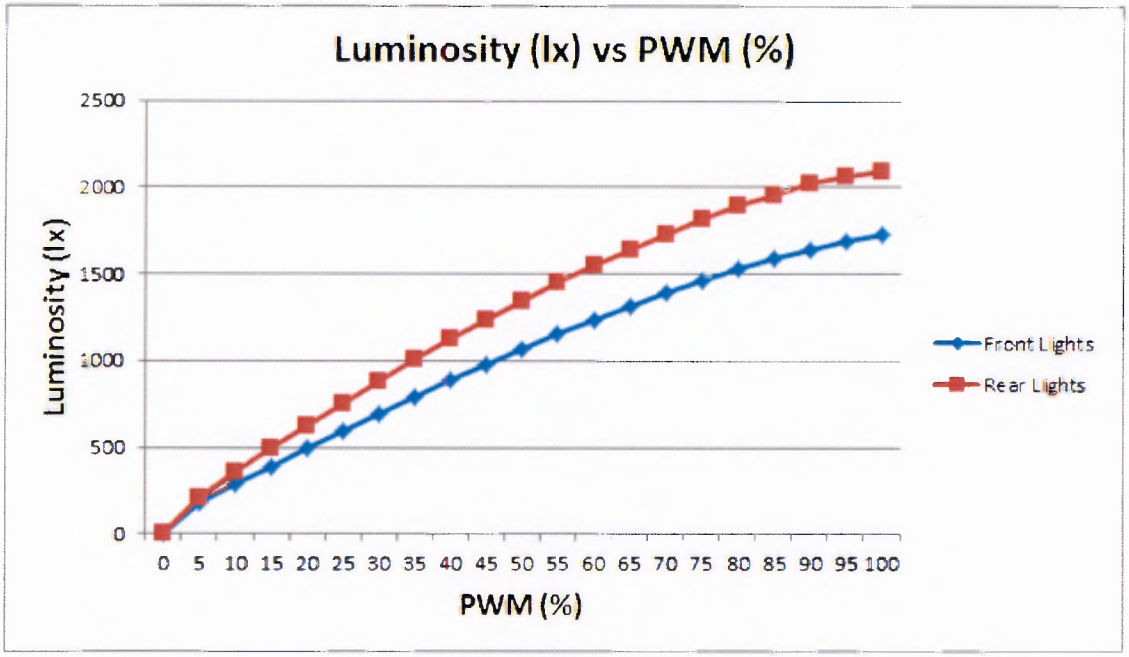

Figure 9.27.: The brightness readings of the lights at different PWM settings.

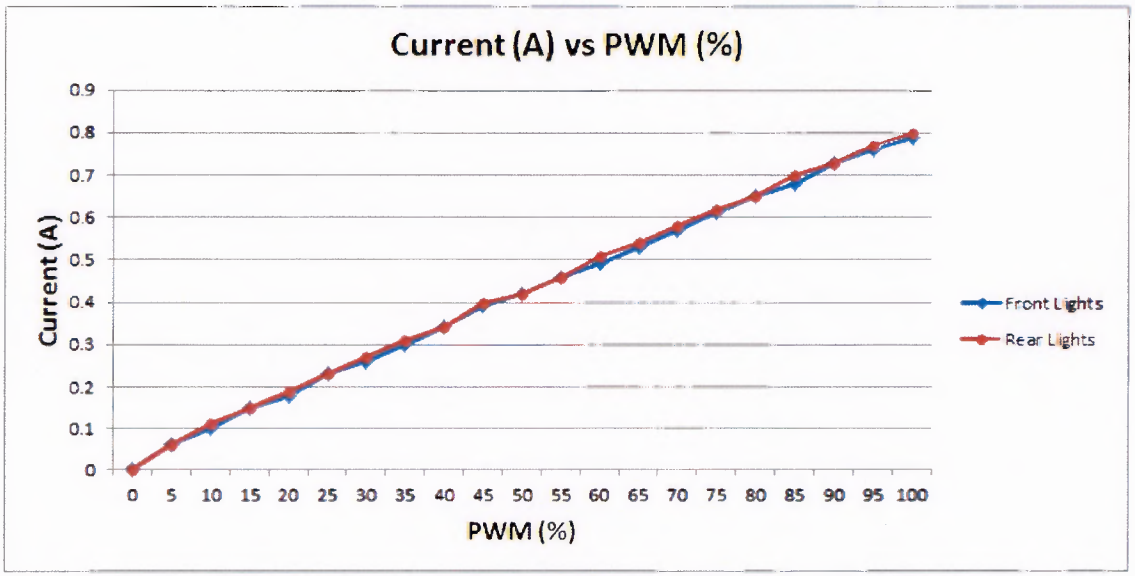

Figure 9.28.: Chart displaying the current of each PWM value for both sets of lights.

The relationship between luminosity and distance of both the rear and the front lights can be seen in Figure 9.29 and Figure 9.30. A trendline was used to determine the equations of the rear and front line values contained in their respective charts. The trendline for the front lights yielded an equation of $5787\times^{-1.836}$, while the one for the rear lights was $7336.2\times^{-1.914}$. The trendline for the front lights and the one for the rear lights had a R^2 value of $0.9887$and 0.9994 receptively, which indicates that both lines fit their respective sets of data well.

Figure 9.31 superimposes the two individual charts in order to illustrate their differences in luminosity at the various distances. It can be seen that the rear lights are brighter as the

distance between the platform and the lux meter was decreased. Other than that it appears that the rest of the data values of the charts were virtually identical.

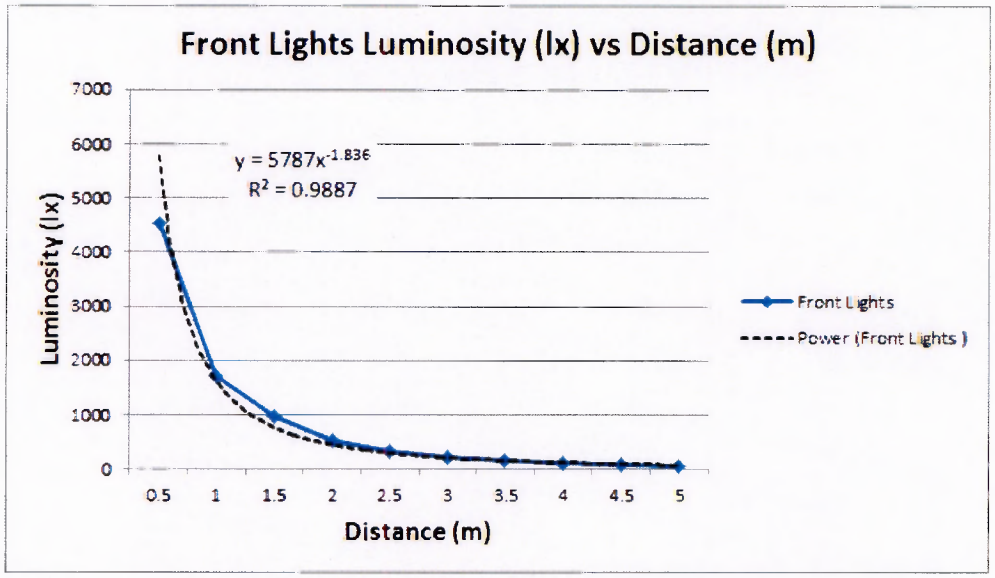

Figure 9.29.: The front lights.

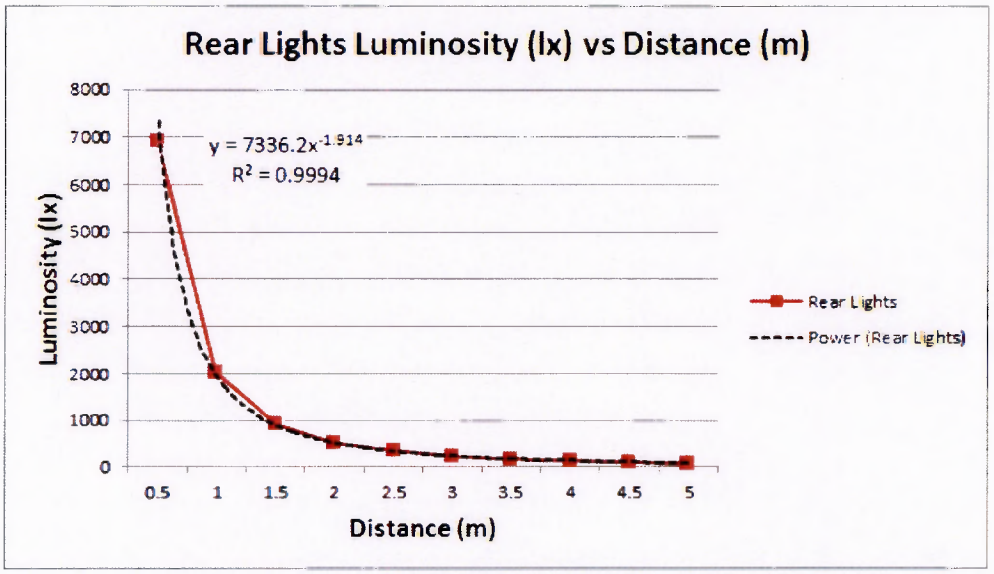

Figure 9.30.: The rear lights.

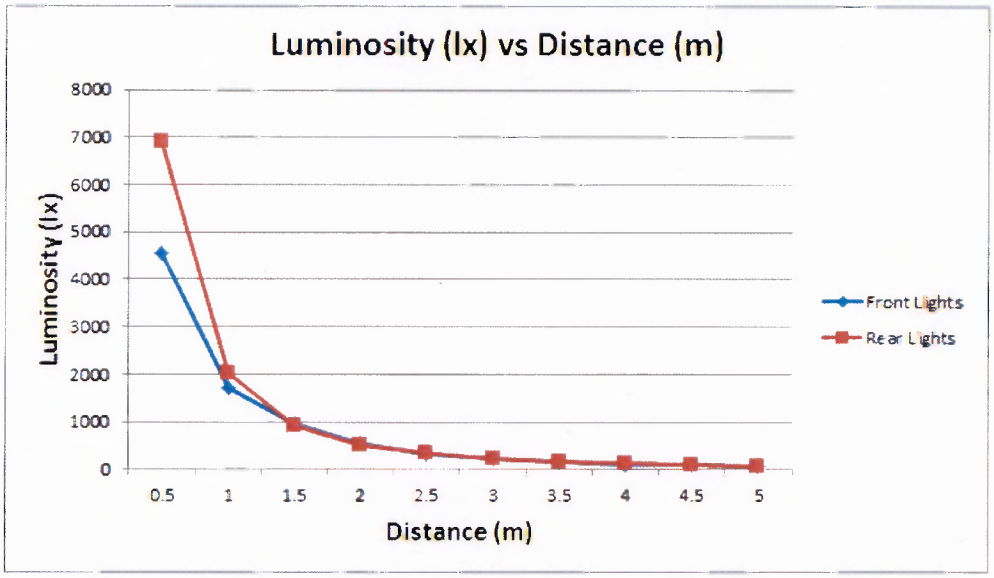

Figure 9.31.: A comparison between the rear and the front lights.

9.6. Mobility and Locomotion System Tests

The addition of the feet to the tracks produced a tread for the system that had the task of improving overall mobility of the platform. This new configuration had to be tested in various ways that mimicked the **RoboCup Rescue** environments. Additionally performance tests had to be performed on the modified pulley assemblies. The platforms ability to climb stairs and inclined planes as well as to drive on level ground had to be tested. The speed setting for the driving configuration was analysed in order to determine if it was sufficient when deployed. The following sections present the tests that were performed to gauge the overall motion systems of the robotic platform.

9.6.1. Entry Triangle

As previously discussed in Chapter 2, a 24" equilateral triangle is cut into the side of a building in order to enter it, should the conventional means of entry not be available anymore. The platform was designed to fit tightly through the entry triangle in order to obtain as much space as possible for the components housed inside the robot platform. The tread that was attached to the drive tracks should allow the platform, including the arm assembly and sensor payload, to fit through the this triangle.

9.6.1.1. Test Procedure

An equilateral 24" entry triangle was cut into one of the walls. A 30° slope was placed on the side of the wall that the robot would emerge from when driving through the triangle. An operator navigated **Ratel** to the the entry triangle and then proceeded to carefully manoeuvre it through through the entrance. Care was taken not to rub against the sides of the triangle

with any part of the robot, especially the sensor payload, as this delicate equipment is essential to navigation can control. The setup of the test can be seen in Figure 9.32.

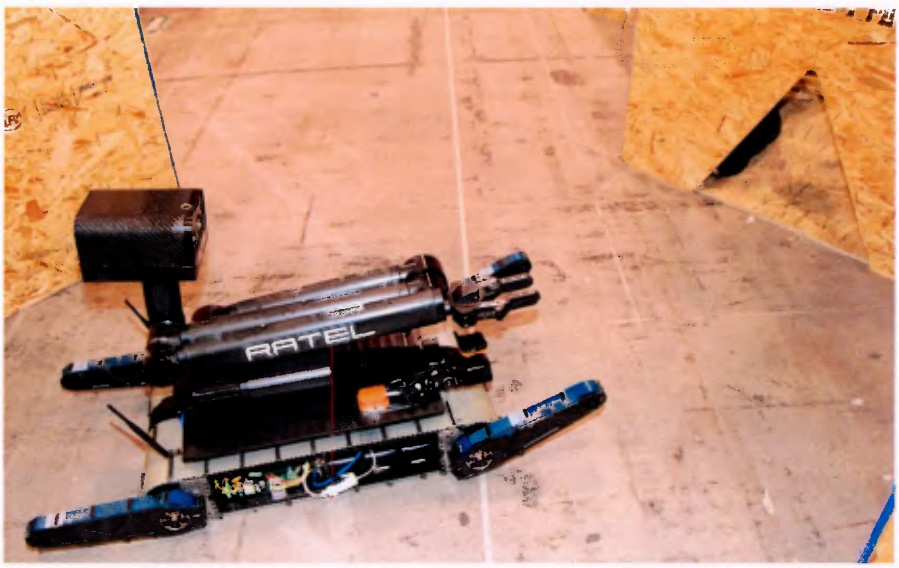

Figure 9.32.: Ratel positioned in front of the entry triangle (Image courtesy of Richard Whittemore).

9.6.1.2. Results

The entire unit managed to fit through the entry triangle, however the rubber feet of the flippers touched the edges of the triangle. Figure 9.33 depicts how the robot fits through the entry triangle.

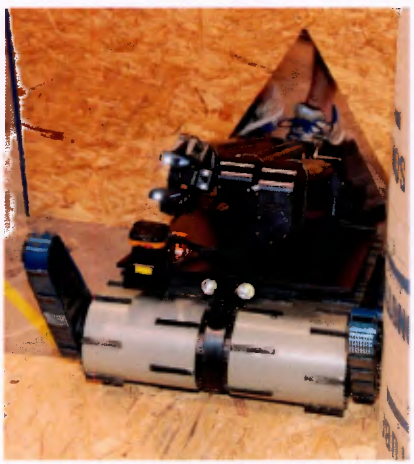

Figure 9.33.: Ratel driving through the entry triangle (Image courtesy of Richard Whittemore).

9.6.2. Straight Line Tests

Besides slopes and stairs,the most fundamental terrain that all rescue robots should be able to traverse are flat terrains, especially over larger distances. This test was done so as to establish the amount of current that was drawn and to test the tracks with the treads. Initially the platform motors would either stall or draw up to 10A. Occasionally the current draw spiked to 17.3A . Journal bearings were introduced to the system, as discussed in Section 6.4.2, to mitigate this problem. This test was therefore performed to gauge the proficiency of the journal bearings as well as that of the new motor assembly.

9.6.2.1. Test Procedure

The platform was placed at a starting position and then driven 1m forward and a set speed value. After that the robot was reversed at the same speed. The current values and the time it took to drive the distance were recorded. This entire procedure was repeated for the **DAC** speed settings of 15, 819, 1638, 5457, 3276 and 4095. The current readings were taken from the power supply's read-out, because using a multimeter to measure current could have been detrimental to the device, because it only has a 10A fuse. It should also be noted that it was significantly difficult to accurately measure the current because of the noise coming from the motors.

9.6.2.2. Results

The journal bearings allowed the platform to function correctly and thus substantially reduced the current draw. As expected, the motors drew more current with higher speed settings. The maximum currents drawn while driving forward or in reverse were below 9A. Figure 9.34 and 9.35 depict the relationship between the motor speed setting and the actual speed for motion in both directions. Thereafter Figure 9.36 and 9.37 illustrate the current draw of the system during the test.

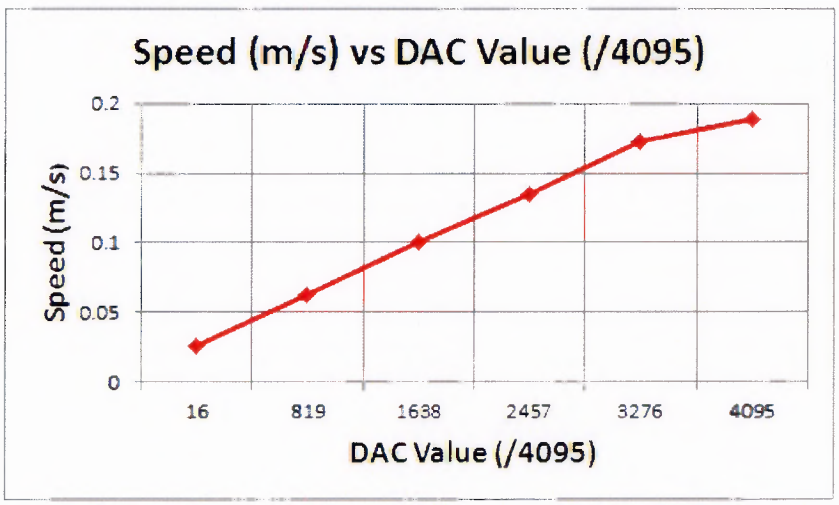

Figure 9.34.: The speed vs DAC speed setting when driving forward.

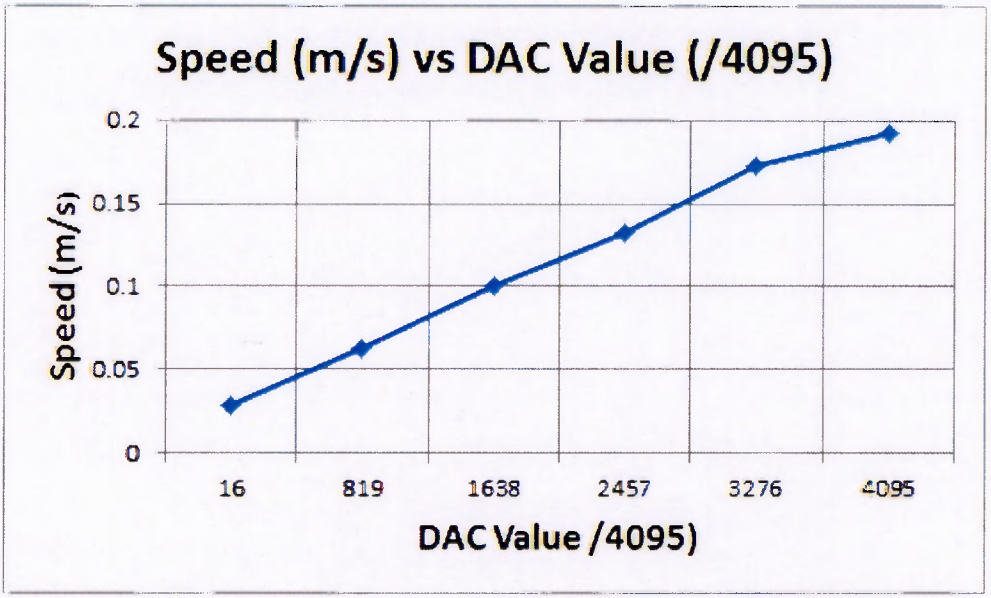

Figure 9.35.: The speed vs DAC speed setting when driving in reverse.

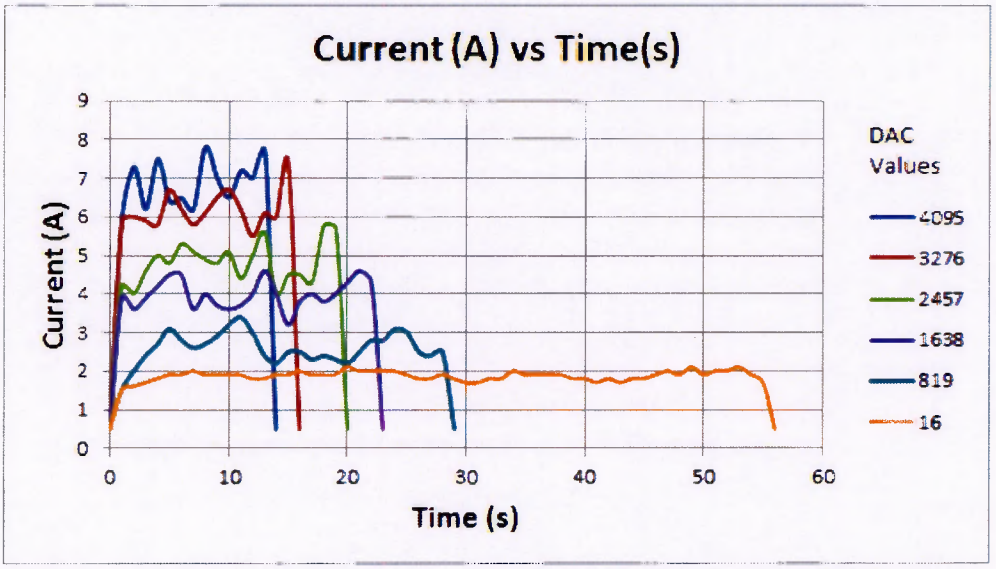

Figure 9.36.: The current draw of the motors over time while driving forward.

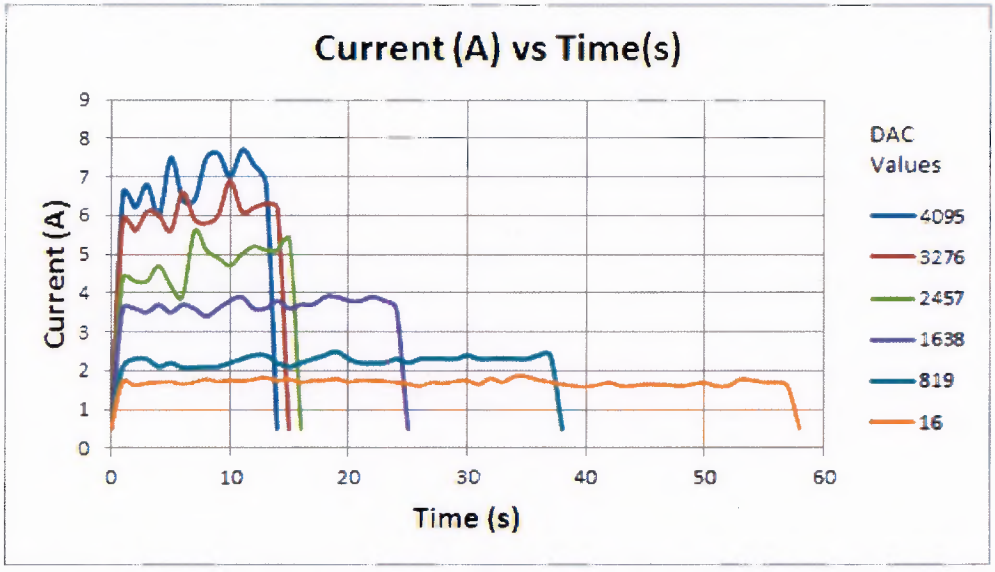

Figure 9.37.: The current draw of the motors over time while driving in reverse.

9.6.3. Mobility while towing a Load

The aim of this test method is to quantitatively evaluate the platform's ability to tow a sleds of varying weights over a flat surface. This is important, because rescue robots can be required to provide logistics support, which means that they are used to transport equipment and supplies [2].

9.6.3.1. Test Procedure

A sled made from a piece of carpet was tied to the platform-arm interface component using a length of cloth line. A weight of 2.5kg was placed on the sled and the robot was driven in a straight line for 5m. The current readings of the 36V line were recorded and the test was repeated with weights increasing in 2.5kg steps, until the robot could not pull the sled anymore. For the reason discussed in Section 9.6.5.1, the power supply's current read-out was used. Likewise, the average current drawn in this test was calculated. Figure 9.38 depicts the the platform towing 5kg a weight.

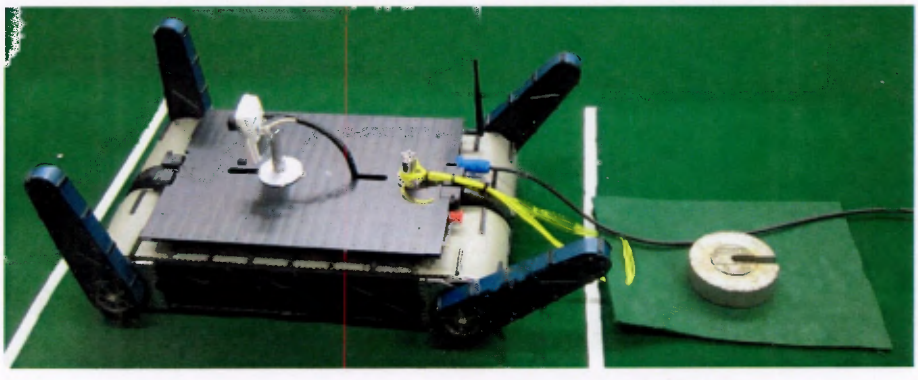

Figure 9.38.: The robot towing a 5kg weight.

9.6.3.2. Results

Weights of up to 70kg were dragged behind the robotic platform. Once a 72.5kg weight was placed on the sled, the motors would attempt to draw more current, which sent the embedded microcontroller into brownout mode and the platform could no longer be controlled. The robotic platform worked properly again, once the weight was reduced or removed. The current drawn by the robot at this weight was 4.58A. The tests in this section and in Section 9.6.4.2 were chronologically performed after the other mobility tests. The platform fell during the stair climbing tests and the front right flipper shaft ended up being bent slightly, as explained in Section 9.2.1.2. The weight the platform had to pull would have had an influence on the shaft and could have caused it to chafe against another component, especially if the weight was large. Seeing that the flipper tracks moved along with the main tracks and seeing that the position of the flipper affected the current drawn as a result of the bent shaft, this is most likely the reason for the discrepancies between the results obtained from the mobility tests performed prior to the fall. The amount of current would spike and the controllers can supply a current of 10A to the motors for only 2s. The controllers will stop taxing the motors if a current that is higher than the prescribed nominal current of 5A is needed. Additionally whenever the controllers switched to their 10A current mode, more current was needed than could be supplied and thus the microcontroller would enter a brown-out mode. The weights that were towed and the corresponding current that was drawn during the test are depicted in Figure 9.39. It can be seen that the current draw rises with the amount of weight that was placed on the sled, however the increase was not consistent. A trendline superimposed on the values provides the equation of a straight line that closest fits this distribution of data. The equation is $y = 0.1077x + 1.0362$ and the R^2 value is 0.9554, indicating a satisfactory fit to the set of data.

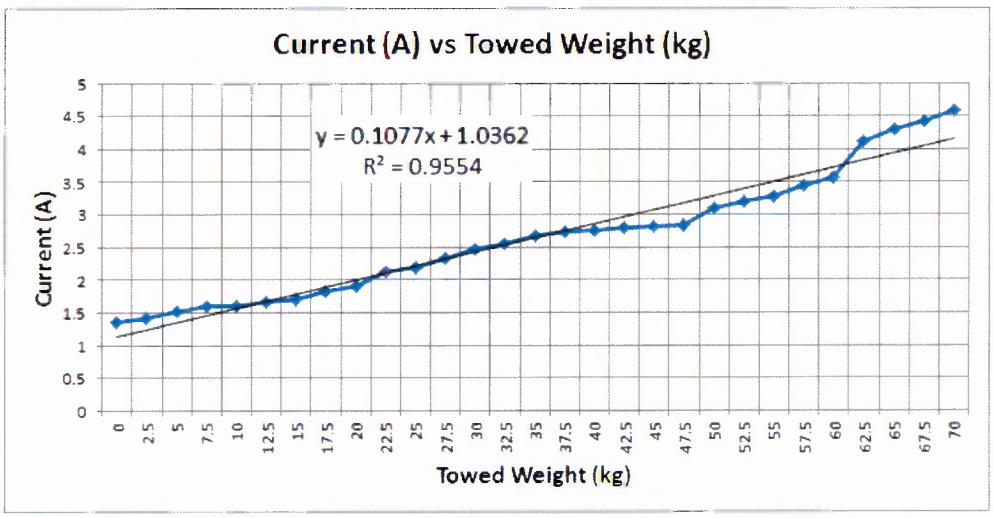

Figure 9.39.: The chart displays the current vs towed weight.

9.6.4. Mobility while carrying a Load

The aim of this test method is to quantitatively evaluate the platform's ability to carry loads of varying weights over a flat surface. The importance of this test is related to the one discussed

in Section 9.6.3.

9.6.4.1. Test Procedure

A piece of carpet was placed on top of the platform so that weights placed on top of it would not scratch the platform. A 5kg weight was positioned on top of the robot and the robot was driven for 1m. During this, the current that was drawn was recorded. The test was repeated for heavier weights that went up in steps of 5Kg. The platform can be seen carrying 40kg in the next figure.

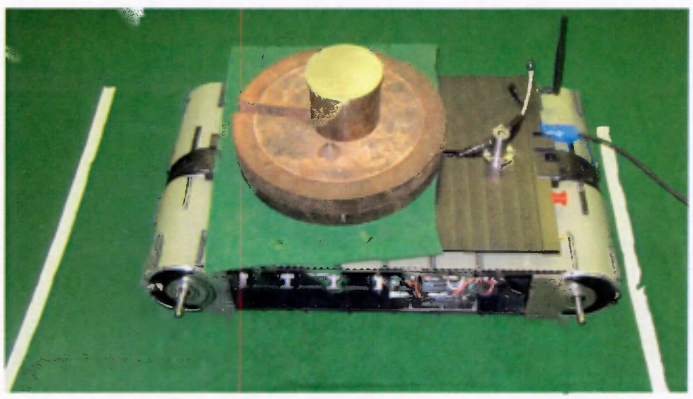

Figure 9.40.: The robot driving while supporting 40kg of weight.

9.6.4.2. Results

Figure 9.41 shows the relationship between the current drawn and the weight carried by the robotic platform. As expected, the current draw rises with the amount of weight carried, even though this does not happen in a consistent manner. A trendline was used to establish an equation for a straight line that is close to the value that were recorded. The equation of the line was $y = 0.3105x + 0.7631$ and the R^2 value was 0.915, which indicates that the trendine associates to the data points in a decent manner. 50kg was the maximum weight that could be carried, since more weight caused the robot to stall or the operator to lose control over the robot's motors. It was established that the robot stalled, because the LM3S8962 microcontroller board would go into brownout mode, as a result of the motors drawing more current. The brownout occurred due to the reasons described in Section 9.6.3.2.

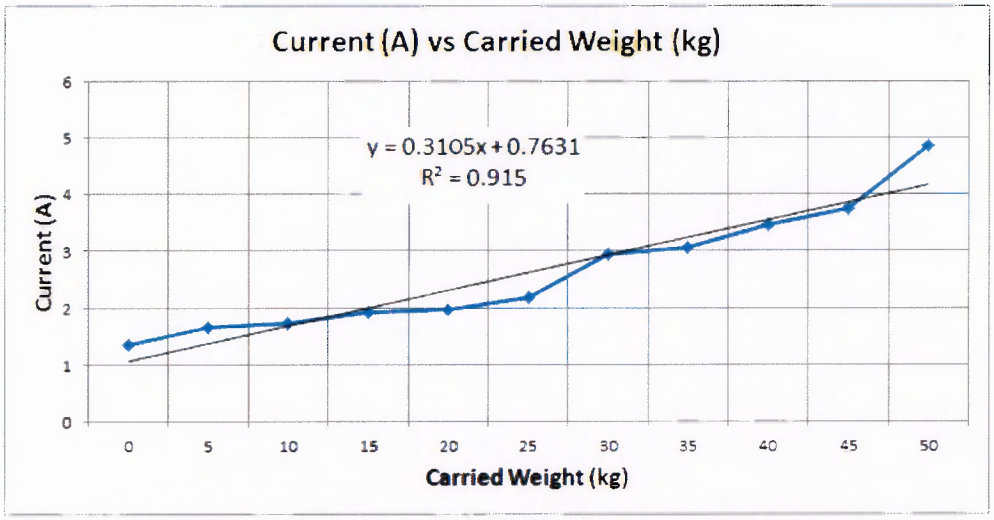

Figure 9.41.: A chart depicting the current that was drawn for each of the weights that the platform carried.

9.6.5. Turning on Flat Terrain

During initial tests it was discovered that the base had significant problems turning on the spot. It turned out that the tracks would be pushed outwards and inwards while turning. Countermeasures were introduced by attaching aluminum circular plates to the pulleys that were designed to act as shoulders that would prevent the lateral movement of the tracks. The effectiveness of the shoulders in preventing the lateral motion of the tracks was gauged in this test.

9.6.5.1. Test Procedure

Once the shoulders were mounted, the operator commenced to make the robot turn left for 30 seconds at a particular speed, stop the robot and then visually inspect if the tracks have moved laterally inwards or outwards. The robot was then placed on the ground once more and it was made to turn in the other direction for 30 seconds. Once again the visual inspection of the tracks for lateral movement will be performed. If a lateral displaced were to be noted it would have had to be measured using a vernier caliper. Thereafter, the test was repeated for 60, 90,120,180, 240 and 300 seconds respectively, each at predetermined **DAC** settings of 16, 819, 1638, 2457, 3276 and 4095. Accurately measuring the current drawn by the motors was a difficult task, because of the noise created by the motors. It was expected that the current could surpass 10A and since the multimeter only has a 10A fuse, it was decided to use the power supply's current read-out.

9.6.5.2. Results

No observable lateral displacement of the tracks occurred. The stalling that occurred prior to the introduction of the shoulders completely ceased and the current draw reduced substan-

tially. The current that was drawn increased as the turning speed was increased. Figure 9.42 illustrates the current drawn versus the rotational speed of the pulleys. Only the average of the current readings are shown. It should be noted that under motion where the platform does not carry, tow or push anything on a flat, even surface, turning required the most amount of current.

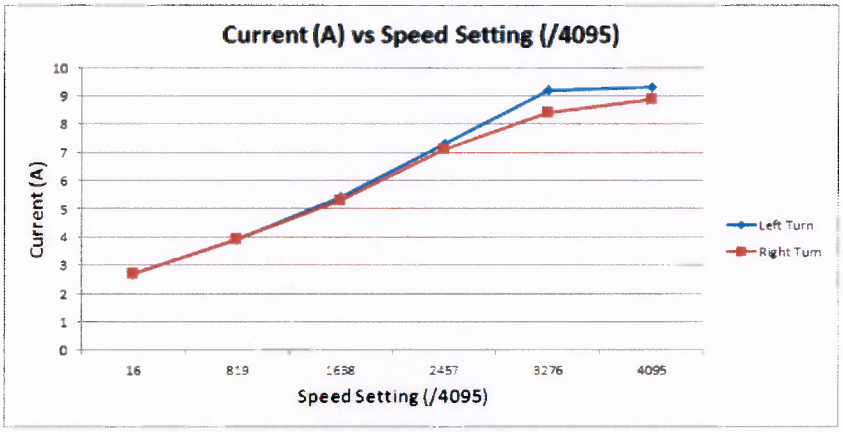

Figure 9.42.: The chart illustrates the current drawn by the motors during turning for a set of DAC values.

9.6.6. Inclined Plane Climbing

The environment of a disaster site often contains slopes that result from fallen walls and other debris. This characteristic property of such environments is also mimicked at the **RoboCup Rescue** competition through wooden slopes. It is thus imperative to most missions to have slope climbing capabilities. The frictional coefficient of the **TPU** feet of the tracks plays a decisive role in this area. Initial tests without the feet attached showed inadequate results, as the platform did not manage to climb a 45° slope, even though a high friction silicon mat was placed on the surface for increased traction. the configuration of the this test can be seen in Figure 9.43. The objective of this test was to determine whether the treads that were attached to the continuous tracks would allow the platform to ascend slopes of different angles of 30° and 45° slopes. This test would additionally be used to inspect the ability of the tracks to provide adequate traction and to evaluate the new pulley assemblies since the introduction of the journal bearings and the LM3S8962 embedded microcontroller.

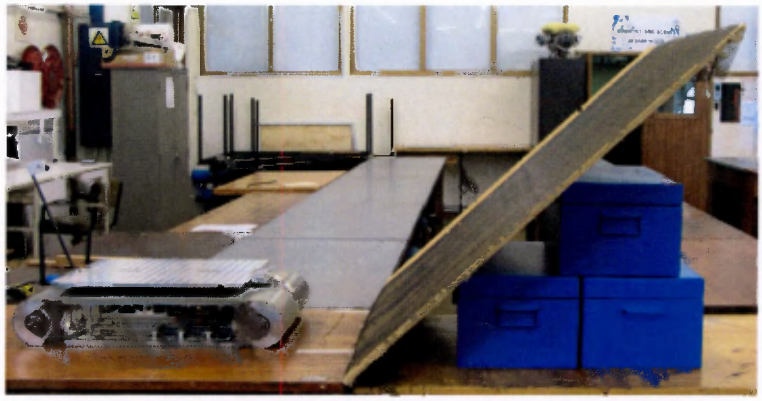

Figure 9.43.: The initial inclined plane climbing test.

9.6.6.1. Test Procedure

A wooden panel covered with carpet is supported by the edge of a table in such a way that both a 30°and 45° slopes could be created. To measure the amount of track slip that would occur during slope ascension some distance was marked out on the carpet and the time to cover that distance was recorded. Once the platform reached the top of the slope, power was removed from the locomotion system and it was observed whether any sliding down occurred and if so then the time taken to slide down 100mm was recorded. These tests were done at six different speeds and the current was recorded each time. It was additionally examined whether the treads would be able to keep the platform assembly in place on a slope once power to the locomotion system has been removed.

9.6.6.2. Results

The platform can be seen ascending a 30° and a 45° slope in Figures 9.44 and 9.45. During ascension it was noticed that the feet would slip occasionally. This became more prominent as the climbing speed was increased. However, the addition of the feet gave sufficient traction and allowed the platform to successfully climb both slopes. The base could be held stationary on both the 30°and 45° slopes in addition to a 60° slope, even when power was switched off. The robot did however very slowly slide down the 60° slope after a while. Figure 9.46 shows the platform on a 60° slope. Turning while climbing slopes was also achieved and did not show any notable increase in current draw that when turning on flat terrain. The speed values with their corresponding current draws were recorded for the 30° as well as the 45° are illustrated in Figure 9.47 and Figure 9.48 respectively.

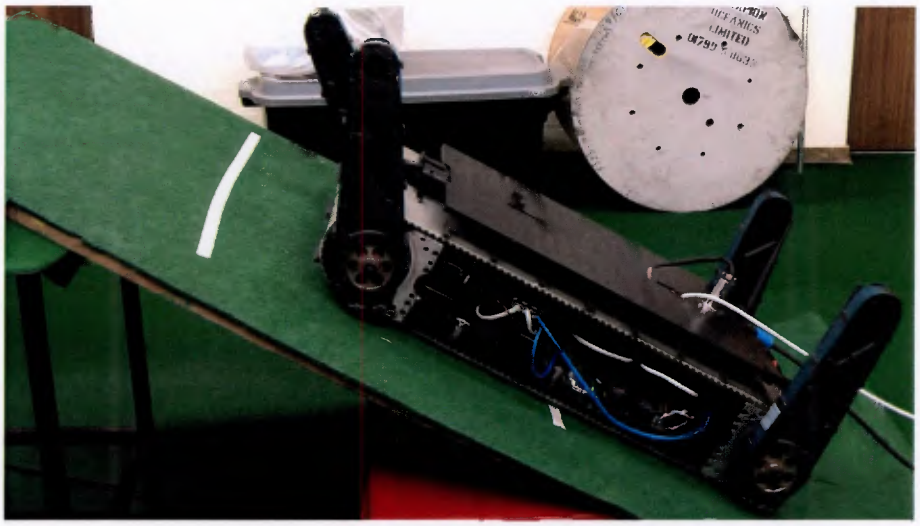

Figure 9.44.: The robot ascending a 30° slope.

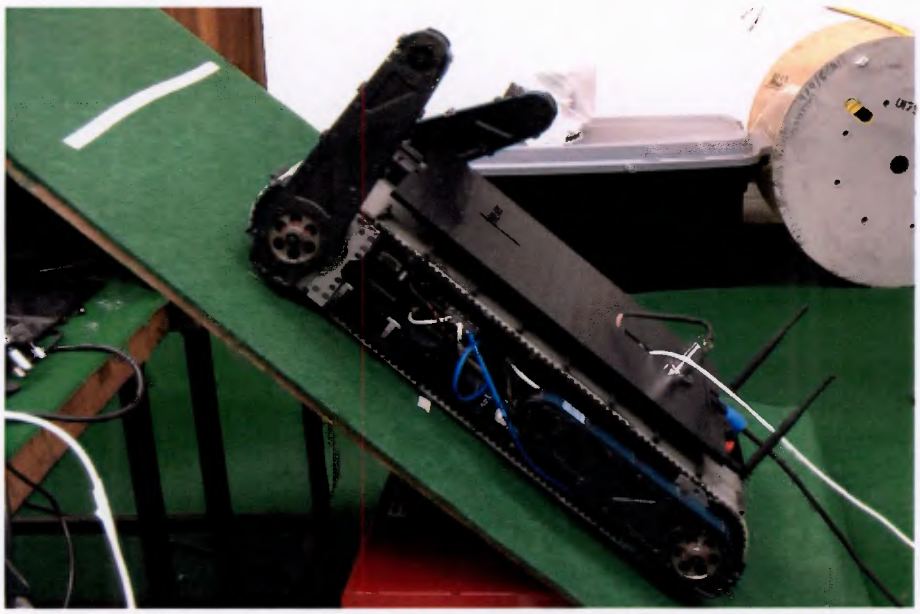

Figure 9.45.: The robot ascending a 45° slope.

Figure 9.46.: The robot ascending a 60° slope.

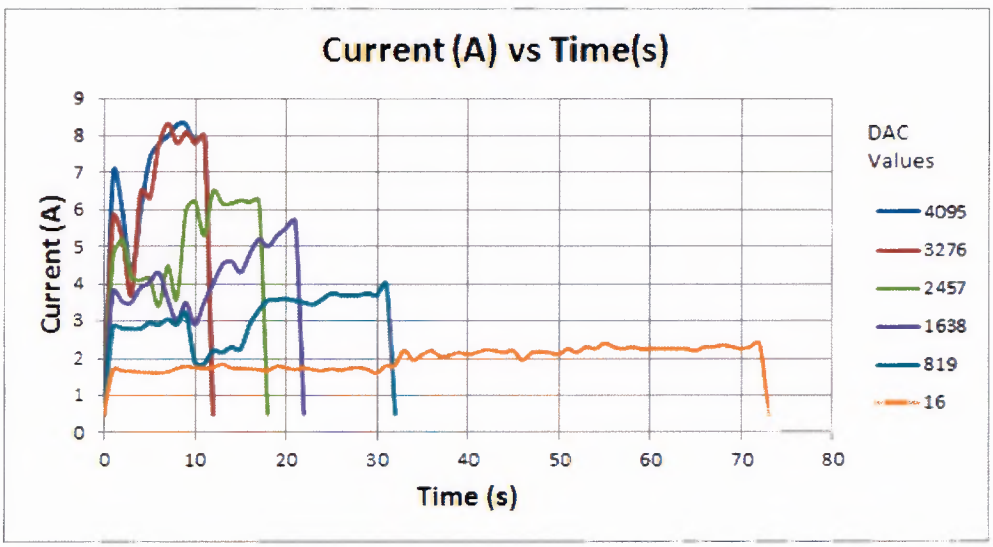

Figure 9.47.: The current draw of the motors over time while ascending a 30° slope.

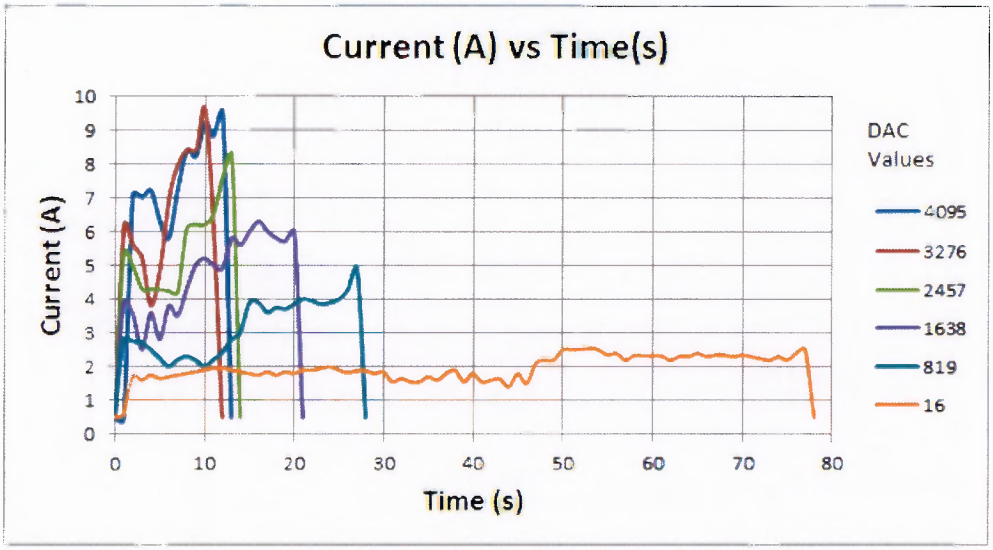

Figure 9.48.: The current draw of the motors over time while ascending a 45° slope.

9.6.7. Mobility on Stairs test

Stairs are characteristic of urban environments and will almost definitely be an obstacle that will be tackled by rescue robots and for this reason it is important to test a robots mobility on stairs. The aim of this test was therefore to gauge the platform's ability to traverse stairs of different dimensions.

9.6.7.1. Test Procedure

The robot was placed at the foot of a staircase and it then commenced to climb those stairs at a particular speed until it reached the top of the staircase. Once the top was reached, right and left pivot turning motions was performed. It was then driven down until it reached the foot of the staircase again. This procedure was repeated for a set of **DAC** values and for different stair geometries.

9.6.7.2. Results

The platform managed to climb and descend stairs of the geometry depicted in Figure 9.49. Steeper staircases were also attempted, however, the feet of the tracks would slip, occasionally causing the entire platform to slip down the staircase. The traction of the drive tracks was not sufficient to allow the platform to climb the steeper staircases and the flippers were utilised as well in order to increase traction between the robot and the stairs. Ascending stairs was successful for all speeds.

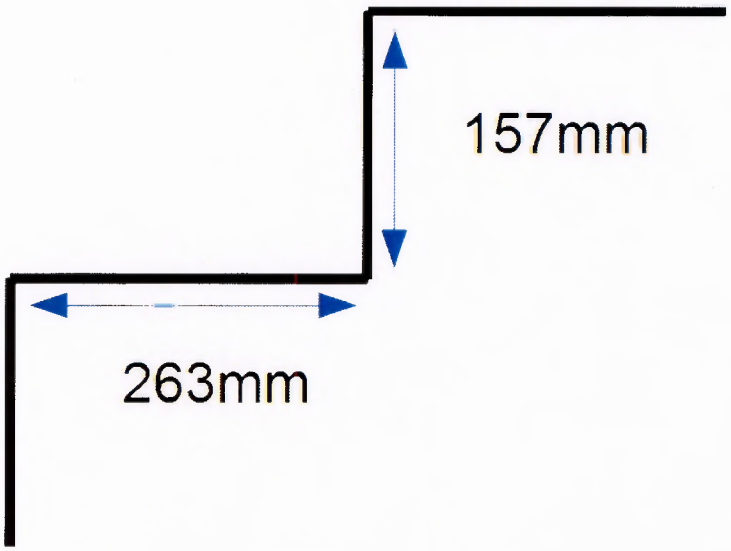

Figure 9.49.: Dimensions of the steps that the platform managed to climb.

9.7. State of Charge Estimation

Having knowledge about the **SOC** would assist the operator in estimating the amount of active mission time left for which the robot could stay fully functional without recharging or exchanging depleted batteries for charged ones.

9.7.1. Procedure

The robot was activated and driven around with the lights on and weight placed on top of it, in order to drain its batteries quickly. The amount of current flowing from the batteries to the platform's components was measured with the custom designed current sensors. A time domain math function in **LabVIEW** was used to sum the current together, thus applying coulomb counting. Once the batteries were depleted and could not be used to drive the platform around anymore, the program was stopped and the final sum of the current that came from the batteries was noted. The batteries were charged and the test was repeated, but the amount of current that was flowing was subtracted from the sum of the current that was measured to have flowed through the system in its first run.

9.7.2. Results

The sum of the current recorded in the first run was determined to be an inaccurate value for the full charge that the batteries could store. It took a considerable amount of time to perform this test and thus it was only performed twice. It turned out that the current sensors were too inaccurate and thus the calculated time that the platform could be active for turned out to

be very long in both cases, since very small values were subtracted from the initially recorded maximum charge value. This is most likely because when the established the charge value, the platform was driven around and thus a large amount of current was drawn. However, while doing the test, the platform was not driven around so it could be monitored more closely and thus less current as flowing. When low current flows, ambient noise inherent in the system can have a greater effect on the readings of the current sensors. After the program indicated that the batteries were depleted, they were removed from the body of the robot and charged. The chargers indicated in both cases that the batteries had more than 80% of their charge left.

9.8. Power Source Switching

Normally when the robot was not being used for a mission it would run off tethered power in order to preserve the charge of the batteries. The batteries were mounted in the sidepods of the platform and used only when needed. Thus the tether would only be removed just before the commencement of a mission. For this reason it was desirable to have a system that could use tether power when the tether was attached and automatically switch to battery power once the tether had been removed, without causing any disturbances to the active electronics devices.

9.8.1. Test Procedure

This test was performed to establish how smooth switching between tether and battery power was. The test was done by having only one module on and then switching from tether to battery power. Thereafter one module was added and the test was repeated.

9.8.2. Results

The platform's power source switching capability functioned adequately and ultimately the fully assembled platform including the arm assembly and the sensor payload retain power during a switching operation.

9.9. Summary

The tests presented in this chapter were performed in order to verify various specifications and to evaluate the functionality and proficiency of the robot's subsystems. As a whole the majority of specifications were met and the platform was deployable without reacquiring any further modifications. Some of the main issues includes the backlash of the flippers, the inability to attain reasonable **SOC** estimations, the lack of suspension and the brown out mode that the embedded controllers go into when excessive currents are drawn by the motors when the platform drags or carries very heavy objects.

Chapter 10 will present the conclusions that were drawn after performing tests and the recommendations that were made to improve future development on the system.

9.10. Wireless Communication

Wireless communication make up an integral part of **Rescue Robots** . It is therefore important to test the capabilities of the wireless link that was used during teleoperation.

9.10.1. Start up time

The amount of time the Bullet M5 radios require to set up a link determines how long it takes before the platform can be deployed.

9.10.1.1. Test Procedure

The radio on the base was switched off, while the operator station's Bullet M5 remained powered. The radio of the platform would then be powered and the time taken to create a link was measured. This was repeated twenty times. Thereafter the roles were reversed and the platform's radio remained powered, while the other one would be switched to check how long it took to create a link. This too was performed twenty times. Lastly both radios were switched off and then powered on to see how long it would take them to connect. This too was repeated twenty times.

9.10.1.2. Results

The Bullet M5 radios took an average of 73.76s seconds to connect throughout all configurations of the test. The longest and shortest times were 110.58s and 36.07s respectively.

9.10.2. Penetration Test

In order to control a rescue robot during rescue missions, wireless signals have to be able to penetrate deep into buildings and through scattered debris. This test was done in order to evaluate the penetration capabilities of the platform's wireless communication system.

9.10.2.1. Test Procedure

The platform was driven around in the Duncan McMillan laboratory. This area was chosen because of the several pieces of equipment as well as desks and cupboards, among other things, that present obstacles to wireless communication. Figure 9.50 depicts a section of the laboratory.

Figure 9.50.: The Duncan McMillan laboratory.

9.10.2.2. Results

The platform was driven from end to end, which is approximately a 50m-60m distance. The wireless link remained stable throughout the test. No lag was noticeable in the video streams and the control of the platform occurred in real time.

10. Conclusions and Recommendations

Throughout the design, further development and testing of the robotic platform, valuable lessons were learnt that made it possible to draw the conclusions presented in this chapter, and make corresponding recommendations for possible future developments on the system.

10.1. Continuous Tracks and Pulleys

10.1.1. Conclusions

In the previous development of this project, the tracks had no adequate means of providing traction to the platform. Trapezoidally shaped **TPU** feet were produced using a band saw and attached to the surface of the tracks which would normally makes contact with the terrain that the robot traverses. This increased the traction capabilities of the tracks and enabled the platform to sufficiently ascend slopes and stairs. Initially when polymer glue from Bondstick was used to attach the feet to the tracks, some feet would detach when the platform was climbing stairs. Once super glue was implemented, the feet did not come off, however, they were not truly bonded to the timing belts and thus they can potentially still come off when enough force is applied.

The platform was designed without any form of suspension and this led to the platform noticeably experiencing significant shock when traversing uneven and rough terrains. Even though the polymer feet added traction to the tracks, the one aspect that was not accomplished, was the introduction of cushioning. Ensuring a smoother ride could not be accomplished with the feet, because being able to drive through a 24" entry triangle, as was specified in the previous development of the system, was essential and this left hardly any space to introduce larger feet capable of decent cushioning. Besides the size of the feet, their shore hardness affected their cushioning abilities. A lower shore hardness would result in a smoother ride and would accomplish higher levels of traction. However, polymers with lower shore hardness values were not as sturdy as ones with higher values. Therefore a rather high shore hardness for the task was chosen, so as to ensure longer lifespans for the feet.

During testing, it was discovered that the tracks had the tendency to laterally move off the pulleys, while the platform was performing a turning motion. This impediment was removed entirely through the addition of shoulders mounted on the pulley assemblies. They guided the tracks and prevented them from walking off the pulleys. The advantage of this solution was that the shoulders rotated at the same rate as the tracks, which meant that the relative velocity between the tracks and the shoulders was zero and thus there was no friction between the components. Overall the modifications to the pulley system significantly increased the mobility of the platform.

10.1.2. Recommendations

The shape of the feet was chosen to be trapezoidal, like the teeth of the timing belts. The choice was made, simply because this shape could be easily manufactured in house and because commercially available robot tracks commonly have such treads. Shapes for feet such as hemispheres should be investigated, because round shapes like that lend themselves to a smoother ride. Another, more versatile method of producing the feet, such as moulding should also be looked at.

The layout of the feet should also be investigated. The benefits of attaching feet in patters where the feet are not parallel to the teeth of the tracks could result in significant improvements and should be looked at. Tread patterns such as those on commercially available tracks, as can be seen in Figure 10.1, should be looked at.

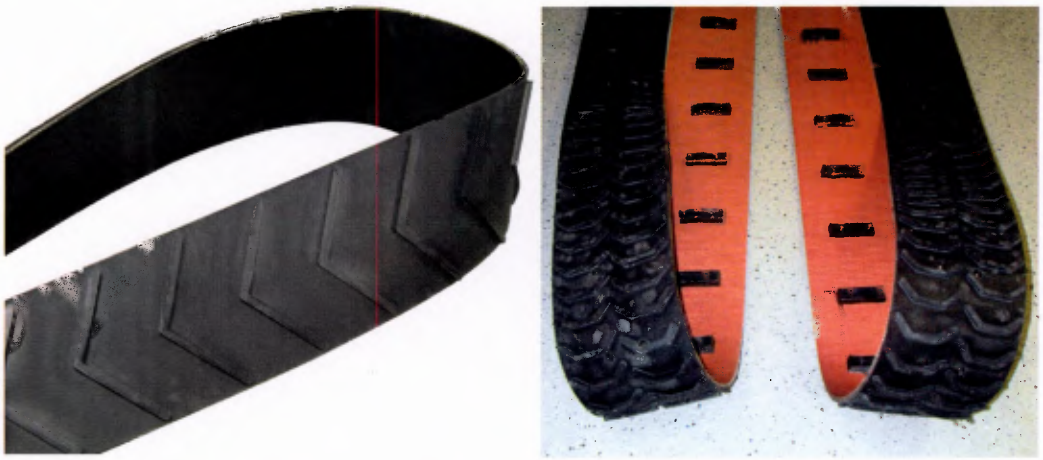

Figure 10.1.: Tread patterns of commercial robot tracks [35],[35].

Although using super glue to attach the feet was ample, more permanent solutions should be researched. A promising bonding method is ultrasonic welding. This method is typically used to join thermoplastics. It employs ultrasonic energy at high frequencies ranging from 20kHz to 40kHz to produce low amplitude mechanical vibrations that heat up the joint interfaces and melt the thermoplastic materials together [36]. The joints produced are very strong and consistent. This method is also the fastest plastic joining method, with the time taken to join components taking between 0.1 to 1.0 seconds. Additionally no fumes are created, eliminating the need for special ventilation.

The dimensions of the feet of the platform were greatly influenced by the requirement to be able to drive through a 24" equilateral entry triangle, as previously discussed. When members of **RARL** attended **RoboCup Rescue** 2012 it was discovered that the driving through this entry triangle was not mandatory and thus larger feet that are better suited for shock absorption could be attached to the tracks. A more elegant solution would be to design a suspension system that uses damping and spring elements to ensure a smoother ride.

10.2. Flippers and Flipper Control

10.2.1. Conclusions

Initially the flippers lacked power, but once the motor assemblies were introduced to the system, a single flipper had the enough power to lift up the fully assembled platform. The addition of the feet to the flipper tracks greatly increased their traction, which was very useful while ascending staircases and climbing over obstacles. When it comes to power and robustness, the flippers performed very well. The one area where the flippers performed inadequately was accuracy. The backlash of the flippers was so large that it made simple position control very challenging. The rear flippers had a backlash of 30°, while the right and the left flipper had a backlash of 22° and 20° respectively. This resulted in the flipper being unable to reach accurate positions and maintain them.

This backlash arose from a combination of components that had loose fits or contacts. The spur gear assembly of the front pulleys and the gear train of the rear pulley inherently had some backlash. Other components, such as the shaft-spring pin assembly of the rear flippers and especially the loose fit of the keys of every flipper increased the overall backlash of this system.

Even though the control aspect of the flippers suffered as a result of the backlash, during testing the maximum difference between the desired and the accomplished angular positions was approximately 1.466°, which is slightly larger than the specified 1°. During testing the flippers were moved by hand, until the limit of the backlash was reached, otherwise such accurate values would not have been accomplished.

10.2.2. Recommendations

Most likely the most effective, yet simple step that could be taken is to ensure that the keys of the flippers fit snugly in their keyways. An additional step to reduce the backlash could come in the form of anti-backlash gears, such as those depicted in Figure 10.2.

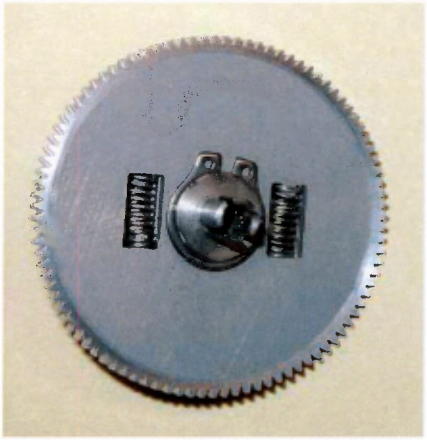

Figure 10.2.: An anti-backlash spur gear [37].

10.3. Wiring and Assembly of the Front Drives

10.3.1. Conclusions

The assembly of the front pulleys was very complicated as a result of the small channel through which the wires had to be guided. During assembly the wires had to be pulled and positioned properly, so that the cable cover could be placed on top of them. To simplify the assembly, thin pico clasp wires replaced the thicker wires that were initially used. Even though this ensured that the wires could fit through in this channel, the male pico clasp plugs had the tendency of coming out of their female plugs during assembly, as a result of having to pull them.

Initially the motor assemblies of the front drives were each being supported on only one side and this caused them to chafe against the inner sides of the pulleys, consequently causing the motors to stall. The introduction of a journal bearing to support the unsupported side eliminated chafing, enabled the motor assembly to function. The maximum current drawn from the motors while was just under 10A at full speed when the platform was driving in straight lines and ascending stairs. This value was high, especially when considering that the maximum available current was 12A and that other devices also require power. The current draw did drop to under 3A when driving slower and which mean that other devices would have enough power to function properly.

10.3.2. Recommendations

The channel cannot be increased in depth any further without creating a hole in the centre spine. Thinner wires that collectively have the same current carrying capabilities as a single one of the wires that were used to supply the drive assemblies with 36V could be introduced. These wires would make the assembly of the drives simpler.

10.4. Sidepods

10.4.1. Conclusions

The sidepods were able to house several electronic components, including the batteries that power the Ratel. They were designed in such a way, that the inside of the sidepods was only accessible from a single side. The large number of threaded holes that were available in the sidepod units added a great amount of versatility to the mounting of additional components to the platform. The more components were added to the sidepods, the more cumbersome it became to mount devices in the sidepods and to work with them. The reduced space made even the simplest tasks, such as screwing a fastener inside a sidepod challenging. Furthermore wiring was difficult to arrange, due to only having access to it from the side.

10.4.2. Recommendations

Having access to the components from above would make wiring and assembly significantly simpler. Seeing that the tensioning system that is built into the top section of the sidepods was not used, one could make that a part of the top platform section removable. Introducing such a feature would be useful, yet could turn out to be difficult to implement. A second and easier option would be to mount all components to a perspex plate that could be easily inserted and taken out of the sidepod units. This would allow one to amount devices onto the plate, while having access to them from all sides. Once the components were mounted, the plate could be inserted and fastened to a sidepod. For this to work, wires that run inside the platform would have to be sufficiently long and loose, enabling the plate to be easily extractable.

10.5. Platform Weight

10.5.1. Conclusions

The overall weight of the platform was specified to be under 20kg, but after assembly the overall weight of the platform was measured to be 42.16kg, which is more than twice the specified limit. The largest contributors to the weight of the **UGV** are sidepods. The sidepods are as heavy as they are, mainly because they house the majority of the electric components. Thus, even though the mass of the structural components of the sidepod cannot be reduced too much, several components can be reduced in weight.

10.5.2. Recommendations

The centre spine is the main support structure of the system and it was designed to be very sturdy, however, this has also led to it weighing 4.96kg. The middle section of the spine can be removed in order to reduce its mass, without weakening its ability to support the rest of the structural components. Furthermore holes could be drilled into some of its sections to further reduce weight. Similarly material can be removed from the sidepod sections as well as the utility plate that sits atop the spine.

10.6. Power Supply and Distribution System

10.6.1. Conclusions

The power supply and distribution system performed satisfactorily. The power board met all its specifications and made the wireless operation of Ratel possible. However, It did not deliver the required means to estimate the **SOC** of the batteries. It was also observed that the embedded LM3S8962 microcontroller boards would brown out when the motors attempted to draw very large amounts of current.

10.6.2. Recommendations

The power board makes use of electromechanical relays, which worked sufficiently, but could be replaced with faster solid state relays. The brownout of the LMS8962 boards or any board used in the future of the project could be prevented by altering the configuration of the power board. Instead of having all regulation occur at the board itself, 18V and 36V could be delivered to the board to be distributed to various locations, and the regulation could occur at the controllers. This way, even if the voltage of the lines were to fluctuate, a DC/DC converter on the boards would handle this and thus brownout could be prevented. Some power regulation would still be on the power board, so that components like the D-Link switch and the cameras could attain their required power.

10.7. Wireless Communication

10.7.1. Conclusions

While members of **RARL** attended **RoboCup Rescue** 2012 the Ubiquiti RouterStation Pro radios were used to create a wireless link between the operator station and the rescue robot. Several complications arose and a reliable link could not be created nor maintained. The introduction of the Ubiquity M5 wireless radios solved all the issues associated with the RouterStation Pro wireless radios. The setup of the new radios was simple and quick and they had the added benefit of having a small footprint, which meant that finding a place to mount them was not difficult.

10.7.2. Recommendations

The radios proved to produce a reliable wireless link and testing showed that they have sufficient penetration capabilities. The remaining aspect of the radios that should be inspected is their line of sight range, as well as the maximum amount of traffic they can tolerate.Additionally the latency and data throughput of the wireless link versus distance or signal strength should be investigated further.

10.8. Cameras

10.8.1. Conclusions

The front and rear cameras that provided visual information to the operator during teleoperation only managed to present adequate picture. The video feed enabled sufficient navigation through areas, however, it did fall short when a more detailed picture was required.

10.8.2. Recommendations

Usually the sensor payload provides the clear pictures, however having more cameras that are capable of producing high resolution images is beneficial. During testing, the Bullet M5 radios showed that they could transmit considerable data without any noticeable delay and therefore real time data streaming of the added high resolution cameras should be acceptable.

10.9. Summary

The platform performed adequately during driving tests. Most of the systems on the platform performed as was expected. Hard track feet and the lack of a suspension system made the ride quality poor, and ways of introducing cushioning to the system, such as using larger and softer polymer components for the tread. Position control was very inaccurate because of the backlash of the flippers. The backlash could be removed by ensuring tighter fits of the components that make up the flipper assembly and through the introduction of anti-backlash gears. The wireless communication system performed well, but it requires thorough testing so that its abilities can be accurately gauged.

Bibliography

[1] FEMA, "Urban Search and Rescue." [Online]. Available: http://www.fema.gov/emergency/usr/

[2] B. Siciliano and O. Khatib, *Springer handbook of robotics*. Springer, 2008.

[3] MEAN WELL Enterprises Co. Ltd, "NID60-SPEC 2009-09-04." [Online]. Available: http://www.meanwell.com/search/nid60/NID60-spec.pdf

[4] Sulekha.com, "India Kashmir Building Collapse Pictures & Photos." [Online]. Available: http://newshopper.sulekha.com/india-kashmir-building-collapse_photo_941870.htm

[5] Myselfanand.com, "New Zealand's earthquakes kills 65 people have died after a 6.3-magnitude earthquake hit Christchurch." [Online]. Available: http://www.myselfanand.com/2011/02/new-zealands-earthquakes-kills-65-people-have-died-after-a-6-3-magnitude-earthquake-hit-christchurch/

[6] GiGazine, "Video Documentary: 15 Years from the Great Hanshin Earthquake - GIGAZINE." [Online]. Available: http://en.gigazine.net/news/20090117_great_hanshin_awaji_earthquake/

[7] RoboCup Rescue, "Building Rescue Systems of the Future." [Online]. Available: http://www.robocuprescue.org/

[8] CRASAR, "World Trade Center 911." [Online]. Available: http://crasar.org/gallery/?g2_itemId=113

[9] iRobot Corporation, "iRobot Â® PackBot Â® Accessories." [Online]. Available: http://www.irobot.com/ /media/Files/Robots/Defense/PackBot/iRobot-510-PackBot-Accessories.ashx

[10] NIST, "RoboCup Rescue Robot League Rules 2011.2." [Online]. Available: http://www.nist.gov/el/isd/upload/Robocup_Rules_2011.pdf

[11] E. Dreyer, "Development of the RATEL UGV Platform," University of Cape Town, 2012.

[12] N. Enayati, G. Mahaseni, and A. Tamjidi, "RoboCupRescue 2010 - Robot League Team < PARS (IRAN) >," 2010.

[13] A. Tangpok, C. Siriphitakchai, and C. Sawatdee, "RoboCup Rescue 2010 - Robot League Team SUCCESS (Thailand)," 2010.

[14] T. Kimura and I. Aida, "RoboCupRescue 2010 - Robot League Team < NuTech-R (Japan) >," *Technology*, pp. 0–5, 2010.

[15] RobotShop Distribution Inc., "Quince the Rescuer Robot." [Online]. Available: http://www.robotshop.com/blog/quince-the-rescuer-robot-517

[16] International Rescue System Institute, "Rescue Robots & Systems." [Online]. Available: http://www.rescuesystem.org/IRSweb/en/robot.html

[17] Evan Ackerman, "FirstLook: iRobot's New Throwable Baby Surveillance Bot - IEEE Spectrum." [Online]. Available: http://spectrum.ieee.org/automaton/robotics/military-robots/firstlook-irobot-new-throwable-baby-surveillance-bot

[18] iRobot Corporation, "IRobot 710 Warrior Image Gallery." [Online]. Available: http://www.irobot.com/gi/ground/710_Warrior/

[19] A. H. Soltanzadeh, A. Chitsazan, S. Azizah, and S. A. Ghazali, "RoboCupRescue 2010 - Robot League Team AriAnA & AVA (Iran + Malaysia)," 2010.

[20] GlobalSpec Inc., "Optical Encoder | Products & Suppliers on GlobalSpec." [Online]. Available: http://www.globalspec.com/industrial-directory/optical_encoder

[21] R. Edlinger, A. Pölzleithner, W. Rokitansky, M. Zauner, B. Fahringer, T. Fink, T. Hatheier, J. Kieslmair, and H. Kneidinger, "RoboCupRescue 2009-Robot League Team, FH-Wels (Austria)," pp. 1–14, 2009.

[22] Xsens Technologies B.V., "xsens mti : miniature ahrs - attitude and heading sensor - xsens," 2011. [Online]. Available: http://www.xsens.com/en/general/mti

[23] W. Xiao-Hong and Y. Xiao-Xin, "Motion control for rescue robot based on PC104 and CPLD," pp. 317–320, 2009. [Online]. Available: http://ieeexplore.ieee.org/xpls/abs_all.jsp?arnumber=5156625

[24] N. S. Nise, *Control Systems Engineering*, 5th ed. John Wiley & Sons, Inc.

[25] T. Wescott, "PID without a PhD." [Online]. Available: http://igor.chudov.com/manuals/Servo-Tuning/PID-without-a-PhD.pdf

[26] Linksys, "Differentiating the 5 GHz and 2.4 GHz bands." [Online]. Available: http://kb.linksys.com/Linksys/ukp.aspx?pid=80&vw=1&articleid=17415

[27] M. Rieger, "Research and Development of a Rescue Robot End-Effector," University of Cape Town, 2013.

[28] R. Collette, "Polyurethane and rubber tires: A comparative overview," Thombert, 2010. [Online]. Available: http://www.thombert.com/white_papers/PolyurethaneRubberTires.pdf

[29] Smooth-on Inc., "Durometer Shore Hardness Scale." [Online]. Available: http://www.smooth-on.com/-Documents-Duromet/c0_1351_1370/index.html

[30] Distrupol Ltd., "Elastollan(TM)_Extrusion_Recommendations.pdf." [Online]. Available: http://www.distrupol.com/images/Elastollan(TM)_Extrusion_Recommendations.pdf

[31] Spyparty.com, "Have an alpha masked Xbox 360 Controller, on me." [Online]. Available: http://www.spyparty.com/2010/08/30/have-an-alpha-masked-xbox-360-controller-on-me/

[32] Applied Image Inc., "QA-70-1 Video Resolution (EIA-1956) Pattern Product Specifications," pp. 1–3, 1956. [Online]. Available: http://www.aig-imaging.com/mm5/PDF/EIA Video Resolution Pattern QA-70-1_v1-07.pdf

[33] Macular Degeneration Support, "Snellen Chart." [Online]. Available: http://www.mdsupport.org/snellen.html

[34] Fredrik Gløckner, "Micro 4/3rds Photography: Geometric distortion correction." [Online]. Available: http://m43photo.blogspot.com/2013/01/geometric-distortion-correction.html

[35] SuperDroid Robots, "Mechanical Robot Parts > Treads." [Online]. Available: http://www.superdroidrobots.com/shop/category.aspx?catid=55

[36] M. Troughton, *Handbook of plastics joining: a practical guide*. William Andrew, 2008.

[37] Ascent Precision Gear Corp., "Anti-Backlash Gears." [Online]. Available: http://www.ascentgear.com/prod06.htm

Index

A. Drawings

A.1. Introduction

This appendix contains a selection of drawings that were made in the process of completing this project.

Table A.1.: Drawing Register.

Drawing Register		
Drawing	**Drawing Number**	**Page**
Final Rescue Robot Platform	RR	Ai
Modified Front Pulley	RR-FP	Aii
Exploded Modified Front Pulley	RR-EFP	Aiii
Modified Rear Pulley	RR-RP	Aiv

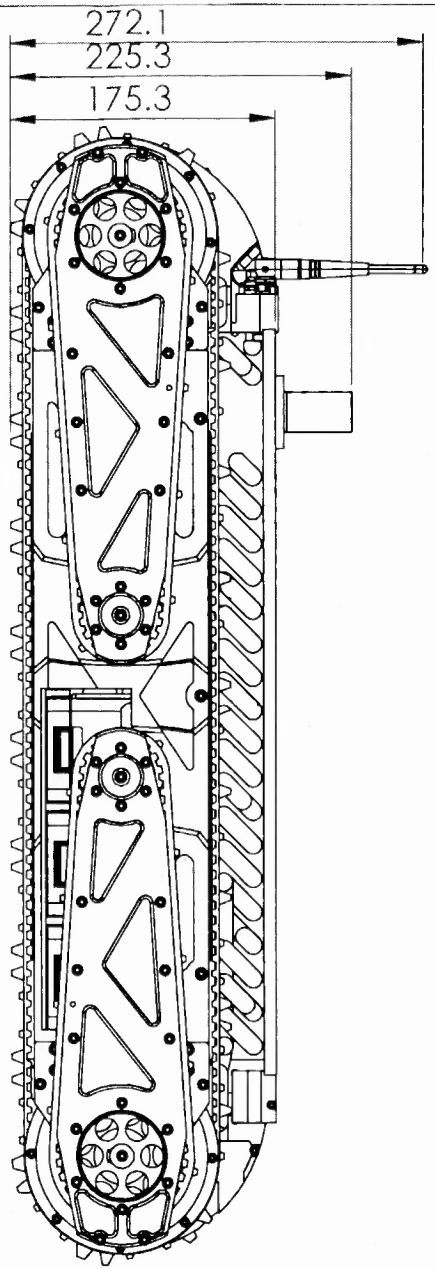

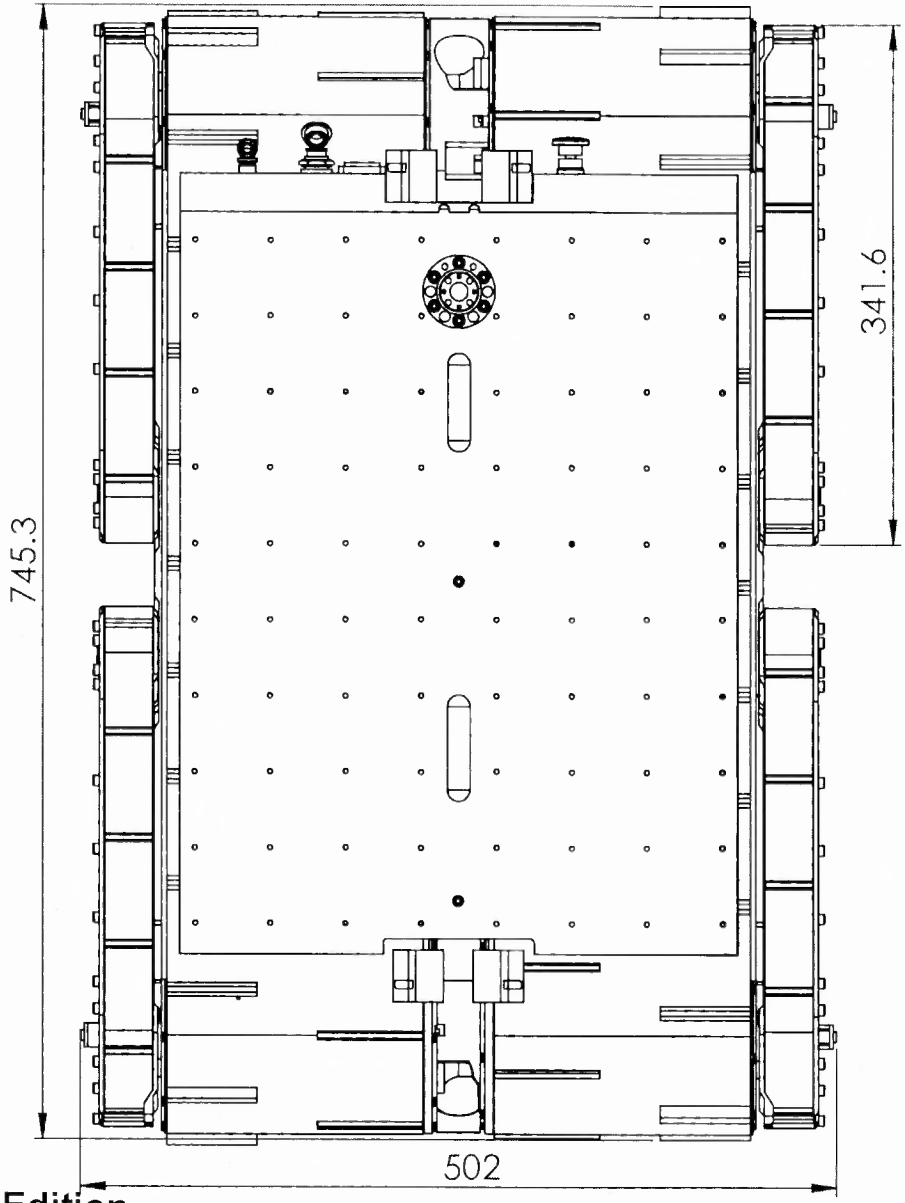

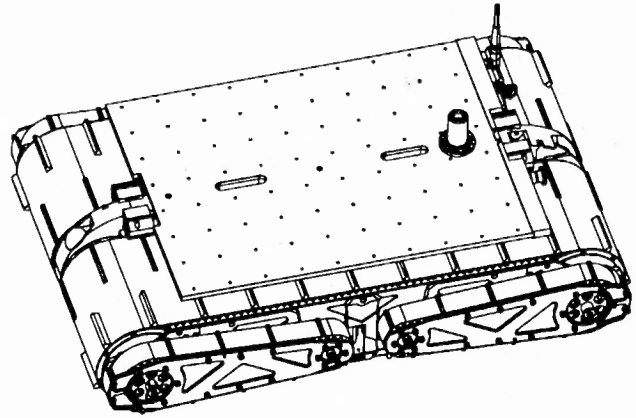

SolidWorks Student Edition.
For Academic Use Only.

A4 Landscape	University of Cape Town Department of Mechanical Engineering				
	Title: Final Rescue Robot Platform				
Quantity: 1	Part Finish	Date: 2013/04/02	Scale: 1:5	Sheet1	of 1
Material:	Drawn By: David Lwabona			Drawing Number RR	

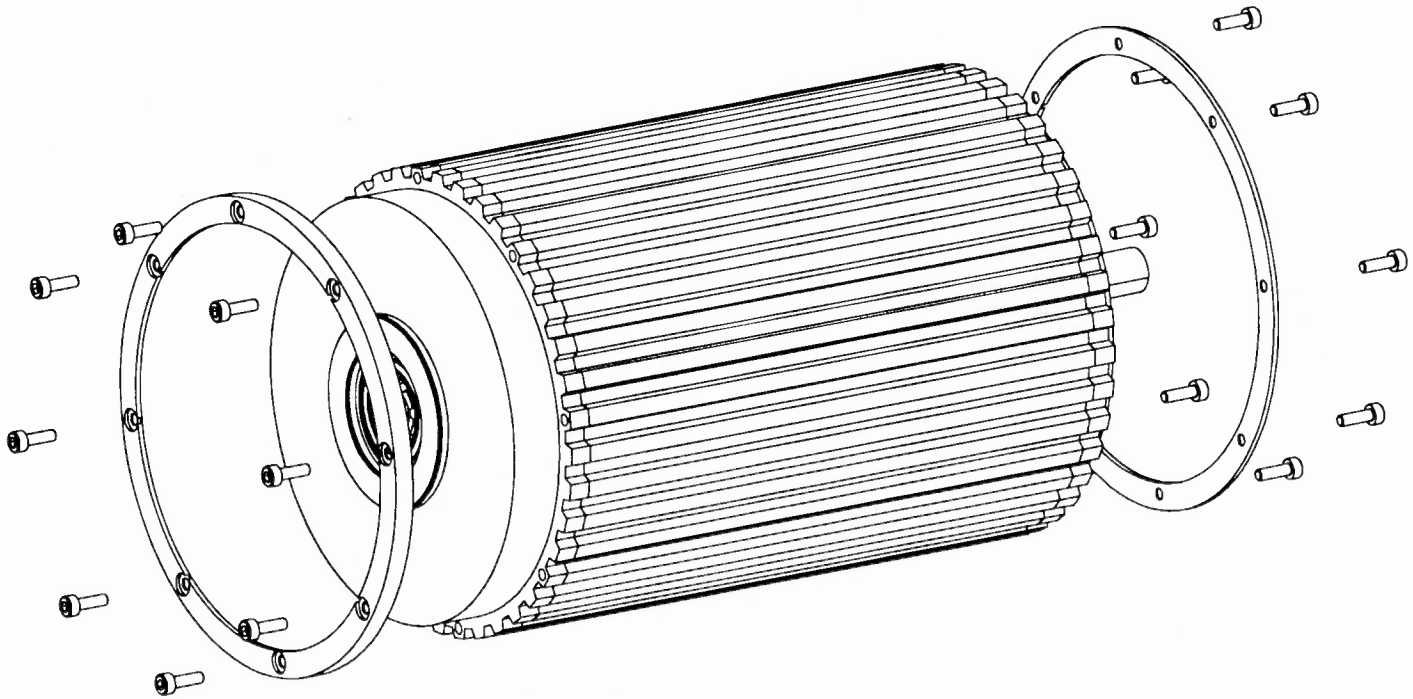

A4 Landscape	University of Cape Town Department of Mechanical Engineering				
	Title: Exploded Modified Front Pulley				
Quantity:	Part Finish	Date: 2013/04/02	Scale: 1:2	Sheet1	of 1
Material:	Drawn By: David Lwabona			Drawing Number RR-EFP	

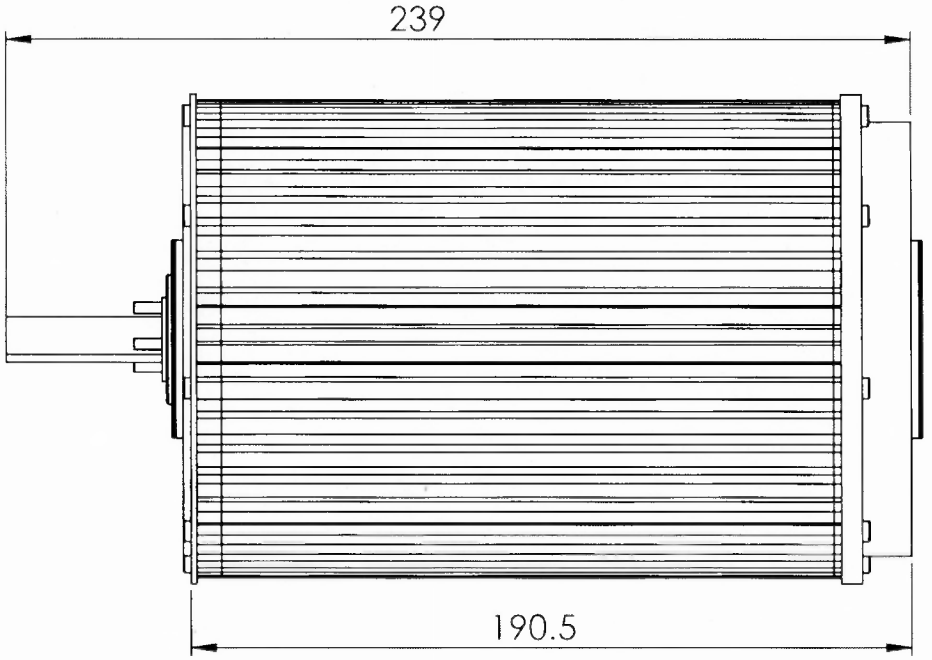

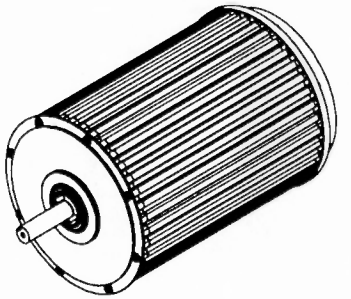

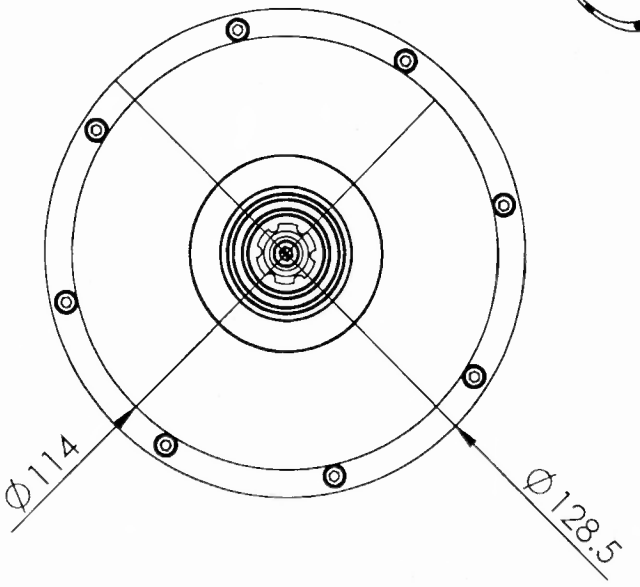

SolidWorks Student Edition.
For Academic Use Only.

A4 Landscape	University of Cape Town Department of Mechanical Engineering				
	Title: Modifeid Front Pulley				
Quantity:	Part Finish	Date: 2013/04/02	Scale: 1:2	Sheet1	of 1
Material:	Drawn By: David Lwabona			Drawing Number RR-FP	

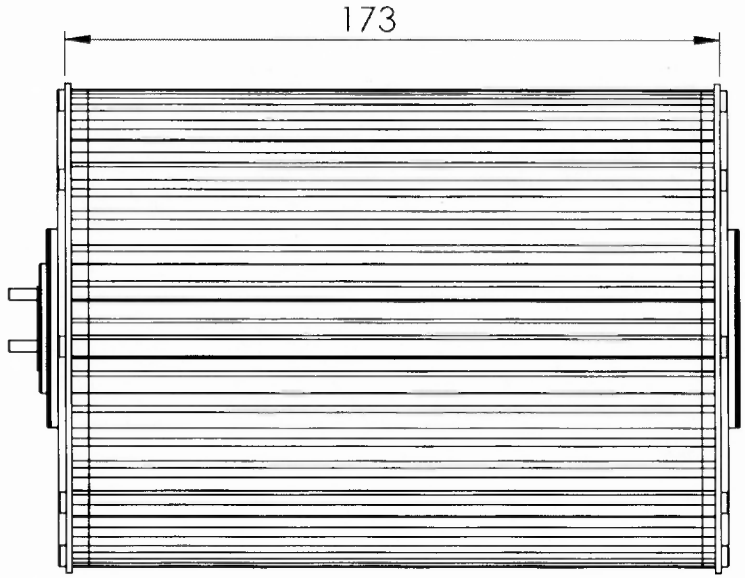

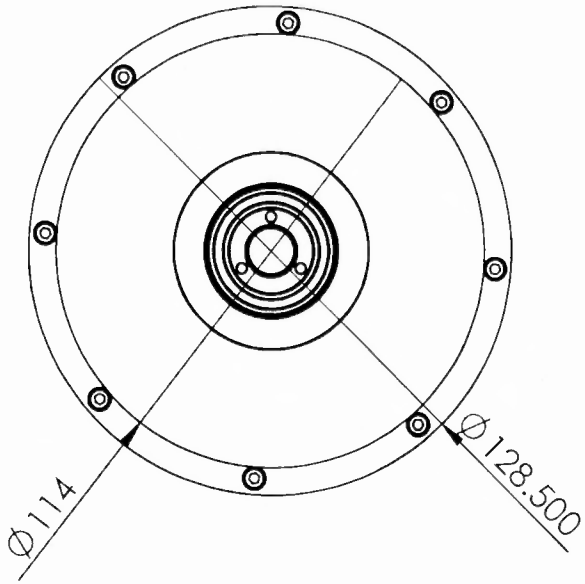

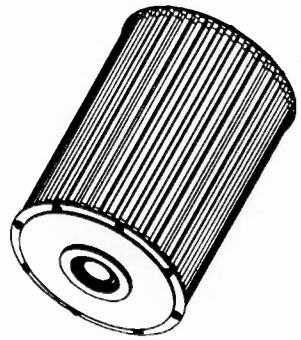

SolidWorks Student Edition.
For Academic Use Only.

A4 Landscape	University of Cape Town Department of Mechanical Engineering				
	Title: Modified Rear Pulley				
Quantity:	Part Finish	Date: 2013/04/02	Scale: 1:5	Sheet1	of 1
Material:	Drawn By: David Lwabona			Drawing Number RR-RP	